The Capture of Suspended Particles by Aquatic Vegetation

Ariaan Purich

Environmental Engineering Project Dissertation

October 2006

Supervisors: Dr Marco Ghisalberti & Prof. Greg Ivey

School of Environmental Systems Engineering

The University of Western Australia

Abstract

In aquatic systems, the fate of suspended particles such as sediments and biological particles is important, as this affects water quality and the population dynamics of aquatic species. Aquatic vegetation is typically coated with a sticky periphyton layer and when particles collide with vegetation this layer facilitates retention. This process is known as direct particle capture. Before conducting this study, the understanding of the efficiency with which suspended particles are removed from the water column by direct particle capture in vegetation arrays, and the importance of stem wakes on this process, was limited. Laboratory experiments were conducted with the aim of measuring the particle capture efficiency of simulated aquatic vegetation under different flow conditions, and investigating how wakes in the modelled vegetation arrays influenced this. Particle capture efficiency is a measure of the efficiency that an individual cylinder captures suspended particles and for the modelled aquatic vegetation this was found to range between 0.02 and 0.67%. Particle capture efficiency was highest for the medium density array tested. Analysis of the velocity measurements made during experiments found that the vortex shedding frequency and speed of eddy rotation were also highest in the medium density array. This suggests that the wakes generated by aquatic vegetation arrays are influenced by the density of the vegetation, and that there is a threshold density which supports the strongest eddy structures. It also suggests that the existence of these eddies influences the particle capture efficiency. Based on the magnitude of particle capture efficiencies determined experimentally, the importance of direct particle capture as a suspended particle reduction mechanism, compared to sedimentation, was assessed. It was concluded that in aquatic systems with low flow velocities and relatively sparse vegetation, such as in freshwater wetlands, sedimentation is the dominant process. Conversely, in aquatic systems with higher flow velocities and denser vegetation, such as in tidal marshes and seagrass meadows, direct particle capture is the dominant process. Understanding of the particle capture by aquatic vegetation and how stem wakes influence this has been improved as a result of this study, however considerable further work is required to fully understand these processes. Recommendations for future work include conducting more laboratory experiments as well as numerical modelling to enable verification and expansion of the conclusions drawn from this study. From this the geochemical and biological functioning of aquatic systems would be better understood, which could lead to improved conservation and management of these important systems.

Acknowledgements

I would like to acknowledge all the people who have contributed to this project.

First and foremost I would like to acknowledge the contributions of both my supervisors, Prof. Greg Ivey and Dr Marco Ghisalberti. Their support and guidance with this project throughout the year has been invaluable and greatly appreciated.

I would also like to thank Hon Leong and Dianne Krikke, whose assistance with my experiments in the lab was really helpful.

Finally I would like to acknowledge my family and friends. In regards to this project, thanks to Mum and Dad for proof reading my report and to Eva for helping me in the lab. In general, thanks to Mum, Dad, Alex, Ingrid and Eva for all of your support and encouragement over the past year and throughout my entire education. Thanks also to Kate, for being a terrific friend and for understanding me better than anyone else, and to James, for always encouraging me and believing in me.

Contents

List of Figures

List of Tables

Notation

A	Frontal area (m^2)
a	Frontal area per unit volume (m^{-1})
B	Width (m)
b	Upstream width of particles captured (m)
C_D	Drag coefficient for a single cylinder
$\overline{C_D}$	Bulk drag coefficient
d	Reynolds number length scale (m)
d_c	Cylinder diameter (m)
D_p	Plant density (shoots m^{-3})
d_p	Particle diameter (m)
F	Particle diffusivity ($m^2\ s^{-1}$)
f_s	Shedding frequency (s^{-1})
g	Acceleration due to gravity (9.81 m s^{-2})
h	Water depth (m)
k	Settling rate constant (s^{-1})
L	Length (m)
l_c	Length of collector cylinder (m)
m_p	Average mass of one particle (g)
m_{total}	Total mass of particles in the flume (g)
n	Number of cylinders or shoots (cylinders, shoots)
N_c	Number of particles collected (particles)
N_p	Number of particles in the flume (particles)
P	Particle concentration (particles m^{-3})
p	Proportion of area occupied by cylinders
P_0	Initial particle concentration (particles m^{-3})
R	Particle to collector ratio
Re	Reynolds number
Re_c	Collector Reynolds number
r_p	Particle radius (m)
S	ADV signal strength (dB)
s	Specific gravity
S_0	Initial ADV signal strength (dB)
St	Strouhal number
Stk	Stokes number

T	Period (s)
t	Time (s)
T_K	Absolute temperature (K)
U	Flow velocity (m s^{-1})
V_f	Flume volume (m^3)
V_p	Average volume of one particle (m^3)
w_s	Stokes settling velocity (m s^{-1})
η	Particle capture efficiency
η_R	Particle capture efficiency due to direct interception
η_D	Particle capture efficiency due to diffusional deposition
κ	Boltzmann constant (1.38 x 10^{-23} J K^{-1})
μ	Dynamic viscosity of fluid (kg m^{-1} s^{-1})
ν	Kinematic viscosity of fluid (m^2 s^{-1})
ρ_f	Fluid density (kg m^{-3})
ρ_p	Particle density (kg m^{-3})
ℓ	Turbulent length scale (m)

1.0 Introduction

1.1 Aquatic vegetation and particle capture in the environment

The unprecedented environmental concern of our times has driven a better understanding of the processes that govern environmental systems. The capture of suspended particles by aquatic vegetation is a topic of considerable interest in a variety of disciplines such as biology, environmental science and engineering. Aquatic vegetation existing in environments such as wetlands, seagrass meadows and tidal marshes plays a critical role in the functioning of such aquatic systems. The presence of vegetation in aquatic systems can reduce the particles suspended in these systems and this can improve water quality, increase water clarity and play a crucial role in the breeding cycles of different species. Sedimentation of particles in vegetated areas which occurs as a result of the reduced flow velocities in these areas is well understood, however another particle removal mechanism also exists. Aquatic vegetation is typically coated with a sticky periphyton layer and when particles collide with vegetation this layer facilitates retention, resulting in a reduction of suspended solids in the water column. This mechanism plays a significant role in removing suspended particles from aquatic systems but is not as well understood or quantified as sedimentation.

1.2 Study objectives

Removal of suspended particles in aquatic systems by direct particle capture has been observed in the field and modelled in laboratory experiments, and it has been found to be an important and significant process. The understanding of the efficiency at which aquatic vegetation removes suspended particles from the water column by direct particle capture is limited. Similarly, there is a limited understanding of the effect of stem wakes on the particle capture efficiency of aquatic systems. The purpose of the study was to investigate the importance of direct particle capture by vegetation in aquatic systems, and to increase the understanding of the factors controlling particle capture efficiency. To do this, laboratory experiments simulating conditions observed in real aquatic systems were conducted, with the goal of helping evaluate the filtration capacity of vegetated wetlands, and improving the understanding of some of the processes which occur in aquatic systems.

1.3 Document overview

This dissertation begins with a discussion of the background information relevant to the study objectives, in Section 2.0. This includes a discussion of the types of suspended particles and vegetation that exist in aquatic systems and why the capture of suspended particles is important. Previous research in the area of particle capture is also presented. Following the

literature review, the study methodology is presented in Section 3.0. This includes a detailed description of the experimental procedures undertaken. The results obtained in experiments are then presented in Section 4.0, followed by a discussion and analysis of these results in Section 5.0. The dissertation concludes with a discussion of the significance of the findings of this study in Section 6.0 and recommendations for future work in the research area of particle capture by aquatic vegetation in Section 7.0.

2.0 Literature Review

The capture of suspended particles by aquatic vegetation has been studied in many different systems and is a topic of interest in a variety of disciplines. Plant ecology and population dynamics of aquatic species are of interest in biology, sedimentation, erosion and contaminant fate are of interest in environmental science and hydrodynamics and wetland design are of interest in engineering. Previous work in the area of aquatic systems has investigated the importance of particle capture by aquatic vegetation in these systems, as well as describing field observations and laboratory experiments of particle capture in different systems.

2.1 Suspended particles in aquatic systems

Suspended particles exist in many different forms in natural aquatic systems, and the capture of these particles occurs by a number of different processes. For example, pollination of seagrasses relies on water currents to transport the suspended pollen particles for submarine pollination (Ackerman 2002), suspension and filter feeding aquatic organisms rely on trapping suspended food particles in both marine and freshwater environments (Ayaz & Pedley 1999), passive accumulation of larvae (for example marine bivalve larvae) is controlled entirely by flow hydrodynamics (Harvey *et al.* 1995) and the fate of heavy metals is controlled by sediment suspension and deposition as these pollutants are often sorbed to sediment particles (Palmer *et al.* 2004). These processes play an important role in the systems in which they occur, and thus an understanding of such processes improves the overall understanding of that aquatic system.

Typical particles which may be suspended in aquatic systems include sediments, biological particles, and pollutants, such as heavy metal colloids and chemicals sorbed to sediments. The size and density of suspended particles can vary considerably, and these influence the fate of particles in aquatic systems.

Suspended sediments may consist of sands, silts or clays. Under the British Standard classification system, sand particles are between 60 – 2000 μm in diameter, silt particles are between 2 and 60 μm in diameter and clay particles are less than 2 μm in diameter. Typically sediment densities are 2650 kg m^{-3} (Whitlow 2001).

Suspended biological particles include larvae and pollen particles. The pollen of seagrasses (such as eelgrass (*Zostera marina*)) is typically filamentous to improve the capture of these particles on the leaves of other plants. *Zostera marina* pollen particles have a diameter of

approximately 7.5 μm, range from 3 to 5 mm long, and have a density of 1070 kg m^{-3}. This size is also typical of other seagrass species (Ackerman 2002). Marine bivalve larvae (species such as mussels and scallops) typically have a diameter between 125 to 300 μm. These particles have a density of approximately 1400 kg m^{-3} (Harvey *et al.* 1995; Lindegarth *et al.* 1991).

2.2 Vegetation in aquatic systems

2.2.1 Types of vegetation

Various types of vegetation exist in different aquatic systems. Seagrasses, tidal marshes and wetlands are three typical aquatic systems and the vegetation that grows in each of these systems plays an important role in the functioning of that system.

Seagrasses are a functional group of about 60 species of underwater marine flowering plants that grow in fully submerged marine and estuarine soft-bottomed environments. In many regions seagrasses cover extensive areas ranging from a fraction of a hectare up to thousands of hectares (Green & Short 2003). These regions are known as seagrass meadows or seagrass beds. Seagrasses vary in morphology significantly and can have long flat bladed leaves (for example eelgrass) to small round leaves (for example the sea vine, *Halophila decipiens*) (Green & Short 2003). Such vegetation arrays are habitat to distinct marine communities, possibly because the seagrass provides shelter from disturbances and predation (Eckman 1983). How seagrasses capture suspended particles, such as pollen and larvae, has a significant impact on the functioning of the ecosystem in which they belong.

Tidal marshes exist in areas intermittently submerged by marine waters as a result of the tidal changes in water level. Marsh vegetation grows in low-energy coastal areas and in estuaries and consists of a variety of plants including grasses, rushes, reeds and sedges. Particle retention in tidal marshes leads to the accretion of sediment in these areas, which is important in controlling the stability of such areas (Leonard & Reed 2002). The processes which control accretion are thus important components moderating tidal ecosystems.

Wetlands are the transition between aquatic and terrestrial systems. They control the exchange of sediments, contaminants and nutrients and are thus very important systems. Riparian vegetation is typically dominated by sedges and rushes (Chambers *et al.* 1995). Knowledge of how wetlands function, through the uptake and biological transformation of particles, and through altering the hydrodynamic conditions, is important for understanding the wetland ecosystem and in designing wetland systems to treat water quality (Nepf 1999).

2.2.2 Typical aquatic vegetation densities

Aquatic vegetation densities vary significantly depending on the type of system in which they exist, such as marine or freshwater, and on the prevailing conditions of that system. Some typical vegetation densities are presented below for the purpose of demonstrating the range of densities present in real aquatic systems.

Shoot densities (measured in shoots m^{-2}) are commonly used as an indicator of seagrass health, and as a result, data for different species of seagrasses in a variety of locations is available. Shoot densities for *Posidonia sinuosa* in Cockburn and Warnbro Sounds, Western Australia were found to be about 2000 shoots m^{-2} in shallow water (less than 0.5 m deep), 1000 shoots m^{-2} in medium depth water (between 2.5 to 4 m deep) and 142 shoots m^{-2} in deep water (maximum depth of 10 m) (Cambridge & Hocking 1997). Summer shoot densities for *Zostera capricorni* in estuarine regions of the Coromandel Peninsula, New Zealand were found to be between 2700 to 3800 shoots m^{-2}, although winter shoot densities were lower than summer shoot densities (Turner & Schwarz 2006).

Shoot densities are less commonly measured in wetland ecosystems. One study investigating the response of wetlands to different water regimes reported *Baumea arthrophylla* shoot densities of between 100 to 1600 shoots m^{-2} (Rea & Ganf 1994). Another study summarising wetland vegetation reported the vegetation densities in terms of void spaces. The void spacing between the stems of wetland vegetation on average was stated as being over 99% at mid-height, decreasing to 90 to 95% in the litter layer. A void spacing of 99% between leaves or stems corresponds to a spacing of approximately ten stem diameters (Kadlec 1990).

2.2.3 Typical flow velocities in aquatic vegetation systems

Flow velocities are of the order of 0.1 to 10 cm s^{-1} in aquatic systems (Palmer *et al.* 2004). For example velocities of 3 to 7.4 cm s^{-1} have been observed in an emergent stand of *Spartina alterniflora* (smooth cordgrass) (Nepf 1999), velocities of up to 10 cm s^{-1} have been observed in a *Juncus roemarianus* marsh (Leonard *et al.* 1995) and velocities up to 8 cm s^{-1} were observed in a *Zostera marina* (eelgrass) canopy (Grizzle *et al.* 1996). Flow velocities in freshwater wetlands are often lower than those in tidal systems. Velocities of 0.4 to 3.3 cm s^{-1} were observed in a lake wetland ecosystem by Kadlec (1990).

2.2.4 Effects of vegetation in aquatic systems

Aquatic vegetation affects the systems in which it exists in a number of different ways. Vegetation improves water quality through the uptake of nutrients and improves water clarity

by reducing turbidity. Vegetation controls sediment deposition and retention, and geochemical exchanges at the sediment water interface as well as influencing the fate and transport of contaminant particles and contaminants sorbed to sediments. Aquatic vegetation also influences biological processes such as submarine pollination, benthic recruitment and settlement of planktonic larvae and controls the fate and transport of contaminant particles and contaminants sorbed to sediments (Leonard & Reed 2002; Palmer *et al.* 2004). The fate of suspended particles in vegetated areas is often very different to what it would be in equivalent un-vegetated areas, which is why vegetation has such an important impact in aquatic systems. Reductions in the concentration of suspended particles commonly occur in vegetated areas and these reductions have a number of causes.

Flow velocities are reduced in vegetated areas because aquatic plants convert the mean kinetic energy into turbulent kinetic energy (Nepf 1999). This reduces suspended particle concentrations as more particles sink at lower flow velocities. Resuspension is also reduced by the presence of vegetation as the flow velocities near the bed are slower, and vegetation roots help stabilise beds. Reduction in suspended particle concentrations due to a slowing of flow velocities has been well documented. It is known that seagrass canopies reduce flow and turbulence (Ackerman & Okubo 1993; Gambi *et al.* 1990) and that as a result of this, seagrasses meadows promote sedimentation (Gacia & Duarte 2001; Gacia *et al.* 1999; Terranos & Duarte 2000). Similar reduction in flow has been observed in wetlands and tidal marshes and reduction in suspended particle concentrations in these systems has been attributed to this (Knight *et al.* 1999; Leonard & Reed 2002).

Reduction in suspended particles also occurs because particles can directly bind onto the leaves and stems of aquatic plants. Particles that collide with aquatic vegetation adhere to the vegetation because a sticky periphyton layer consisting of epiphytes and organic biofilm is present. Periphyton layers typically grow on submerged surfaces, such as vegetation stems and leaves. Epiphytes excrete exopolymeric substances, which form the sticky layer facilitating particle retention (Palmer 2003). The appreciation of direct particle capture as a significant particle removal mechanism in aquatic systems is emerging in the literature. Recent evidence that seagrasses affect particle flux by directly capturing particles, as well as by inducing sedimentation has been reported (Agawin & Duarte 2002). Direct particle capture is also known to have a significant contribution to the reduction of suspended particles in tidal marshes and coastal wetland systems (Leonard *et al.* 1995; Stumpf 1983). Direct particle capture has also been observed for modelled vegetation (Harvey *et al.* 1995; Hosokawa & Horie 1992; Palmer *et al.* 2004).

In this dissertation the process by which particles are removed from the water column by directly binding to the surface of vegetation is referred to as direct particle capture, or just particle capture. The process by which particles are removed from the water column by settling to the bed is referred to as sedimentation. Both processes result in a reduction in suspended particles in aquatic systems but it is important to note that they are different processes. These processes may occur individually or simultaneously in aquatic systems to varying degrees of importance.

2.2.5 Effects of vegetation in terrestrial systems

There has also been significant research on atmospheric particles, and the removal of these through various processes, some involving terrestrial vegetation. Trees have been found to act as effective biological filters for atmospheric particles as they have a high leaf area relative to the ground they stand on (Beckett *et al.* 1998). Forest canopies are most effective at capturing particles due to their great surface roughness. Turbulence causes increased local wind speed resulting in deposition and impaction processes (Beckett *et al.* 1998). This is analogous to the submerged seagrass canopies trapping suspended particles.

2.3 Aquatic vegetation and hydrodynamics

2.3.1 Fluid mechanics of flow around a cylinder

To understand how vegetation influences the hydrodynamic conditions of aquatic systems, the fluid mechanics of flows around obstructions must be understood. Vegetation can be modelled as cylindrical stems, as typical of various types of wetland reeds and rushes in natural systems. The theory of flow around cylindrical cylinders is discussed below. Vortex shedding and wake generation are also discussed, and are of importance in particle capture as they influence the local flow field around particle collectors.

The Reynolds number (*Re*) is a dimensionless number used to describe how turbulent a flow is. The Reynolds number is the ratio of inertial forces to viscous forces and is widely used in fluid mechanics. It can be expressed in terms of the mean flow velocity (U), the dominant length scale (d) and the fluid kinematic viscosity (ν):

$$Re = \frac{Inertial\,forces}{Viscous\,forces} = \frac{Ud}{\nu} \tag{1}$$

Laminar flow occurs at low Reynolds numbers, where viscous forces are dominant, and is characterized by smooth, constant fluid motion. Turbulent flow occurs at high Reynolds numbers and is dominated by inertial forces, producing random eddies, vortices and other

flow fluctuations. There is a transition region between laminar and turbulent flow, which is described below. Flow around circular cylinders can be described analytically for limiting Reynolds numbers: low Reynolds numbers ($Re << 1$) and high Reynolds numbers ($Re >> 1$). Analytical solutions for transitional Reynolds numbers have not been found, so calculations depends on numerical and experimental solutions (Kundu 1990).

At low Reynolds numbers ($Re < 1$ for flow around cylinders) inertia forces are negligible over most of the flow field. At low Reynolds numbers the flow is laminar as shown in the first situation (A) in Figure 1 below. As Reynolds number is increased from low to transitional values the character of the flow becomes more turbulent. Vorticity is generated close to the cylinder surface as a result of the no slip boundary condition at the interface between the cylinder and fluid. As Reynolds number increases the vorticity is increasingly confined behind the cylinder as a result of advection. In ideal two dimensional flows, when the Reynolds number is greater than 4, two small standing eddies form behind the cylinder and these remain attached to the cylinder, as shown in the second situation (B) in Figure 1. The wake behind the cylinder remains laminar up until a Reynolds number of approximately 40. As Reynolds number is increased from 4 to 40 the length of the eddies behind the cylinder increase (Kundu 1990).

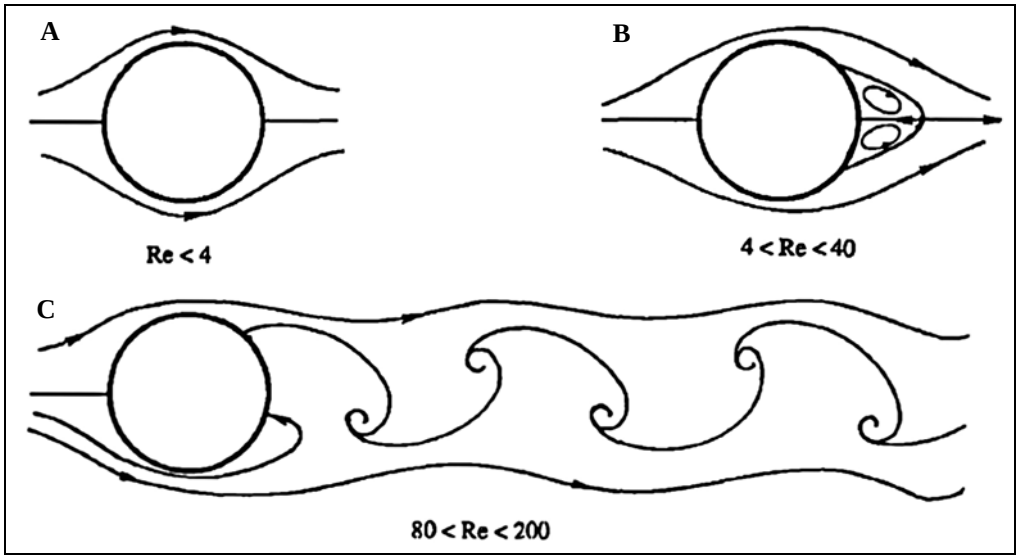

Figure 1: Vortex production behind a circular cylinder for ideal two dimensional flow (Kundu & Cohen 2002).

Beyond a Reynolds number of 40 the wake behind the cylinder becomes partially turbulent and is described as being in the transition region. When the Reynolds number is increased above 40 the wake behind the cylinder becomes unstable. It develops a slow oscillation resulting in the velocity downstream of the cylinder being periodic in both time and distance.

The amplitude of oscillations increases downstream. In ideal two dimensional flows, these oscillations form two staggered rows of vortices downstream of the cylinder with the vortices having opposite rotation directions. This staggered formation is known as a von Karman vortex street (Kundu 1990).

For a Reynolds number between 40 and 80 the von Karman vortex street does not interact with the eddies attached to the back of the cylinder. As Reynolds number is increased further, the attached eddies begin to oscillate and then these break off periodically and alternatively, making the flow near the cylinder unsteady as shown in the third situation (C) in Figure 1. This periodic shedding causes wake velocity measurements to have a dominant periodicity as a result of the passage of regular vortices. This periodicity is an important component of the flow and can be described by the Strouhal number (*St*). The Strouhal number is a dimensionless number describing oscillating flow mechanisms and can be expressed in terms of the mean flow velocity, the shedding frequency (f_s) and the cylinder diameter (d_c):

$$St = \frac{f_s d_c}{U} \tag{2}$$

When the Reynolds number is below 200 the wakes behind the cylinder are laminar but above 200 the vortices become unstable and irregular (Kundu 1990). The Strouhal number has been found to be equal to approximately 0.21 for a large range of Reynolds numbers (Kundu 1990), however a more accurate description of Strouhal number variation with Reynolds number is shown in Figure 2 (Norberg 2001).

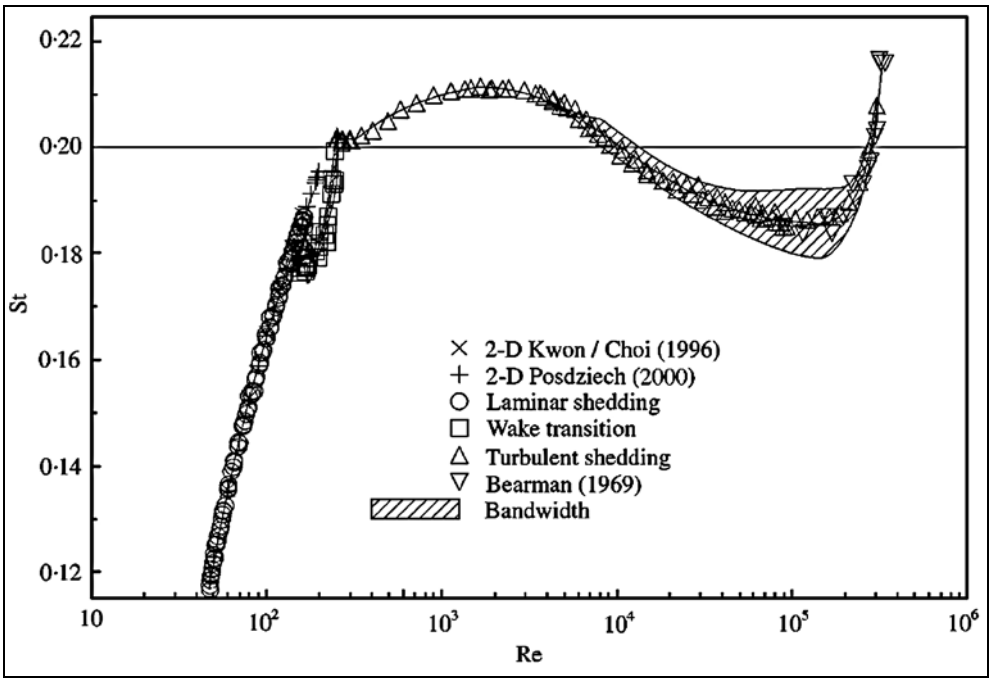

Figure 2: Strouhal number versus Reynolds number for a single circular cylinder (Norberg 2001).

At high Reynolds numbers (Re > 1000 for flow around cylinders) viscous forces are negligible except close to the fluid surface. Wake generation behind cylinders means that the flow is turbulent. Above very high Reynolds numbers (Re > 5000 for flow around cylinders) there is no periodicity in the wakes and the flow is fully turbulent (Kundu 1990).

2.3.2 Observations of hydrodynamic disturbance

Laboratory experiments and field observations have been undertaken to investigate how aquatic vegetation affects the hydrodynamics of aquatic systems. These previous investigations into the impacts of vegetation on the hydrodynamics of aquatic systems and particle capture in aquatic systems have been conducted because this knowledge is important in understanding biological and geological processes (Eckman 1983). Understanding flow characteristics is important because these are often the dominant factors shaping the ecology of aquatic ecosystems. Aquatic organisms are not only recipients of water flow, but also influence the flow, often to their advantage by increasing their protection, nourishment and reproductive success (Lopez & Garcia 1998; Paterson & Black 1999). Laboratory experiments and field observations have been undertaken to investigate how aquatic vegetation impacts the hydrodynamics of aquatic systems.

Lopez & Garcia (1998) investigated how aquatic vegetation affected open channel flow in laboratory experiments. It was found that the drag exerted by flowing water on vertical cylinders in open channels is not uniform. Rather, it reaches a maximum approximately one-third of the cylinder height above the bed. It was also observed that the presence of vegetation in open channel flow promotes a slightly more uniform distribution of suspended particles (Lopez & Garcia 1998).

Experiments conducted by Nepf (1999) found that compared to un-vegetated channels, the turbulence intensity of vegetated systems increases with the introduction of sparse vegetation, and then decreases as the stem population is increased further. Nepf (1999) also investigated the influence of vegetation on drag in aquatic systems. The drag exerted by plants in aquatic systems is important because it reduces the mean flow in vegetated areas allowing sedimentation to occur, and reduces erosion (Nepf 1999).Wake structure affects the drag coefficient (C_D) for an isolated cylinder, which is thus dependent on the Reynolds number whereas the bulk drag coefficient ($\overline{C_D}$) for an array is a function of population density (Nepf 1999).

The bulk drag coefficient is dependent on the proportion of area occupied by cylinders (p), the change in head per unit length (dh/dx) and the frontal area per unit volume ($a = nd_c$), and can be expressed as:

$$(1-p)g\frac{dh}{dx} = \frac{1}{2}\overline{C_D}aU^2 \qquad (3)$$

White & Nepf (2003) investigated the pressure distribution and vortex shedding associated with flow through arrays. It was found that the rate of entrainment into the primary wake was dependent on Reynolds number. Vortex shedding was found to begin at Reynolds numbers of 55 to 70 and the total wake volume was proportional to the cylinder density. Pressure disturbances were mainly localised near the cylinder however there was also some disturbance between laterally adjacent cylinders. This slightly elevated pressure compensated for the loss in mass flux caused by the wake, and drove flow through the gaps (White & Nepf 2003).

Field observations of how seagrass structures affect the near-bed hydrodynamic environment have been conducted by Eckman (1983). These observations found that the size, numerical density and geometry of structures determined the magnitude of the shear stress exerted on the bed, as well as other near-bed properties such as turbulence and the rate of fluid transport. It was found that in environments subjected to frequent sediment entrainment and transport, recruitment is likely to be dominated by lateral advection. The effect on flow of a single cylinder was also observed, and it was found to influence sediment deposition and entrainment, creating regions of both on an otherwise smooth bed (Eckman 1983).

A study on the hydrodynamics and sediment transport through tidal canopy marshes (Leonard & Reed 2002) found that the flow speeds in vegetated areas were much lower than those of the near by non-vegetated areas. In all of the flow systems investigated, the presence of tidal canopy marshes attenuated the flow by a similar degree: approximately 2.5 to 3 times that of the non-vegetated surroundings (Leonard & Reed 2002).

A study by Gacia *et al.* (1999), involving measuring the particle flux and sediment retention in a seagrass meadow (*Posidonia oceanica*), measured the velocity and energy profiles for vegetated and non vegetated situations. These measurements showed that in the absence of vegetation the energy dissipation was at a maximum near the bed, and the flow velocity decreased logarithmically over depth, to zero at the bed (no-slip condition). With the presence of vegetation, the peak energy dissipation occurred above the sea bed as a result of the canopy influence on water flow. Canopy flow velocities decayed downwards through the canopy, and

in general to the bed, except near the stem base, where a slight increase in velocity was observed. This lower flow velocity through vegetated areas was predicted to increase particle deposition on the sea bed and also reduce resuspension. Modelling results predicted that particle retention in vegetated beds could be up to 15 times greater than the equivalent non-vegetated beds (Gacia *et al.* 1999).

2.4 Particle capture in aquatic systems

2.4.1 Theoretical description of particle capture

Understanding particle capture in aquatic systems is an important research field and findings can be applied to improve the functionality of designed wetlands, and to improve scientific research of aquatic ecosystems. To understand how particle capture occurs in aquatic systems the different capture processes must be considered.

The particle to collector ratio (R) and the collector Reynolds number (Re_c) are two numbers used to describe the capture of suspended particles by collectors such as aquatic vegetation. Assuming that the collector is cylindrical the particle ratio can be expressed in terms of the cylinder diameter (d_c) and the particle diameter (d_p):

$$R = \frac{d_p}{d_c} \tag{4}$$

The collector Reynolds number is expressed as in Equation 1, with the relevant length scale specified as the cylinder diameter:

$$Re_c = \frac{Ud_c}{\nu} \tag{5}$$

The rate at which particles settle from the water column and the mechanisms by which particles can be deposited are also important when considering particle capture by aquatic vegetation. For particles with a density greater than the fluid that they are suspended in, settling of the particles over time will occur. The settling velocity (w_s) of particles depends on gravity (g), the particle radius (r_p), fluid density (ρ_f) and kinematic viscosity (μ) and particle specific gravity ($s = \rho_p/\rho_f$) and can be described by the Stokes settling velocity equation:

$$w_s = \frac{2}{9}\frac{r_p{}^2 g\rho_f (s-1)}{\mu} \tag{6}$$

This leads to a decrease in particle concentrations over time if particles are not resuspended by processes such as turbulence. This decrease in concentration must be accounted for when

considering the particle capture efficiency of the collectors. Palmer *et al.* (2004) showed that the particle concentration (P) at some time (t) depends on the Stokes settling velocity and the water depth (h) and can be expressed as:

$$\frac{dP}{dt} = \frac{-w_s}{h} P \tag{7}$$

Considering k as the settling rate constant such that:

$$k = \frac{w_s}{h} \tag{8}$$

Then the concentration of particles in the flume can be expressed as a function of the initial particle concentration (P_0) and time (Martin & Nokes 1988; Palmer *et al.* 2004):

$$P(t) = P_0 e^{-kt} \tag{9}$$

Once sedimentation processes have been accounted for, particle capture processes can be considered. For a particle to be trapped by a solid obtrusion, such as a plant in nature or a cylinder in a laboratory, the centre of the particle must pass within one particle radius of the solid surface (Ayaz & Pedley 1999). Then contact occurs, and the particle may be retained by adhesion or electrostatic forces (Ayaz & Pedley 1999). In the case of particle capture by aquatic vegetation, the particle is retained by adhesion to the biofilm layer. The capture of suspended particles can occurs through a number of mechanisms: direct interception, inertial impaction, gravitational deposition and diffusional deposition (Palmer *et al.* 2004).

Particle capture via direct interception is due to streamline kinematics and occurs when the streamline that a particle is travelling along comes within one particle radius of the collector. Particle capture via direct interception (η_R) can be described analytically for creeping flow where $Re_c < 1$ (Equation 10) and potential flow where $Re_c > 1000$ (Equation 11):

$$\eta_R = \frac{1}{(2 - \ln Re_c)} \left[(1+R)\ln(1+R) - \frac{R(2+R)}{2(1+R)} \right] \approx \frac{R^2}{(2 - \ln Re_c)} \tag{10}$$

$$\eta_R = 1 + R - \frac{1}{(1+R)} \approx 2R \tag{11}$$

No analytical solutions exist for intermediate Reynolds numbers which typically dominate natural systems (Palmer *et al.* 2004).

A particle travelling along a streamline that does not come within one particle radius of a collector may still be captured if the particle deviates from the streamline as a result of its inertia. In this case the particle capture mechanism is known as inertial impaction. The Stokes number (*Stk*) describes the importance of inertial forces in particle capture, where the Stokes number is a function of the collector Reynolds number, the particle to collector ratio and the specific gravity (Palmer *et al.* 2004):

$$Stk = \frac{1}{9}\mathrm{Re}_c R^2(s - 1) \tag{12}$$

It has previously been shown that for inertial impaction to be an important capture mechanism $Stk \geq 0.125$ (Palmer *et al.* 2004).

Gravitational deposition is another capture mechanism. It is the process where a particle may be captured on a collector as it settles out of the water column. Gravitational deposition will occur when the specific gravity of the particle is greater than one, and when the collector has a horizontal component. In situations where gravitational deposition is relevant, particles will fall through the water column with a velocity as described in Equation 6. Gravitational deposition is not the same as sedimentation as gravitational deposition involves settling of particles onto vegetation, whereas sedimentation involves particles settling onto the bed.

Diffusional deposition occurs when random motion (such as Brownian motion or turbulence) of a particle results in its deposition on a collector. Diffusional deposition is more significant at lower Reynolds numbers, when the flow is creeping, as direct interception is less significant under these conditions, and for small particles, when inertial impaction is less significant (Li & Park 1996). Diffusional deposition (η_D) for creeping flow can be expressed as (Palmer *et al.* 2004):

$$\eta_D = \frac{1.17\pi F^{2/3}}{ud_c}\left[\frac{Re_c \nu}{2(2 - \ln Re_c)}\right]^{1/3} \tag{13}$$

Where the particle diffusivity (F) is described in terms of the Boltzmann constant (κ) and the absolute temperature (T_K) (Palmer *et al.* 2004):

$$F = \frac{\kappa T_K}{3\pi\mu d_p} \tag{14}$$

Particle capture efficiency (η) describes both the rate at which suspended particles are removed from the water column and the rate at which particles collect on a surface. The

particle capture efficiency of a cylindrical collector is defined as the width of upstream particles (b) that is ultimately captured on the frontal area of the collector (which is the cylinder diameter d_c) as shown below in Figure 3 (Palmer *et al.* 2004). Based on this definition, particle capture efficiency is defined as (Palmer *et al.* 2004):

$$\eta = \frac{b}{d_c} \tag{15}$$

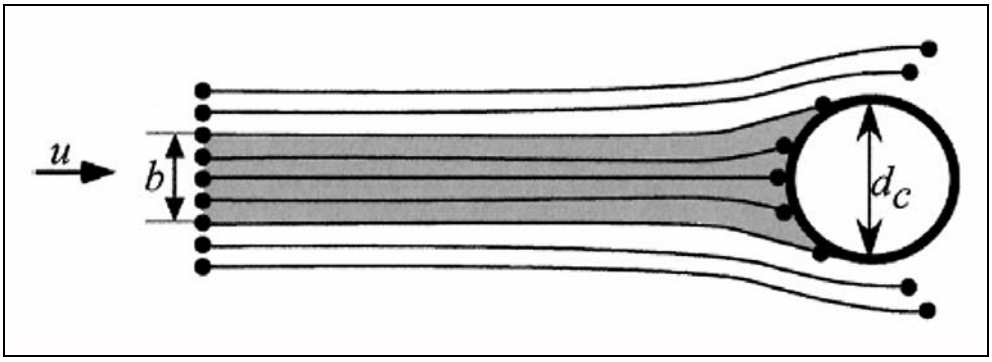

Figure 3: Definition of capture efficiency for a cylindrical collector (Palmer *et al.* 2004).

Various parameters affect particle capture efficiency in practice. Considering the number of particles N_c collected on the surface of a collector of length l_c over a duration t, Palmer *et al.* (2004) showed that:

$$\frac{dN_c}{dt} = \eta P U d_c l_c \tag{16}$$

Combining this with Equation 9 gives an equation which can be used to calculate the particle capture efficiency of collectors in aquatic systems from parameters that can be measured:

$$\eta = \frac{N_c k}{P_0 U d_c l_c \left(1 - e^{-kt}\right)} \tag{17}$$

2.4.2 Field observations of particle capture

Field observations of reduction in suspended particles attributed to direct particle capture have been made. Examples of observations demonstrating the importance of this mechanism for removing suspended particles from the water column are included below.

Research by Stumpf (1983), motivated by the sequestering of mud by seagrasses found that the sediment adhering to the leaves and stems of seagrasses can make up a significant proportion of the total amount of mud sequestered. Sediment on the stems and leaves of seagrasses above 3 cm from the seabed was collected, and accounted for 50% of the suspended sediment lost during a spring tide (Stumpf 1983).

Adhesion of particles to the leaves and stems of marsh plants (creating a thin layer of sediment over these structures) is also thought to contribute to the overall sedimentation of tidal marshes (Leonard *et al.* 1995). Field observations by Leonard *et al.* (1995) found that up to 10% of the sediment accreted in tidal marshes is due to adhesion on vegetation.

2.5 Laboratory modelling of particle capture

As well as field observations of particle capture, there has been significant laboratory work modelling particle capture in different situations. Laboratory experiments are important in increasing the understanding of environmental processes because they allow investigation of specific processes under controlled situations and are repeatable whilst also obtaining real data.

Laboratory experiments conducted by Elliot (2000) suggested that particle settling in blade type vegetation can enhance sediment removal efficiency. These experiments also showed that in some situations, vegetation may result in sediment destabilisation, as a result of the increased turbulence and local flow acceleration around the base of vegetation. In these experiments vegetation was not made sticky, thus re-entrainment from vegetation surfaces was possible. If vegetation was made sticky, for example by coating with a layer of grease, re-entrainment would be lower (Elliott 2000).

Palmer *et al.* (2004) conducted laboratory experiments similar to those conducted in this study. Simple cylindrical collectors were used, as these approximated a variety of natural collectors including vegetation (reeds, benthic plants and algae) as well as suspension feeding structures (cilia, bristles and tube-feet) (Palmer *et al.* 2004). This study found that the relevant Reynolds length scale in the flume set-up was the cylinder diameter, and collector Reynolds numbers between 1 and 1000 were investigated (Palmer *et al.* 2004).

Experiments conducted by Harvey *et al.* (1995) investigating the recruitment of marine bivalve larvae on aquatic structures simulating seagrasses found that some larvae preferentially settled on filamentous substrata. This is possibly a result of the interactions between flow in the benthic boundary, as well as the three-dimensional heterogeneity of the filamentous structures (Harvey *et al.* 1995). The plant structures in this experiment affected turbulence in two ways. Turbulence was suppressed entering the vegetation field, and also generated as a result of the vortices in branch wakes. At low Reynolds numbers ($Re_c << 1$) the flow dynamics around a cylinder were smooth and vortex-free. At intermediate Reynolds numbers ($10 < Re_c < 40$) attached vortices form on the downstream side of the cylinder,

allowing particles to be captured on areas of the downstream face previously inaccessible to capture. At higher Reynolds numbers, (Re_c < 40) the downstream side vortices are periodically shed on each side of the wake. This phenomena was believed to account for the lower capture efficiency at higher Reynolds numbers than at intermediate Reynolds numbers (Harvey *et al.* 1995).

2.6 Study motivation

Understanding the capture of suspended particles by aquatic vegetation is important as it has implications for the understanding of population dynamics of a variety of aquatic organisms as well as in the development of engineering tools to assess environmental impacts, estimate contaminant and sediment transport processes and evaluate design options for the management of wetlands.

Typical collector Reynolds numbers in aquatic systems can be determined from Equation 5. Based on the observed range of velocities (O (0.1 to 10 cm s^{-1})) in aquatic systems (Section 2.2.3), for a typical plant stem diameter of 0.5 to 1 cm (Chambers *et al.* 1995), the collector Reynolds number in aquatic systems is found to range from 5 to 1000, which is within the transitional range of Reynolds numbers. The dominance of intermediate Reynolds numbers (O (1 to 1000)) has also been reported in the literature (Palmer *et al.* 2004; Nepf 1999). Such flows cannot be described analytically as discussed in Section 2.3.1. Thus experiments and numerical modelling are required to understand the flow in such systems and account for field observations of flows and particle capture in these systems.

The reduction of suspended particles in seagrass meadows has been attributed to both sedimentation and direct particle capture. For example Gacia *et al.* (1999) investigated the velocity profiles in seagrass canopies and attributed the reduction of suspended particles in vegetated areas to a reduction in flow velocities due to the presence of vegetation, whilst Stumpf (1983) observed that sediments can adhere to seagrasses, and that this accounted for half of the reduction of suspended particles that occurred in a seagrass meadow. To predict what processes are likely to control the reduction of suspended particles in different seagrass environments, a better understanding of these processes is required.

As with seagrass meadows, different processes have been identified as causing accretion of sediments in tidal marshes. These different processes have been quantitatively investigated in Florida, USA, by Leonard *et al.* (1995) and by Leonard & Reed (2002). An improved understanding of the relative magnitude of adhesion to vegetation as a sediment reduction

process and what factors influence this process would allow the results from previous studies to be used to predict what factors cause reduction of suspended particles in different marsh and estuarine environments.

The rehabilitation of riparian areas and wetlands, as well as the construction of artificial wetlands provides the opportunity to design these areas to reduce the particles suspended in water flowing through the areas above what may naturally occur. An understanding of what sorts of vegetation types and densities lead to the greatest reduction in suspended particles whilst also being economically viable would be advantageous in wetland type projects.

Previous laboratory experiments focussing on how particles suspended in the water column can be captured on aquatic vegetation have been important in improving the understanding of these processes in nature; however these investigations have had limitations. For example, Elliot (2000) observed re-entrainment of particles captured on aquatic vegetation because modelled vegetation was not made sticky to simulate the biofilm layer typically coating aquatic vegetation. Palmer *et al.* (2004) investigated the capture efficiency of a single cylinder, but arrays of vegetation dominate aquatic systems, and turbulent processes that exist in natural systems would not have been present in these experiments, thus limiting the applicability of the determined capture efficiencies to real systems. The results from these experiments form a basis to understand how aquatic vegetation captures particles suspended in the water column, but more realistic experiments would further increase this understanding.

This study will build on the findings of previous laboratory experiments, in particular those conducted by Palmer *et al.* (2004), to investigate particle capture under more realistic conditions, and in doing so, potentially improve the understanding of particle capture in aquatic systems. This is important because a better understanding of vegetation in aquatic systems could lead to better conservation and management of these important systems.

3.0 Methodology

Laboratory experiments were conducted to investigate the efficiency of particle capture by aquatic vegetation and what factors influence this efficiency under controlled conditions. These experiments were conducted in an open channel flume, using wooden dowel rods to simulate vegetation and white synthetic particles as the suspended solids. A total of 18 experiments were conducted with three different density arrays and six different flow velocities, where flow velocities were measured with an acoustic Doppler velocimeter (ADV). Black test cylinders were coated in grease and placed near the end of the dowel array for specific time intervals. The particles captured on black test cylinders were photographed and counted, and the distribution of these particles observed. The particle capture efficiency for the different experiments was then calculated.

3.1 Experimental design

3.1.1 Flume details

An open channel flume of length 400 cm, width 25 cm and height 24 cm was used in experiments. The flume base was sloped at 1:340 to the horizontal, so the base at the downstream end was 1.2 cm below the base at the upstream end. The flume was filled with approximately 120 L of water. This gave a downstream still water depth of approximately 12 cm. A recirculating pool pump (Davey Power Ace CR 300, model number PACR300-0) was used to provide the desired flow rates. Flow rates less than 100 L min^{-1} were estimated with a flow meter (Burkert Easy Flow, SE35/8035).

At the upstream end of the flume two plastic screens 1.5 cm thick, with holes of diameter 1.3 cm, spaced on average 7 cm apart, were placed between the pump inlet and the rest of the flume, creating two stilling basins to distribute the flow evenly. After these stilling basins, 55.5 cm of honeycomb (supplied by Plascore, Inc.) with a cell size of 1.3 cm was positioned in the flume to straighten flow. The 199 cm of pegboard positioned on the floor of the flume began 148.5 cm from the flume inlet. The dowel cylinders were arranged haphazardly in the pegboard. The black test cylinders were located 18 cm from the downstream end of the pegboard. The ADV probe was positioned downstream of the test cylinders, but still within the dowel array. This set-up is shown below in Figure 4 and Figure 5. Figure 6 shows a photograph of the experimental set-up. The flume was covered when not in use to prevent dust and other debris falling into it.

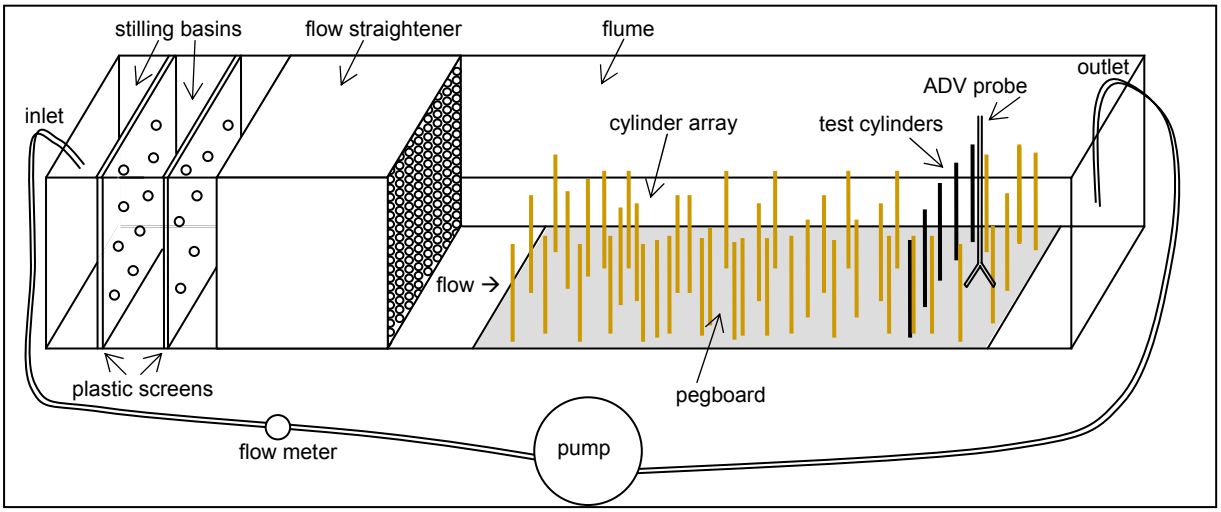

Figure 4: Experimental set-up (not to scale). Water is pumped in at the inlet, flows through the stilling basins and then through a honeycomb flow straightener to ensure that the flow entering the cylinder array is straight and evenly distributed. Cylinders are held in place in pegboard. The pump recirculates water to maintain a constant number of particles.

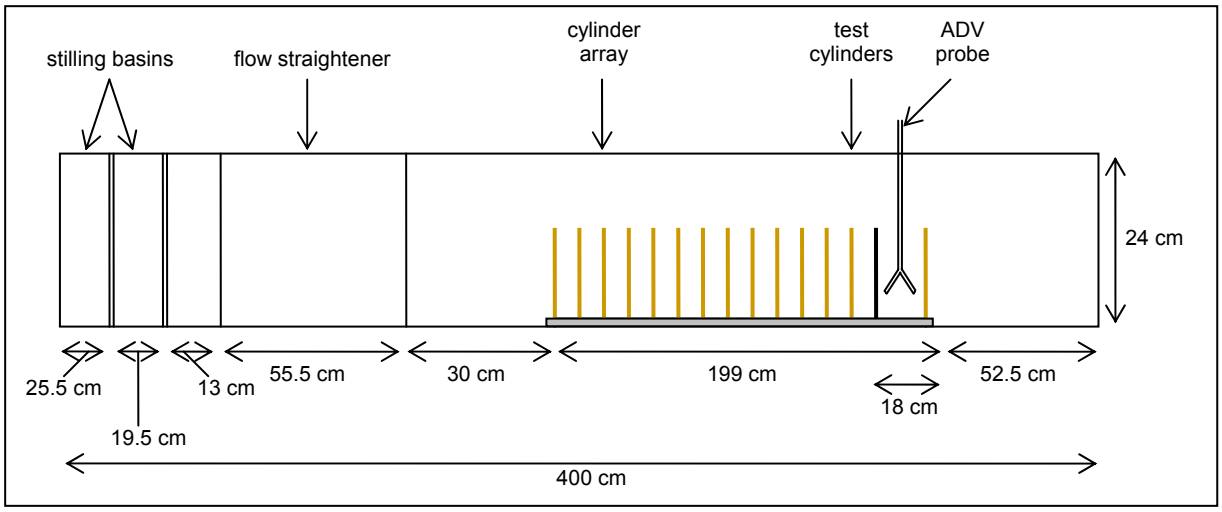

Figure 5: Measurements of experimental set-up.

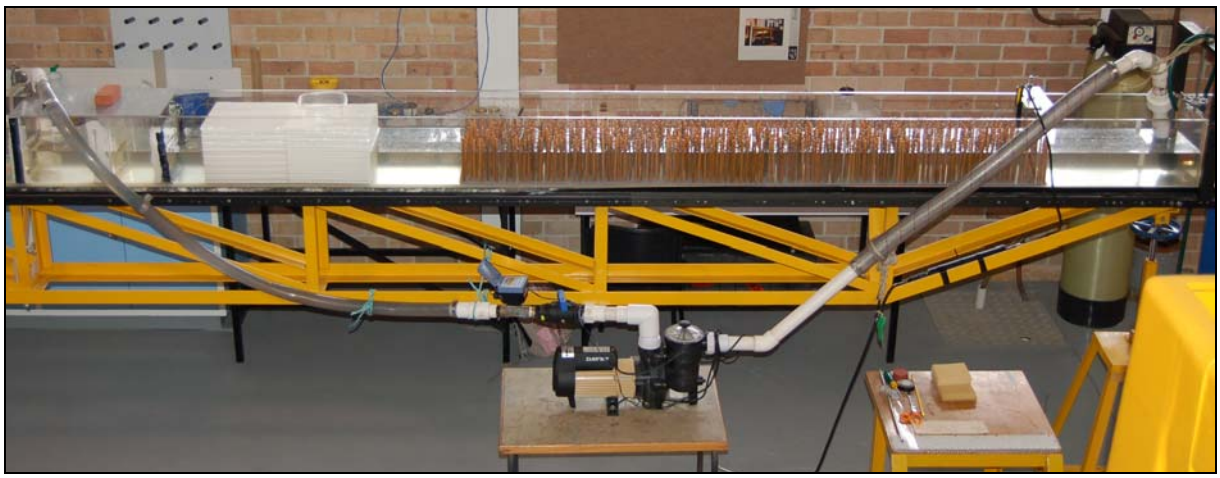

Figure 6: Photograph of the experimental set-up for the medium density array.

3.1.2 Cylinders and array densities

Dowel rods of diameter 0.63 cm and length 16 cm were used to simulate emergent aquatic vegetation in experiments. This diameter approximates the diameter of a number of different aquatic collectors such as the stalks of marsh grass (Eckman 1983) or reed stems (Elliott 2000). Pegboard with ordered holes of 0.65 cm was used to hold the dowel in place. The dowel was left in the pegboard, partially submerged for at least a day prior to experiments to allow the dowel to absorb water and expand, resulting in a tight fit in the pegboard. Three different densities of dowel rods were used: low density, medium density and high density. Details of these densities are shown in Table 1.

Table 1: Array densities tested in experiments.

Array density	Number of rods in pegboard	Density (rods m^{-2})	Percentage of area (%)
Low density	500	1013	3.16
Medium density	1000	2026	6.32
High density	2000	4053	12.63

These array densities were chosen based on natural stem densities found in marine and freshwater environments (Section 2.2.2). For each array density, the number of rods required and the length of pegboard were divided into four parts. Equal numbers of rods were then placed in a haphazard manner to each sub-section. This gave an even distribution of dowel rods over the whole pegboard section.

Black Ertacetal rods (supplied by DOTMAR Engineering Plastic Products, product number ACRB0060) of diameter 0.6 cm and length 16 cm were used as the test cylinders. These rods were used instead of dowel because they had a smoother surface and photographed more clearly than dowel which had been painted black. Each test cylinder was marked with two silver rings around the circumference, 3 cm and 7 cm above the base of the cylinder. The test region was the 4 cm between these two rings. Three marks were made above the top ring, 120° apart. This divided the test region into three sections: the front face, back left face and back right face. The test cylinders were coated in a liberal amount of grease (Comma Multipurpose Grease, lithium-based NLGI No. 2 grease), which was then smoothed by sliding a washer with inner diameter of 0.63 cm over the cylinders. This gave an even coating of grease over the cylinder, was repeatable and increased the diameter of the test cylinders to the same as that of the dowel.

Five test cylinders were used in each experiment. These were placed evenly across the width of the flume, 18 cm from the end of the dowel array. The same cylinder positions were used in all experiments. In each experiment the five test cylinders were placed in the flume one

after another, and then removed in the same order after ten minutes. The test cylinders were removed at the same rate they were inserted, ensuring that all cylinders remained in the flume for the same time interval. After removal the test cylinders were stored upright to maintain the grease surface and particle distribution for future reference.

3.1.3 Particles

Pliolite particles (Vinyltoluene-acrylate copolymer, supplied by The Goodyear Tyre & Rubber Company) were used as the suspended solids in the capture experiments. These particles were used because they are white and easily visible against the black test cylinders, and because their specific gravity of 1.03 is not much denser than water. The particle size range used in experiments was chosen by calculating the Stokes settling velocity (Equation 6) for different particle sizes and assessing the visibility of the particles in trial photographs. The 212 to 250 μm size range had minimal settling of particles whilst allowing suitable visibility of particles in photographs and so was determined to be the most appropriate size range for use in experiments. Particles were sieved using standard British sieves stacked in a mechanical shaker. The 212 to 300 μm size range was collected and then sieved through 250 μm mesh (supplied by Sefar Filter Specialists Pty Ltd). This gave a particle size range of 212 to 250 μm as desired. Particles were assumed to be spherical and sizes evenly distributed within this size range. Thus, the average particle diameter was taken as 231 μm. Natural particles of this size include medium sand grains and marine bivalve larvae (Section 2.1).

A trial run found that sedimentation of particles in tap water was significant. To minimise the settling of particles during experiments salt was added to the flume to increase the density of the water: 3 kg of salt was added to the 120 L in the flume, giving a solution with a salinity of approximately 26 g L^{-1}, and a specific gravity of 1.025. The water in the flume was mixed by hand immediately before each experiment to resuspend any particles that had previously settled to the bottom of the flume.

An accurate mass of pliolite particles (14.0011 g) was weighed for use in experiments (Electronic Balance ER-180A, A&D Company Ltd). The particles were mixed with a surfactant solution to prevent clumping (Photo-Flo 200 Solution, Kodak Professional) before being added to the water in the flume. These particles were recirculated and it was assumed that the number of particles removed from the system during experiments (O (1000 particles)) was insignificant compared to the total number of particles present (O (1 x 10^6 particles)).

The number concentration of particles in the flume was estimated by calculating the approximate volume (V_p) and mass (m_p) of one particle:

$$V_p = (\pi/6)\, d_p^3$$
$$= 6.454 \times 10^{-12}\ \text{m}^3$$
$$m_p = V_p/\rho_p$$
$$= 6.648 \times 10^{-6}\ \text{g}$$

Then the total number of particles added to the flume (N_p) was calculated:

$$N_p = m_{total}/m_p$$
$$= 2.106 \times 10^6 \text{ particles}$$

From this, the number concentration of particles in the water (P_0) was calculated:

$$P_0 = N_p/V_f$$
$$= 1.755 \times 10^7 \text{ particles m}^{-3}$$

3.1.4 ADV

The acoustic Doppler velocimeter (ADV) was used in experiments to measure the flow velocity and monitor the particle concentration. The ADV probe used was a SonTek Doppler current meter (microADV). The ADV operates by using the Doppler shift to detect particle motion in water. The ADV probe transmits a sound pulse at a known frequency and measures the reflection from particulate matter in water. The signal strength, or amplitude, of ADV measurements is related logarithmically to the particle concentration in the sample fluid. For the experiments conducted, velocities in the x, y and z-directions as well as the amplitude of measurements were of interest.

In experiments the ADV settings used were a frequency of 25 Hz and a salinity of 26 g L^{-1}. The temperature of the water in the flume was measured to the nearest 0.5° at the beginning of each experiment and the ADV setting adjusted as required. The maximum flow velocity range was set at 10 cm s^{-1} for the lowest flow rate tested for each density array, and 30 cm s^{-1} for all other flow rates. These ranges encompassed the maximum velocities that were present during experiments, whilst minimising loss in instrument resolution.

3.2 Obtaining results

3.2.1 Calibrating the ADV

To calculate the particle capture efficiency of the test cylinders, the particle concentration in the water must be known. Although adding salt to the water in the experiments reduced the settling rate of the Pliolite particles, sedimentation still occurred to a small extent, as can be

seen in Figure 7. Hence, although a known mass of particles was added to a known volume of water, to determine the concentration of suspended particles more accurately, measurements throughout each experiment were required.

The ADV was used to measure the concentration of particles suspended during experiments. Calibration of the ADV was required to convert the amplitude measurements to a particle concentration. Two calibrations were conducted: an in-flume calibration conducted with the medium density array set-up and a bucket calibration conducted on a smaller scale.

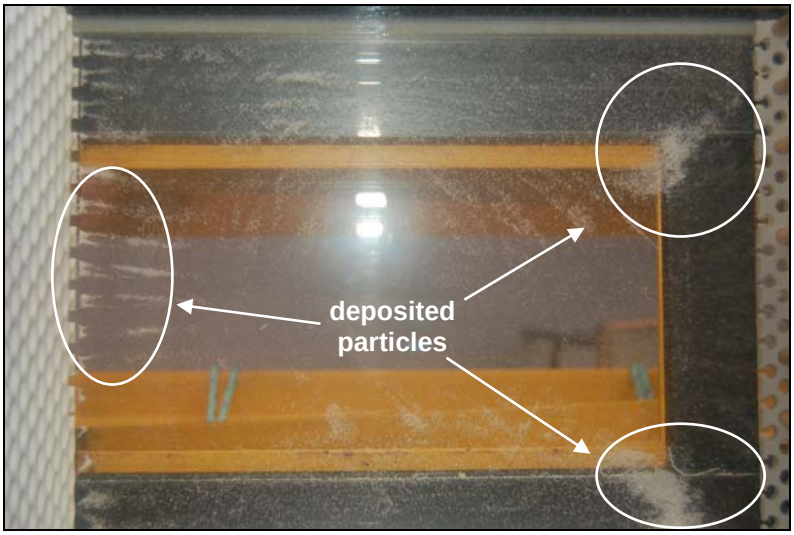

Figure 7: Photograph taken from above, showing the settled particles on the bottom of the flume after a ten minute run. The photograph was taken above a section of the flume between the honeycomb flow straighteners (left side) and dowel array (right side).

The mass of particles used in experiments (~ 14.0 g) was added incrementally to the flume and the ADV run between increments to measure the signal amplitude for different particle concentrations. Initially a mass of 8.0 g was added to the flume, and increments of 0.5 g and then 1.0 g added. The mass of particles in the flume during calibration were thus 8.0 g, 8.5 g, 9.0 g, 9.5 g, 10.0 g, 11.0 g, 12.0 g, 13.0 g and 14.0 g. After adding particles, the water in the flume was mixed thoroughly by hand to suspend any settled particles and amplitude measurements recorded for an intermediate flow velocity (approximately 6 cm s^{-1}). Three ADV records for each particle concentration were taken and the first minute of measurements used to determine the average amplitude corresponding to each particle mass concentration.

Due to some adhesion of particles to dowel rods and sedimentation of particles during the in-flume calibration runs, a bucket calibration was also conducted to provide an alternate calibration curve. A salt solution (26 g L^{-1}) was made up for this calibration and a known mass of particles (0.7782 g) was added to 6 L of this solution. The amplitude was recorded

with the ADV for a twenty minute period, during which the bucket was stirred every two minutes. Dilutions of this solution were made to volumes of 7 L, 8 L, 9 L and 10 L, and the same recording procedure conducted. The concentrations tested in the bucket calibration corresponded to a mass of particles in the flume of 9.3 g, 10.4 g, 11.7 g, 13.3 g and 15.6 g.

Unfortunately the ADV amplitude results (Section 4.1) suggest that there are factors other than just suspended particle concentration affecting the ADV amplitude measurements. This prohibited the use of the ADV amplitude measurements to determine particle concentration for each experiment. Thus the initial particle concentration in the flume was assumed to be constant for all experiments, and was used in particle capture efficiency calculations. Errors associated with this assumption are discussed in Section 5.6.1.

3.2.2 Measuring flow velocity

To test particle capture under reasonable natural flow regimes, various flow velocities were investigated. Six flow velocities (Table 2) were tested for each array density. Due to the limited accuracy of the pump control it was possible only to measure similar velocities for each different density array. The collector Reynolds number (Table 3) changed between experiments due to changes in flow velocity only. Reynolds numbers between 70 and 660 were investigated.

Table 2: Flow velocities (cm s^{-1}) tested in experiments.

Experiment	Low Density Array	Medium Density Array	High Density Array
Run 1 (cm s^{-1})	1.12	1.10	1.79
Run 2 (cm s^{-1})	2.86	2.86	2.35
Run 3 (cm s^{-1})	3.97	4.39	3.65
Run 4 (cm s^{-1})	6.42	5.43	5.63
Run 5 (cm s^{-1})	7.70	6.83	8.71
Run 6 (cm s^{-1})	9.09	10.18	9.92

Table 3: Collector Reynolds numbers tested in experiments.

Experiment	Low Density Array	Medium Density Array	High Density Array
Run 1	72.34	71.02	115.88
Run 2	185.67	184.54	152.07
Run 3	256.65	283.29	235.98
Run 4	414.25	350.84	363.78
Run 5	497.03	440.80	562.42
Run 6	586.90	657.27	640.82

3.2.3 Measuring water level

With the different flow velocities and array densities, different water depths were present. The water levels at the beginning and the end of the array were measured during each experiment. The water depth was recorded to allow the drop in head across the array to be determined and from this, the bulk drag coefficient ($\overline{C_D}$) for each array density to be calculated.

3.2.4 Measuring particle capture

To count the number of particles collected during the experiments digital photographs were taken (Figure 8). Each section of the test region (front face, back left face and back right face) on each cylinder was photographed using a Nikon D50 single-lens reflex digital camera. Cylinders were placed beneath a fluorescent light to take photographs as this was found to minimise reflection.

Figure 8: Sample photograph of the front face of a test cylinder taken to enable particle counting.

Each photograph was rotated and cropped in Adobe Photoshop so that the image could then be loaded directly by MATLAB. It was planned that the number of particles in each photograph would be counted using MATLAB (see Appendix A for details). This was found to be inaccurate as imperfections in photographs, edge effects and clumping of particles resulted in count errors. These problems could not be resolved by improving the MATLAB code, so particles were counted manually. A particle counting template (Figure 9) was used during counting to ensure consistency between photographs. The number of pixels that the

smallest (212 µm) and largest (250 µm) particles were in photographs were calculated. Particles of this size were marked on the template photograph. The required level of whiteness for a mark on the photograph to be classified as a particle rather then an imperfection in the grease or a reflection was determined by comparing the template photograph with the actual test cylinder. Particles of appropriate whiteness were also marked on the template photograph. This template was referred to during particle counting so that the particles counted in all photographs were consistent with those classified as particles on the counting template.

Figure 9: Counting template used to ensure consistency during manual counting of particles. The marks circled in yellow were counted as particles, the mark circled in magenta was counted as two particles and the marks circled in red were not counted as particles. The marks pointed to by green arrows were part of the silver ring used to mark the test region.

3.2.5 Observing resuspension

It was assumed that all particles captured on the test cylinders remained on these cylinders during experiments. To test this assumption a greased test cylinder with a known number of particles was placed in a flume containing clean, fresh water. This cylinder was subjected to a flow velocity of approximately 8 cm s^{-1} for ten minutes. The cylinder was then removed and

the number of particles remaining on the surface counted. The cylinder was then replaced in the flume and rotated 90° from its original position, and left for a further five minutes, after which the number of particles were again recounted.

3.3 Analysing results

3.3.1 Spectral analysis of velocity records

Spectral analysis of the velocity measurements recorded during each experiment was undertaken to determine if a dominant frequency existed in the data. The ADV records for each experiment contained x-direction, y-direction and z-direction velocity data. Spectral analysis was conducted for the velocity directions as outlined in Table 4. Spectral peaks were most pronounced in the y-velocity, so results from the y-velocity spectral analysis were used in further analysis. Spectral analysis of the x and z-velocity data was conducted for some of the runs for comparison to the y-velocity spectral plots.

Table 4: Velocity time series data for which spectral analysis was conducted.

Array Density	Run	Velocity Component(s) Analysed
Low	1, 6	x, y, z
	2, 3, 4, 5	y
Medium	1, 6	x, y, z
	2, 3, 4, 5	y
High	1, 6	x, y, z
	2, 3, 4, 5	y

3.3.2 Calculating capture efficiencies

Capture efficiencies for each experiment were calculated based on the equations detailed by Palmer *et al.* (2004). The reduction in particle concentration during and between experiments was ignored in calculations. This assumption was required because as discussed further in Section 4.1.3, the particle concentration could not be calculated based on ADV amplitude measurements. Errors associated with this assumption are discussed in Section 5.6.1. From this assumption, Equation 17 was simplified to:

$$\eta = \frac{N_c}{P_0 U d_c l_c t} \tag{18}$$

The experimental capture efficiencies were thus calculated and were dependent on the number of particles collected, the concentration of particles in suspension, the flow velocity, the collector diameter, the length of the collector over which particles were collected and the collection time.

3.3.3 Analysing particle deposition patterns

The patterns in particle deposition on cylinder faces were analysed using MATLAB. This required the number of particles on each cylinder to be counted in MATLAB. As mentioned previously in Section 3.2.4, this method did not count particles as accurately as they could be counted manually, over counting the number of particles by on average 7.5% compared to manual counts, however for the purpose of analysing spatial deposition patterns only, this was decided to be acceptable in most cases. Errors were determined to be unacceptable in cases where few particles (approximately less than ten particles) were captured per face because in these cases, due to the way particles were distinguished from the background in MATLAB, imperfections were amplified and counted as particles. Particle counts in such cases were approximately an order of magnitude higher than they should have been. Enough particles (to allow acceptable counting in MATLAB) were captured on the front faces of the test cylinders for all of the low and medium density array experiments, so the deposition patterns on these were analysed. Enough particles were also captured on the back faces of the test cylinders for the higher three Reynolds numbers for the low and medium density array experiments were also analysed.

To analyse the particle deposition patterns, the vertical distribution of the particles on the cylinder faces was investigated. Cropped cylinder photographs were divided up into 32 vertical sections and a histogram of the number of particles in each section created. Spectral analysis of the histogram was conducted to detect any patterns in the spacings between particles. The MATLAB code used for this analysis is included in Appendix A.

4.0 Results

Calibration results, velocity measurements and variations, particle capture and capture efficiency results obtained from experiments are presented in this section. These results are then discussed in Section 5.0.

4.1 ADV calibration and amplitude results

The results from the two different calibrations and the particle concentration used in capture efficiency calculations are presented below. Tables of calibration data are included in Appendix B.

4.1.1 In-flume calibration

The average ADV amplitude measurements from the in-flume calibration are graphed in Figure 10. The amplitude increases with an increase in the particle concentration and the gradient of the linear regression line is 0.1354.

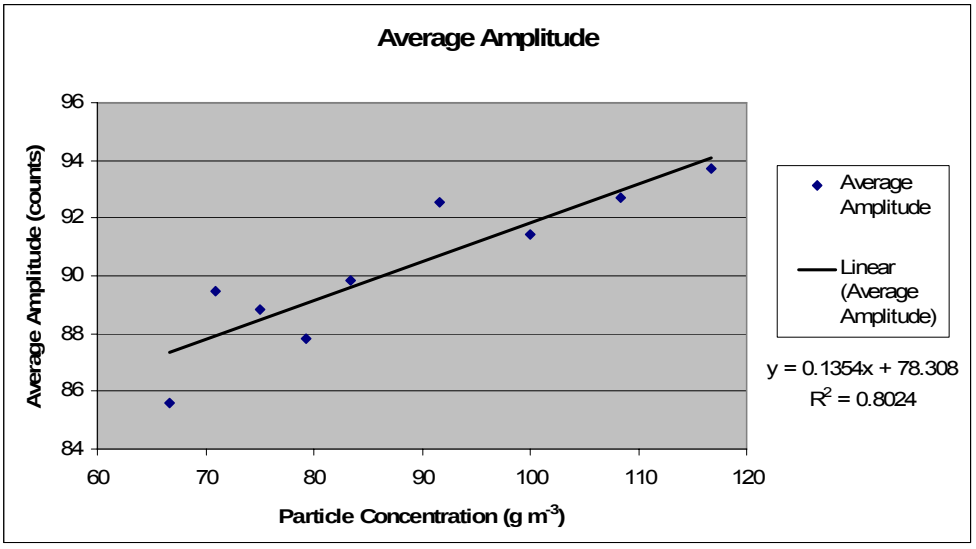

Figure 10: Average ADV amplitude measurements for the in-flume calibration.

4.1.2 Bucket calibration

The ADV amplitude measurements for the bucket calibration are graphed in Figure 11. As with the in-flume calibration the amplitude increases with an increase in particle concentration. In this calibration the dependence of amplitude on particle concentration was not as large, demonstrated by the small gradient of the linear regression line: 0.0309.

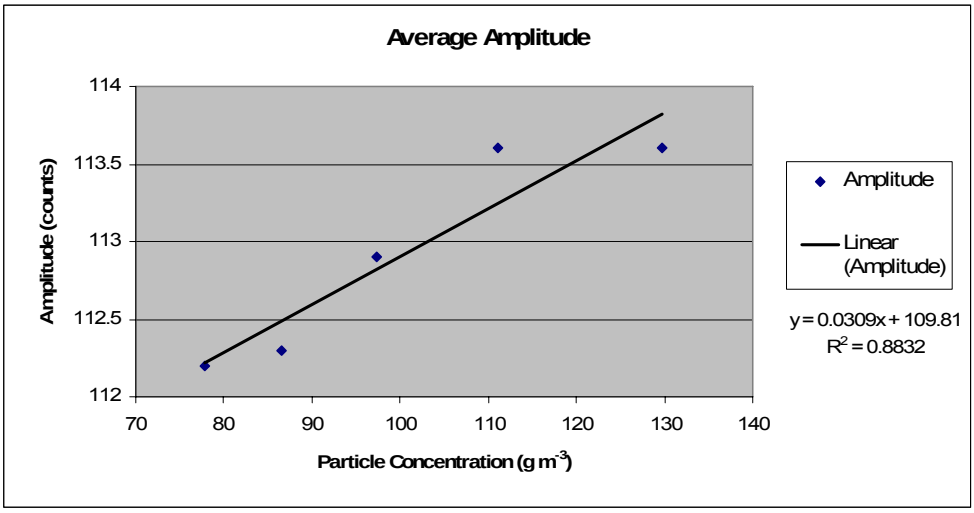

Figure 11: Average ADV amplitude measurements for the bucket calibration.

4.1.3 Experimental amplitude measurements

The amplitude measurements from the 18 particle capture experiments conducted range between 77 and 94 counts. As can be seen in Figure 12, there was noticeable variation in the measured amplitudes for the medium and high density array experiments.

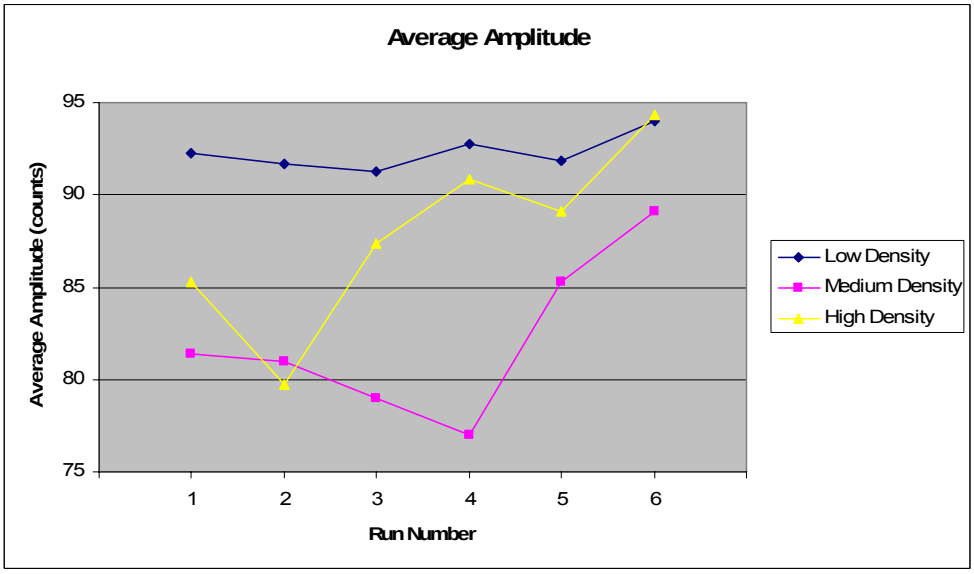

Figure 12: Average ADV amplitude measurements for the particle capture experiments.

Based on the in-flume calibration the experimental amplitude range corresponds to a particle concentration range of approximately -10 to 116 g m^{-3}. Based on the bucket calibration the experimental amplitude range corresponds to a particle concentration range of approximately -1062 to -512 g m^{-3}. A negative particle concentration is not possible, indicating that factors other than particle concentration also influence the amplitude of ADV measurements. As a result of this, the ADV amplitude measurements were not used to determine particle concentrations.

4.2 ADV velocity results

The velocity measurements made with the ADV during each experiment are presented in this section. Velocity measurements in the x-direction (direction of flow), y-direction (lateral) and z-direction (vertical) were recorded. The averages and standard deviations for each experiment as well as velocity time series presented. A table of average ADV measurements is included in Appendix B.

4.2.1 Average velocity measurements

The x-velocities were controlled in experiments by controlling the flow rate. These velocities increased approximately linearly between experiments and ranged between 1.1 and 10.2 cm s^{-1} to give the desired collector Reynolds numbers. Figure 13 shows the ADV measured x-velocity for each experiment. It can be seen in this figure that similar x-velocities were tested for each density array. The collector Reynolds numbers were calculated from the x-velocities shown in Figure 13 and these used as the dependent variable in further plots.

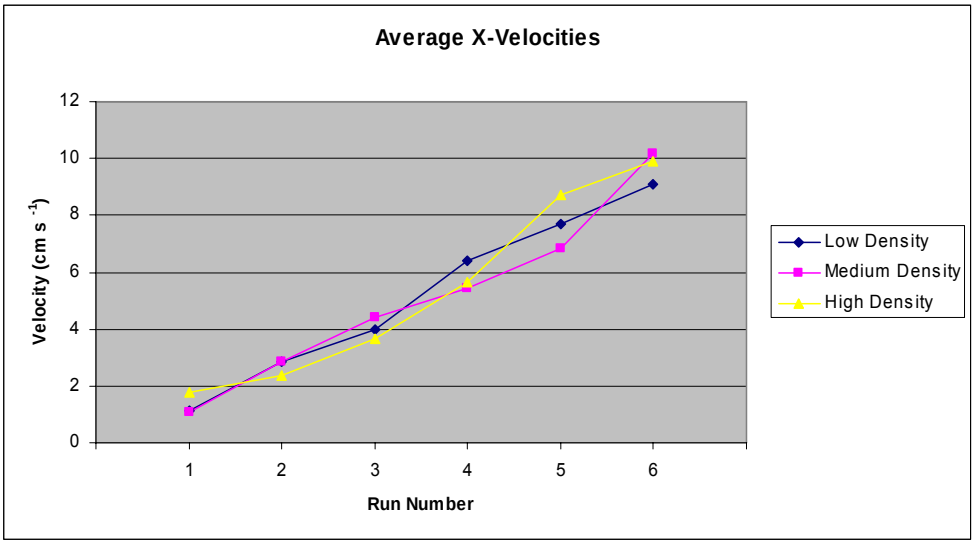

Figure 13: Average ADV x-velocity measurements for particle capture experiments.

Unlike the x-velocities present in the experiments, the y and z-velocities did not have a fixed directionality. For this reason the average velocities were graphed (Figure 14 and Figure 16), and the average of the absolute value of velocities were also graphed (Figure 15 and Figure 17). From these figures, it is evident that the magnitude of y and z-velocities increased with run number.

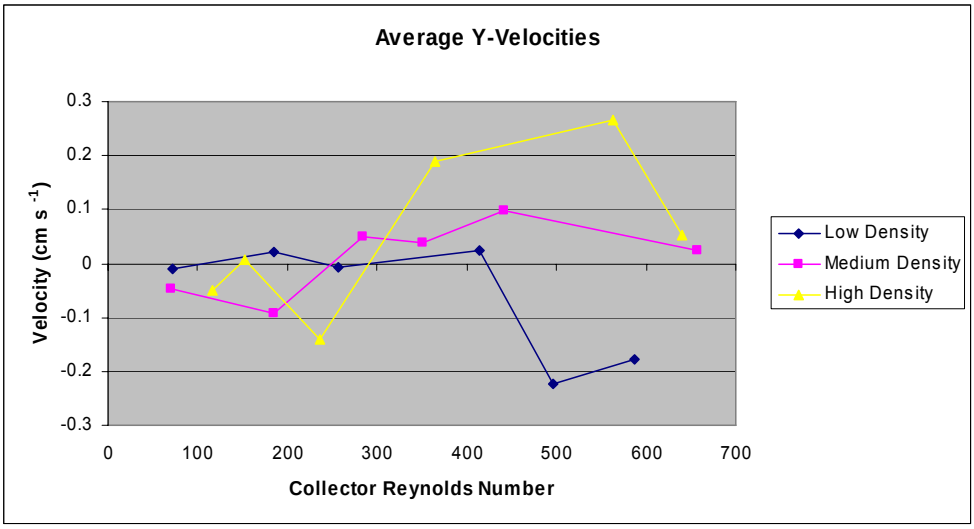

Figure 14: Average ADV y-velocity measurements for particle capture experiments.

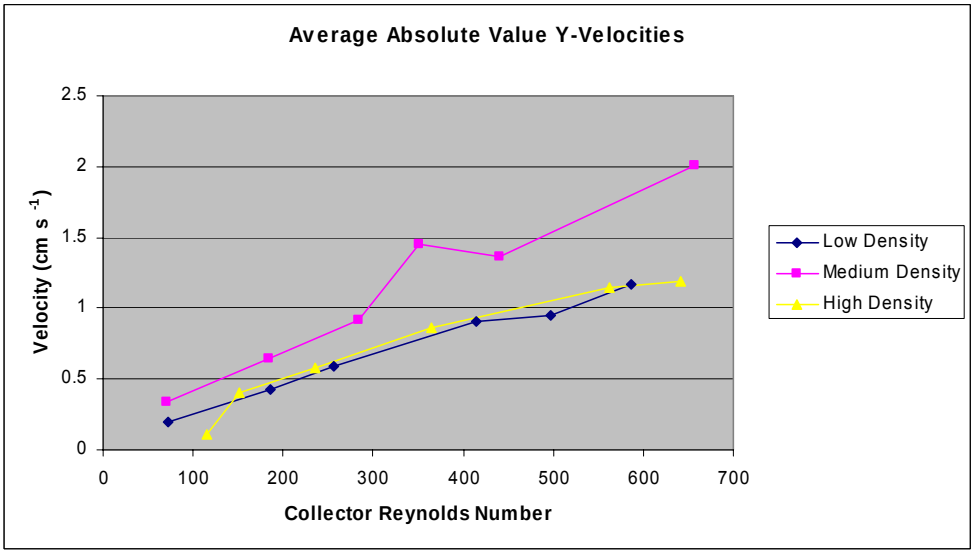

Figure 15: Average absolute value of ADV y-velocity measurements for particle capture experiments.

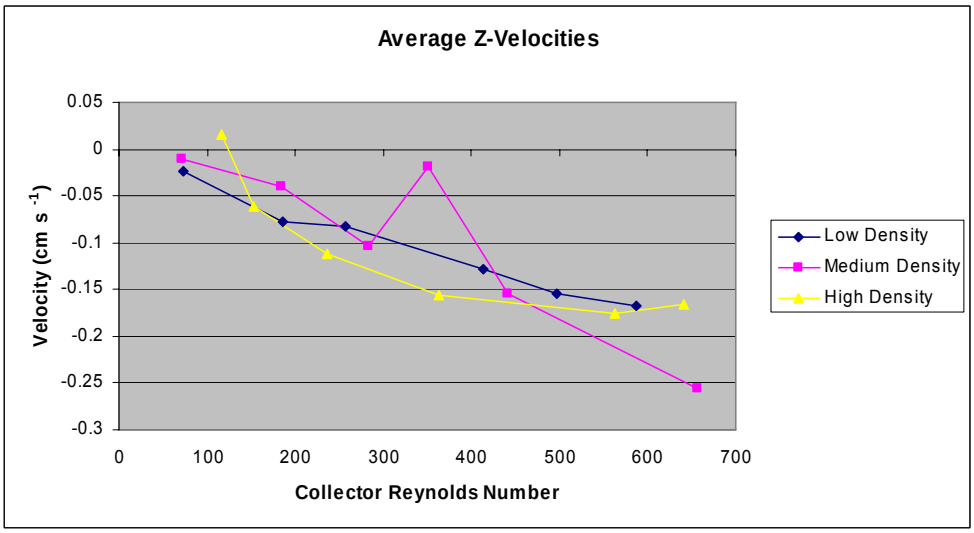

Figure 16: Average ADV z-velocity measurements for particle capture experiments.

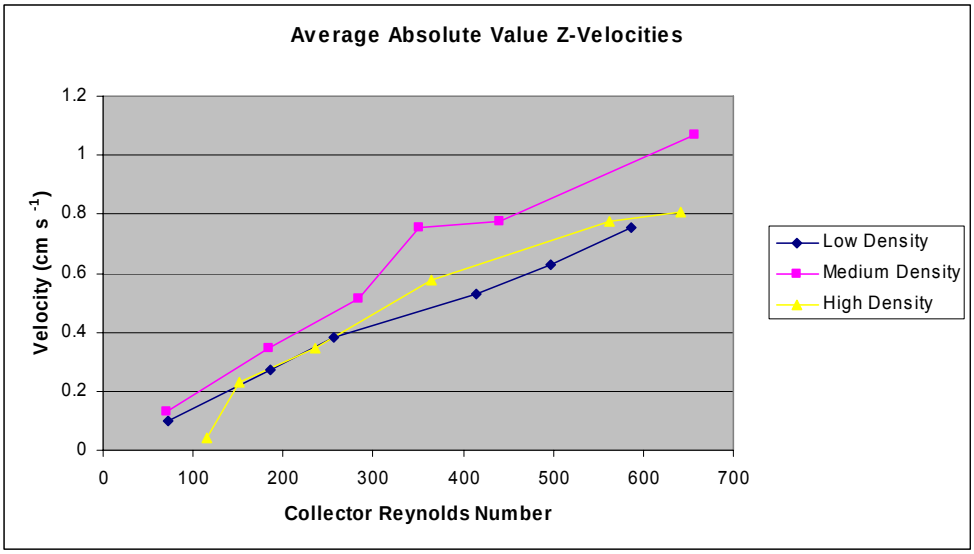

Figure 17: Average absolute value of ADV z-velocity measurements for particle capture experiments.

The standard deviations in the velocities measured by the ADV are shown below in Figure 18, Figure 19, and Figure 20. The standard deviations in velocity measurements made over the duration of each experiment increase with run number, and thus with an increasing flow rate. Standard deviations ranged from 0.2 to 2.0 cm s^{-1} in the x-direction, 0.1 to 2.5 cm s^{-1} in the y-direction and 0.05 to 1.3 cm s^{-1} in the z-direction.

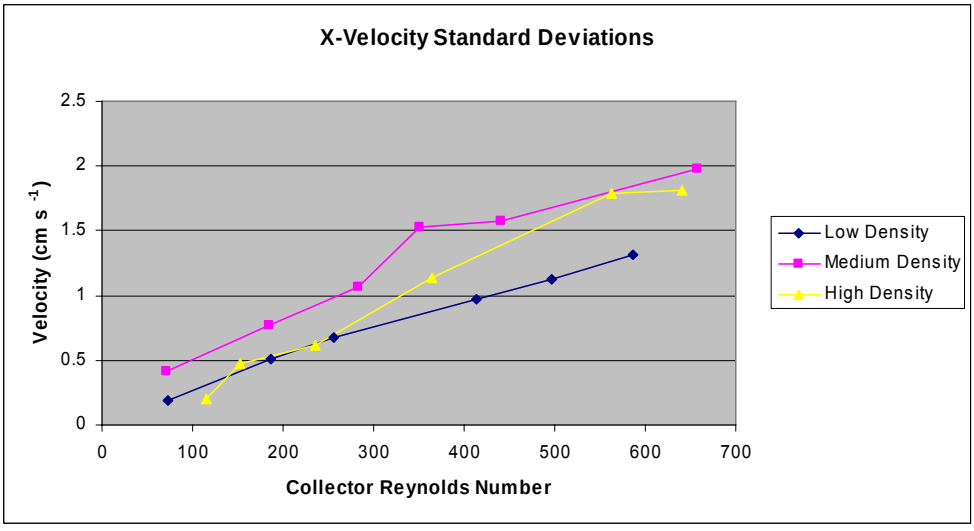

Figure 18: Standard deviation of ADV x-velocity measurements for particle capture experiments.

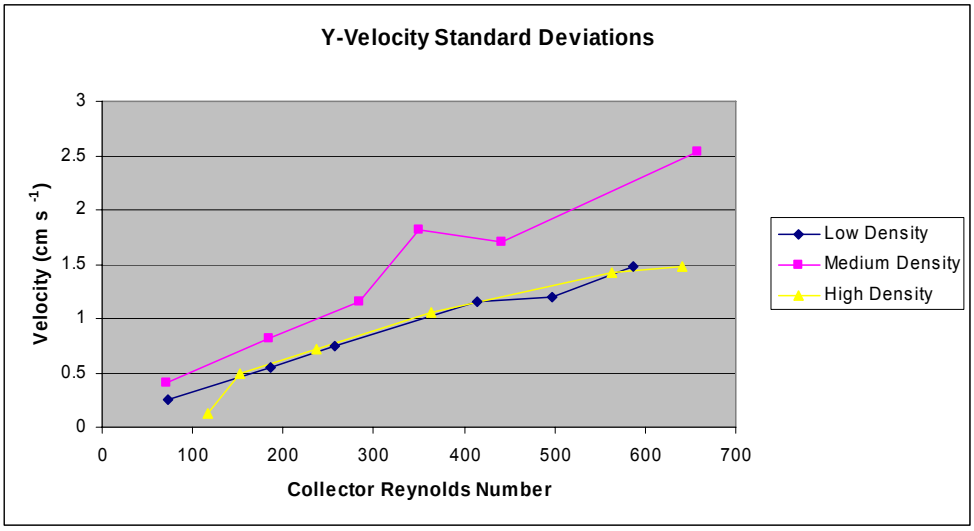

Figure 19: Standard deviation of ADV y-velocity measurements for particle capture experiments.

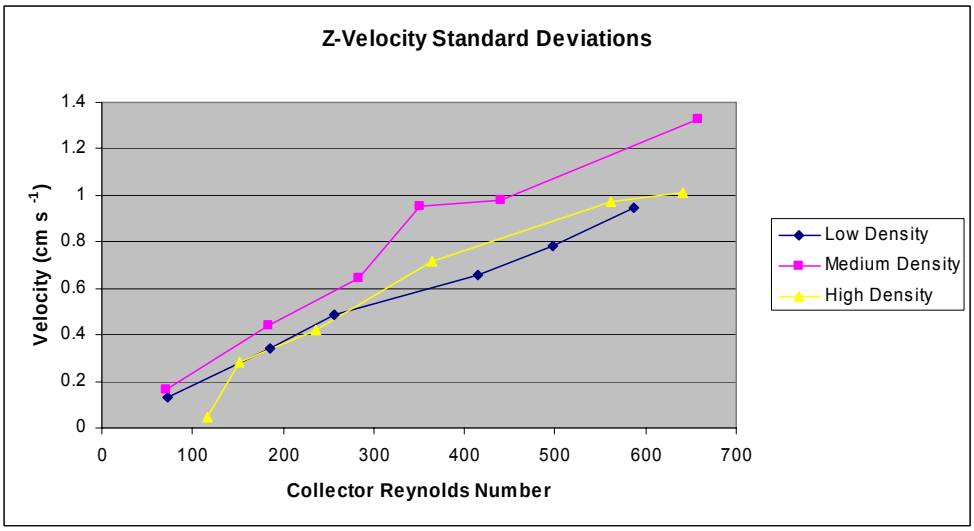

Figure 20: Standard deviation of ADV z-velocity measurements for particle capture experiments.

The standard deviations measured for the different density arrays are all within similar ranges however the standard deviations associated with the medium density array experiments were predominantly higher than those measured in the low and high density array experiments, as shown in Table 5. The standard deviations in the y-velocities measured were higher than the corresponding x and z-standard deviations.

Table 5: Average standard deviations associated with velocities measurements for the different array density experiments.

	Standard Deviations in Velocities (cm s^{-1})		
Array Density	**X**	**Y**	**Z**
Low density	0.80	0.97	0.61
Medium density	0.90	1.41	0.75
High density	0.56	0.88	0.57

4.2.2 Velocity time series

The results presented above were obtained by averaging a large number of data points, as the ADV sampled at 25 Hz for approximately eight minutes for each experiment, giving approximately 12000 data points per experiment. The first forty seconds of velocity data recorded during the lowest and highest Reynolds number experiments (runs 1 and 6) for each array density are included below (Figure 21 to Figure 26). These graphs demonstrate how the velocities recorded varied with time, as well as with flow rate and array density. The trends observed in the first forty seconds of data were observed over the whole time interval. The graphs produced for the intermediate Reynolds number experiments (runs 2, 3, 4 and 5) are not included in this report, but were similar to those included.

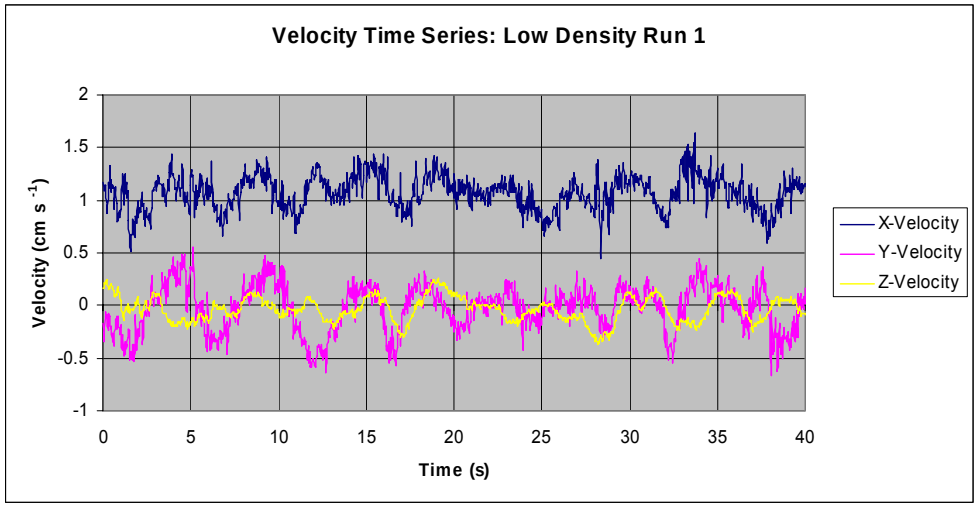

Figure 21: Forty second sample section of ADV data for the low density array, run 1 experiment.

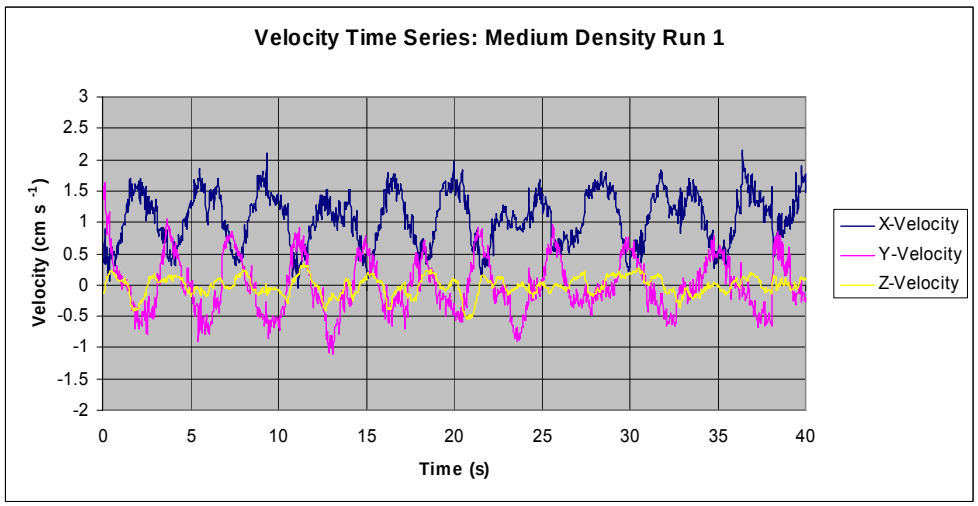

Figure 22: Forty second sample section of the ADV velocity data for the medium density array, run 1 experiment.

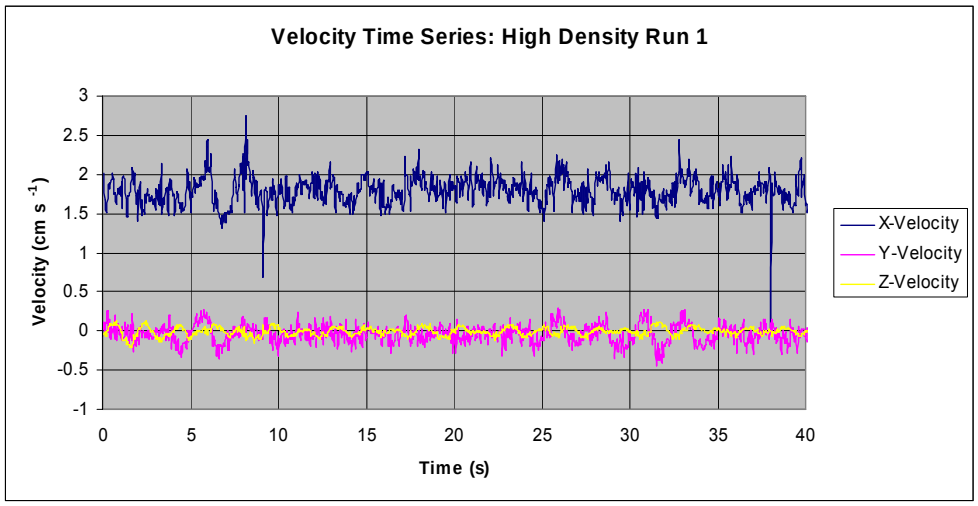

Figure 23: Forty second sample section of the ADV velocity data for the high density array, run 1 experiment.

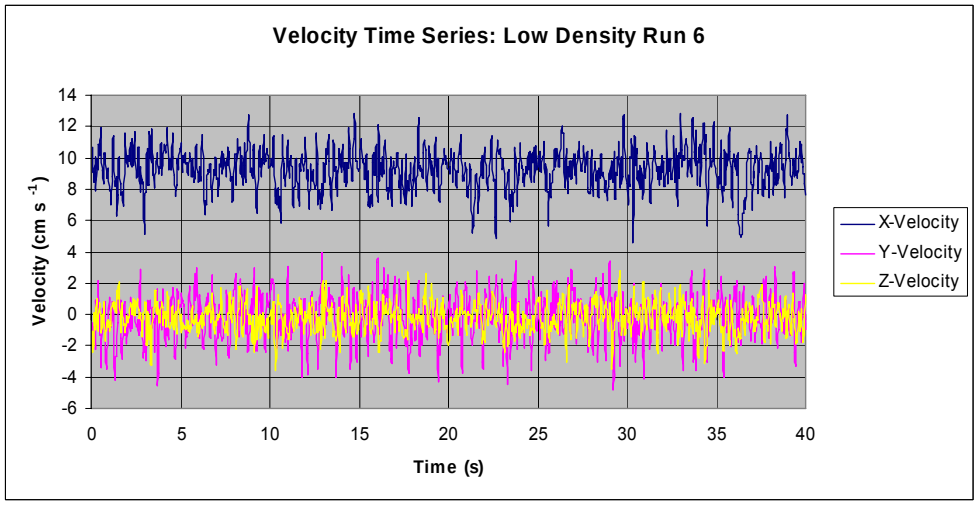

Figure 24: Forty second sample section of the ADV velocity data for the low density array, run 6 experiment.

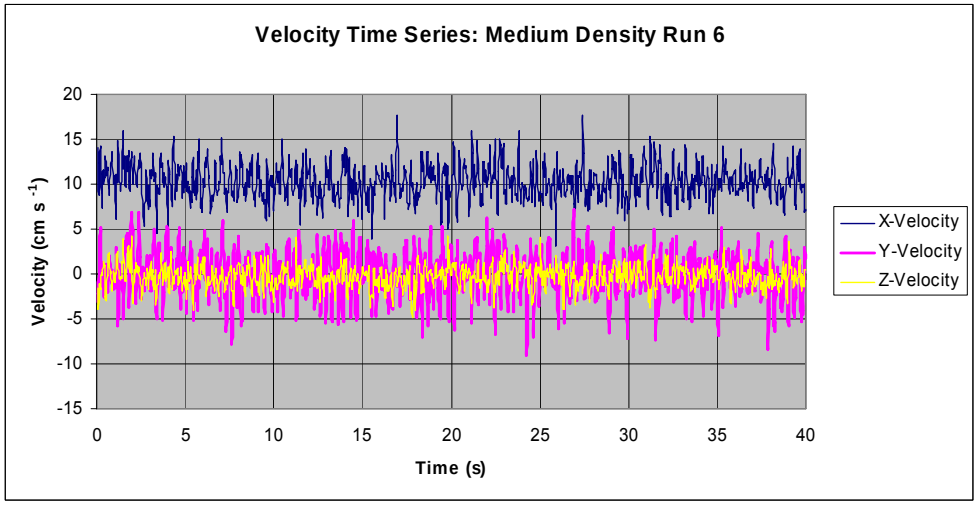

Figure 25: Forty second sample section of the ADV velocity data for the medium density array, run 6 experiment.

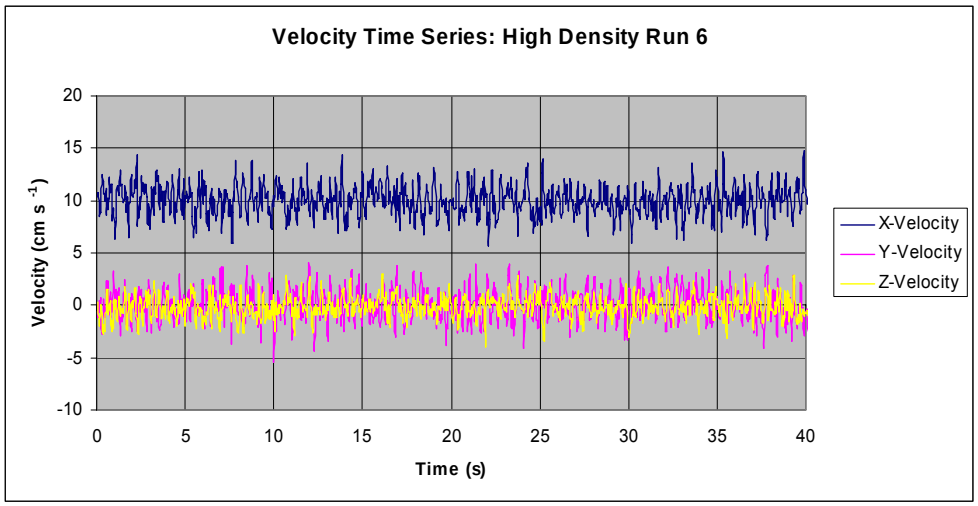

Figure 26: Forty second sample section of the ADV velocity data for the high density array, run 6 experiment.

From these graphs it can be seen that there is a periodic component associated with the velocities measured in run 1 for all density arrays (Figure 21, Figure 22 and Figure 23). This periodicity can easily be seen in the low and medium density array experimental data (Figure 21 and Figure 22), but is less obvious in the high density array experimental data (Figure 23). The periodicity associated with the x, y and z-velocities is similar in all cases. From these graphs the periodicity (T) can be estimated:

Low density array, run 1: ~ 9.5 cycles/40 s → T ~ 4.2 s

Medium density array, run 1: ~ 10.5 cycles/40 s → T ~ 3.8 s

High density array, run 1: ~ 20 cycles/40 s → T ~ 2.0 s

This periodicity is not immediately evident in the graphs of velocities measured in run 6 (highest flow rate) for any of the array densities (Figure 24, Figure 25 and Figure 26). If however, the scale of these graphs is changed, periodicity becomes more obvious. This is shown below in Figure 27, where the x-axis from Figure 25 has been reduced to only include eight seconds of data.

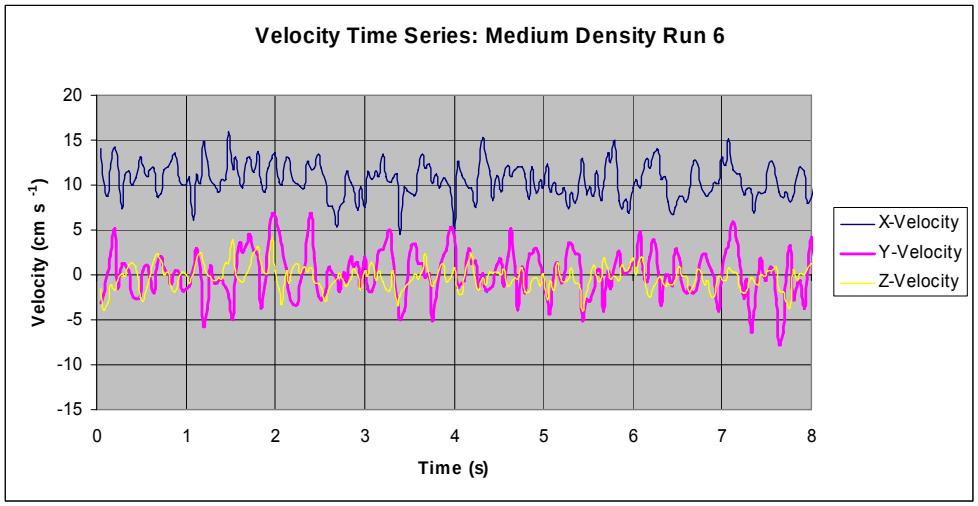

Figure 27: Eight second sample section of the ADV velocity data for the medium density array, run 6 experiment.

From this figure the periodicity can be estimated:

Medium density array, run 6: ~ 21 cycles/8 s → $T \sim 0.4$ s

Spectral analysis of the velocity data was used to determine the dominant frequencies present in the data, and thus to calculated the periodicity in the data more accurately. Figure 28 below is a sample graph produced by performing spectral analysis on the y-velocity data for the medium density array, run 1 experiment. This graph has a peak at a frequency of 0.29 Hz, corresponding to a period of 3.41 s.

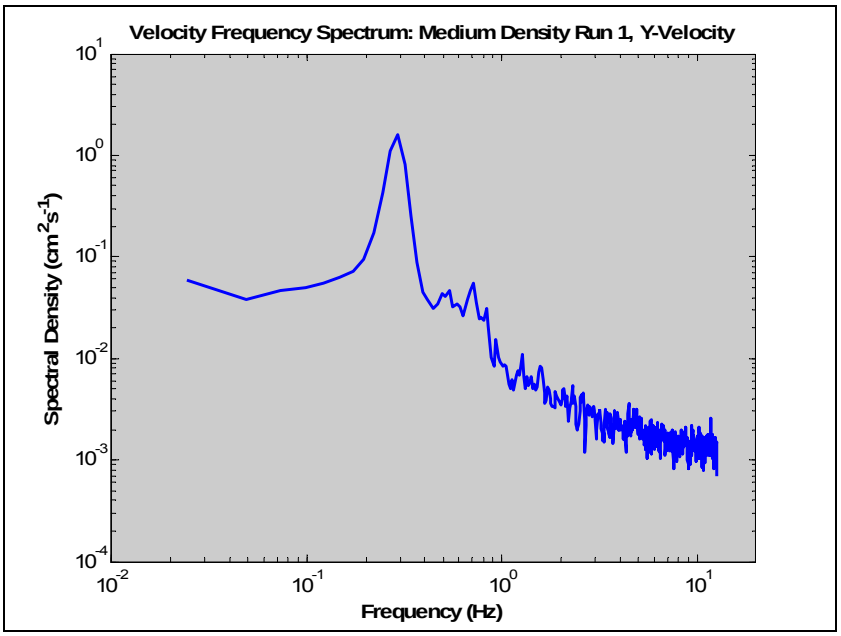

Figure 28: Sample velocity frequency spectrum for the y-direction velocity data from the medium density array, run 1 experiment.

Spectral analysis for the x, y and z- velocities was conducted for runs 1 and 6 of the low, medium and high density array experiments. This showed that the peak frequency remained approximately constant for all velocity directions (Figure 29).

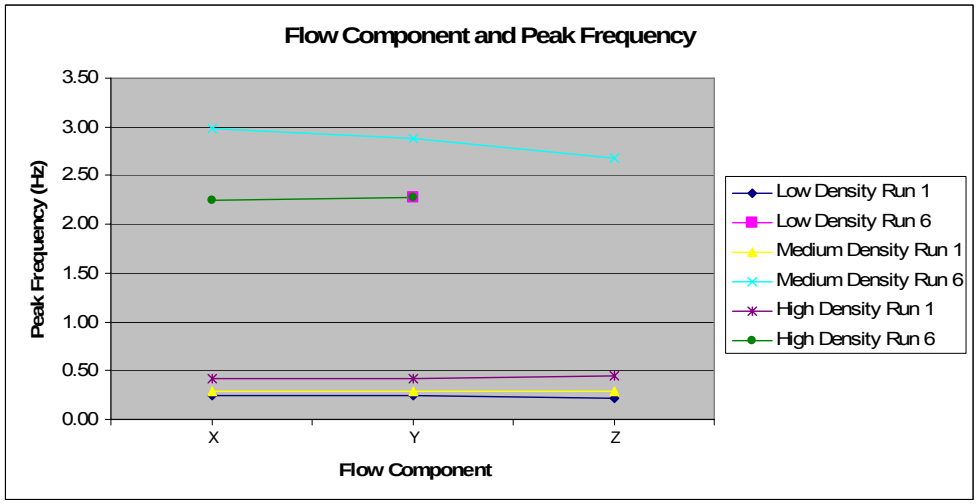

Figure 29: Peak frequencies observed in the x, y and z-velocities for runs 1 and 6 of all array densities.

The y-velocity data produced the largest peaks in the spectral graphs produced for runs 1 and 6 in all cases except for the high density array, run 1 experiment, where all peaks were a similar size (Figure 30). In the low density array, run 6 data, a peak in the x and z-velocity was not observed. In the high density array, run 6 data, a peak in the z-velocity was not observed.

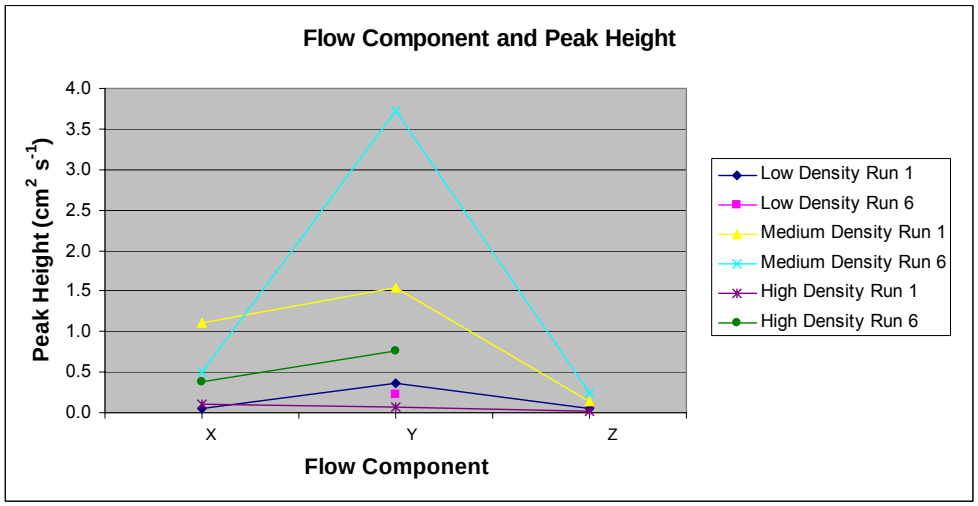

Figure 30: Peak height in the spectral plots of the x, y and z-velocities for runs 1 and 6 of all array densities.

It was thus decided to be appropriate to only use the y-velocity data in further analysis to compare all experiments, as this data showed the clearest peaks, and these peaks were a similar frequency to those in the x and z-velocity. Figure 31 shows that the peak frequency

observed in the y-velocity data increased linearly with collector Reynolds and this increase was observed for all density arrays. The dominant period associated with the y-velocity decreased exponentially with collector Reynolds number for all density arrays, as shown in Figure 32.

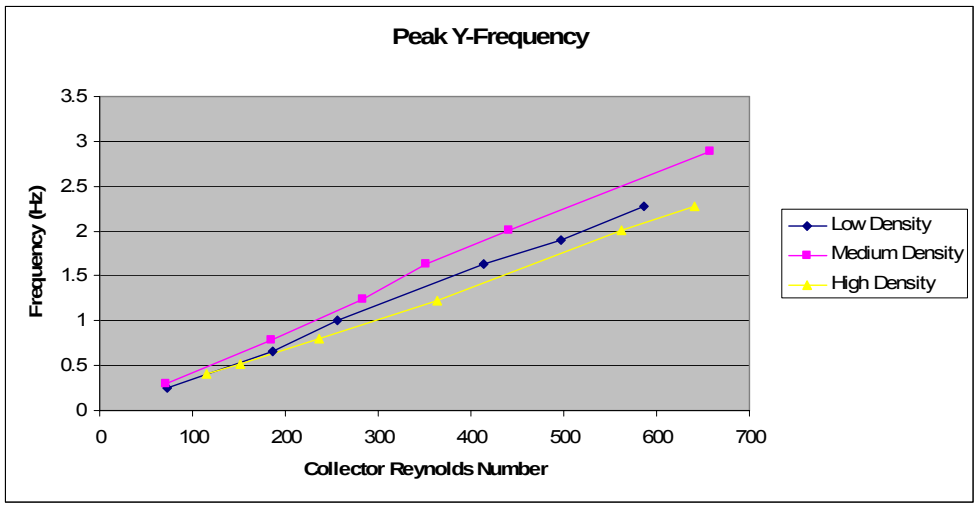

Figure 31: Peak frequencies observed in the y-velocity data.

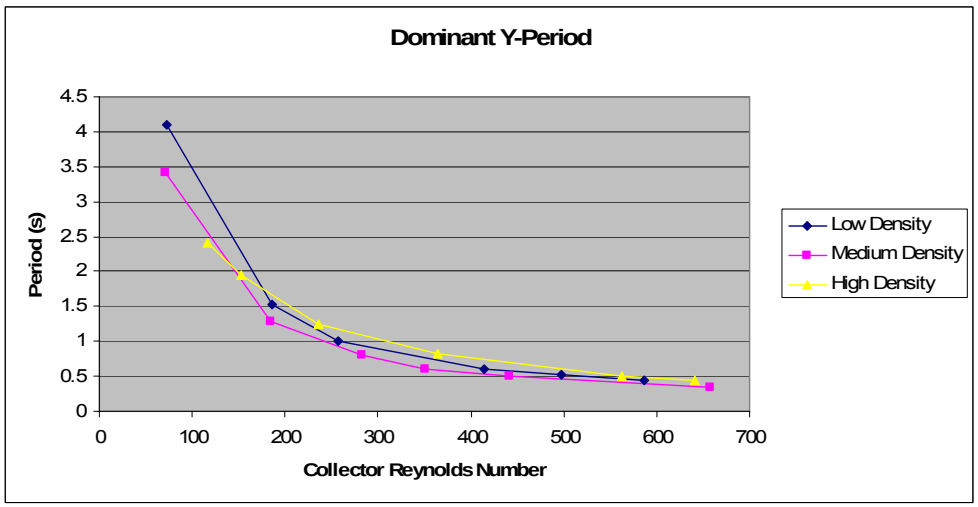

Figure 32: Dominant periods calculated for the y-velocity data.

The Strouhal number for each experiment was calculated from Equation 2, using the observed peak frequencies as shown in Figure 31. Values calculated are shown in Figure 33. The highest Strouhal numbers were calculated for the medium density array experiments, and the lowest Strouhal numbers were observed for the high density array experiments. In the low density array experiments the Strouhal number varied between 0.137 and 0.161, in the medium density array experiments it varied between 0.168 and 0.190, and in the high density array experiments it varied between 0.137 and 0.146.

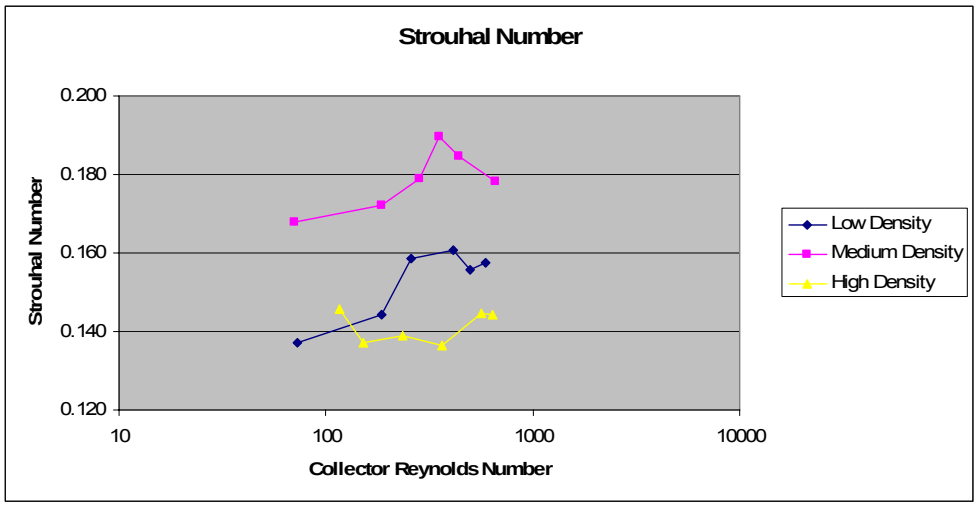

Figure 33: Calculated Strouhal number versus collector Reynolds number.

4.3 Water levels

The measured change in hydraulic head across the 1.99 m of modelled vegetation for each experiment is shown below in Figure 34. There is a reduction in hydraulic head as water flows through the array (shown as a positive head loss in Figure 34). This reduction was observed for all density arrays. As the collector Reynolds number increased the reduction in head across the array also increased. The greatest reduction in head was observed in the high density array experiments and the lowest reduction in head was observed in the low density array experiments.

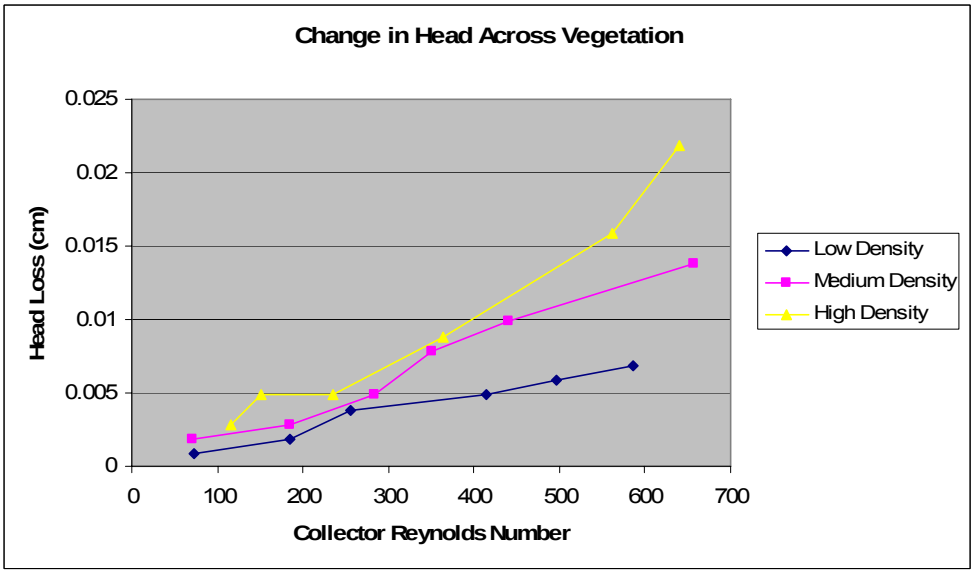

Figure 34: Change in hydraulic head across the model vegetation arrays versus collector Reynolds number.

From the change in hydraulic head, the bulk drag coefficient for the different density arrays was calculated as shown in Figure 35. There is an initial decrease in the bulk drag coefficient

with an increase in collector Reynolds number. Above a collector Reynolds number of 200 to 300 the bulk drag coefficient for each density array remains approximately constant. The bulk drag coefficient decreased with increasing array density for most of the Reynolds numbers tested in experiments. In some cases the bulk drag coefficient of the medium density array was greater than that of the low density array, but generally the bulk drag coefficient for these two densities were very similar, with the medium density array experiments having slightly lower values. The bulk drag coefficient for the high density array experiments was consistently the lowest coefficient of all three array densities.

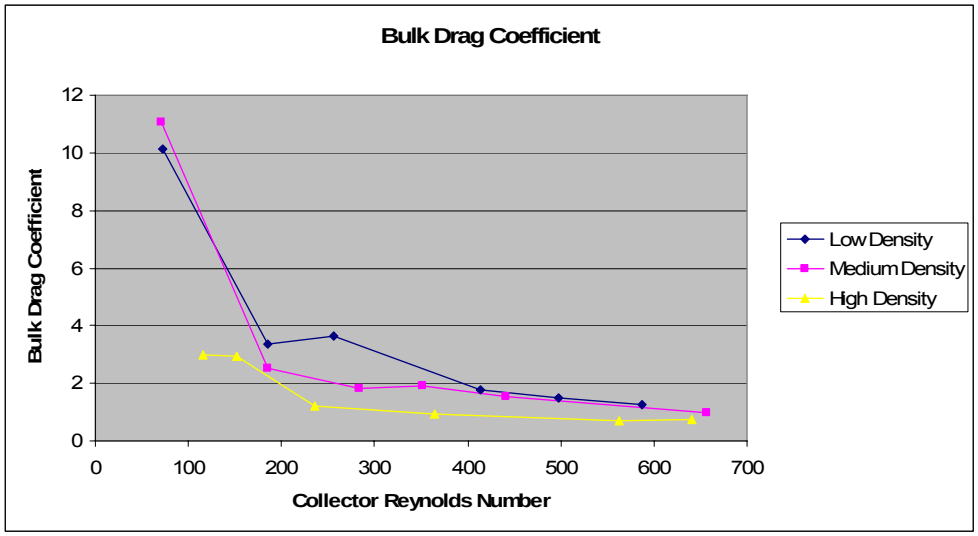

Figure 35: Bulk drag coefficient for the model vegetation arrays versus collector Reynolds number.

4.4 Particle capture

The numbers of particles captured in each experiment are presented below. A table of particle counts is included in Appendix B. Variations in capture between front and back faces of cylinders, as well as variations in capture between different cylinders are presented in this section.

4.4.1 Number of particles captured

The numbers of particles captured in each experiment are graphed below. These show the combined capture of all five test cylinders used in each experiment. Figure 36, Figure 37, and Figure 38 show the number of particles captured in the low density array, medium density array and high density array experiments respectively. These graphs show the capture for the individual cylinder faces for each experiment as well as the total particle capture for each experiment. Figure 39 shows the total particle capture for all the experiments.

The total number of particles captured in the low density array experiments (Figure 36 below) increased as the collector Reynolds number increased. The number of particles collected ranged from 78 for a Reynolds number of 72, to 514 for a Reynolds number of 587. The proportion of particles that were captured on the back faces (back left face and back right face) compared to the total number of particles collected increased as the collector Reynolds number increased. At the lowest Reynolds number the proportion of particles captured on the back faces was 47%. At the highest Reynolds number this proportion had increased to 66%, an increase by a factor of 1.4.

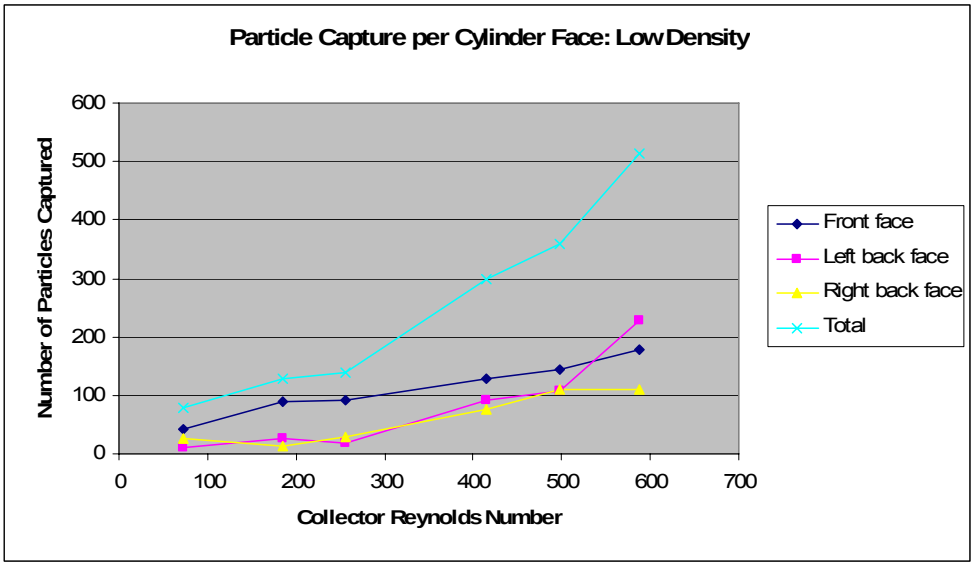

Figure 36: Particle capture per cylinder face versus collector Reynolds number for the low density array experiments.

The number of particles captured in the medium density array experiments (Figure 37 below) increased overall as collector Reynolds number increased, but this increasing trend was not consistently observed. The number of particles collected at a Reynolds number of 71, the lowest tested, was 179, and the number of particles collected at a Reynolds number of 657, the highest tested, was 527. A peak in particle capture of 558 particles was observed for an intermediate Reynolds number of 351. The proportion of particles captured on the back faces increased with Reynolds number. At the lowest Reynolds number 19% of the particles captured were on the back faces of the test cylinders. At the highest Reynolds number this proportion had increased by a factor of 4 to 76% of the particles captured.

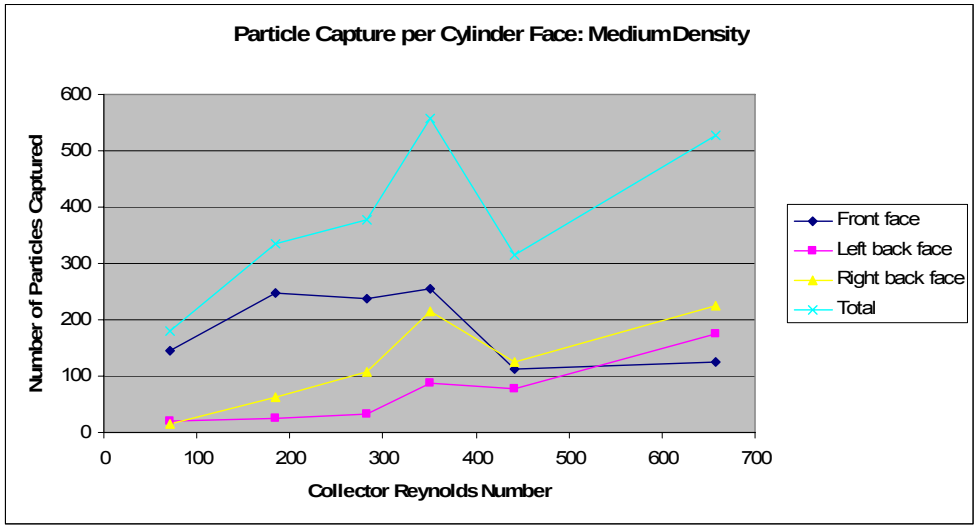

Figure 37: Particle capture per cylinder face versus collector Reynolds number for the medium density array experiments.

An increase in the number of particles captured was also observed in the high density array experiments (Figure 38). The numbers of particles captured in these experiments was lower than in the low and medium density array experiments. For a Reynolds number of 116, the lowest number tested, only 17 particles were captured. At the highest Reynolds number tested, 641, 78 particles were captured. The proportion of particles captured on the back faces of cylinders did not increase with an increase in Reynolds number as observed in the other experiments; however, this proportion was higher at low Reynolds numbers than in the other experiments. The proportion of particles captured on the back faces ranged between 42 and 70% for these experiments.

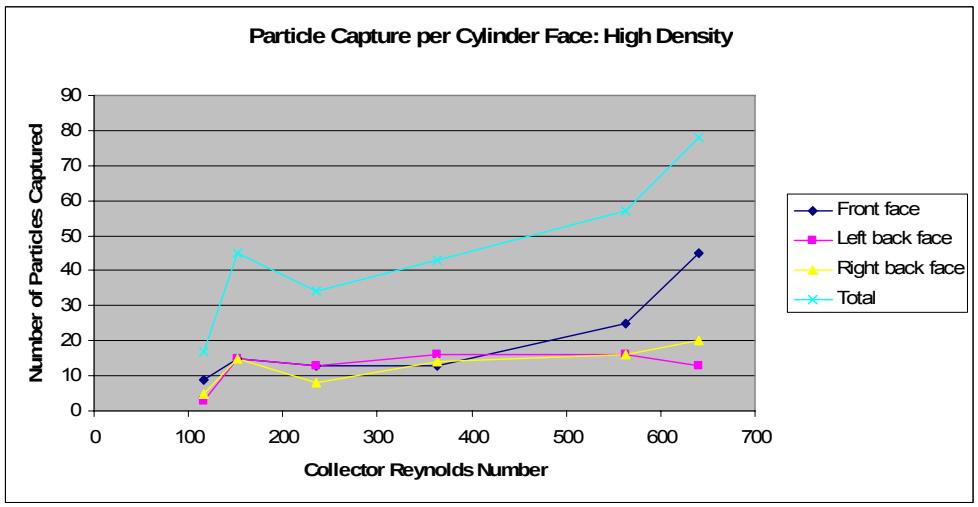

Figure 38: Particle capture per cylinder face versus collector Reynolds number for the high density array experiments.

Figure 39 demonstrates the difference in the overall number of particles captured for the different experiments. This graph shows that the numbers of particles captured in the high

density array experiments was considerably lower than in the other experiments, particularly for high Reynolds number experiments. At the highest Reynolds numbers tested, the number of particles captured in the medium density array experiment exceeded six times the number of particles captured in the high density array experiment. For most Reynolds numbers tested the medium density array experiments captured the most particles.

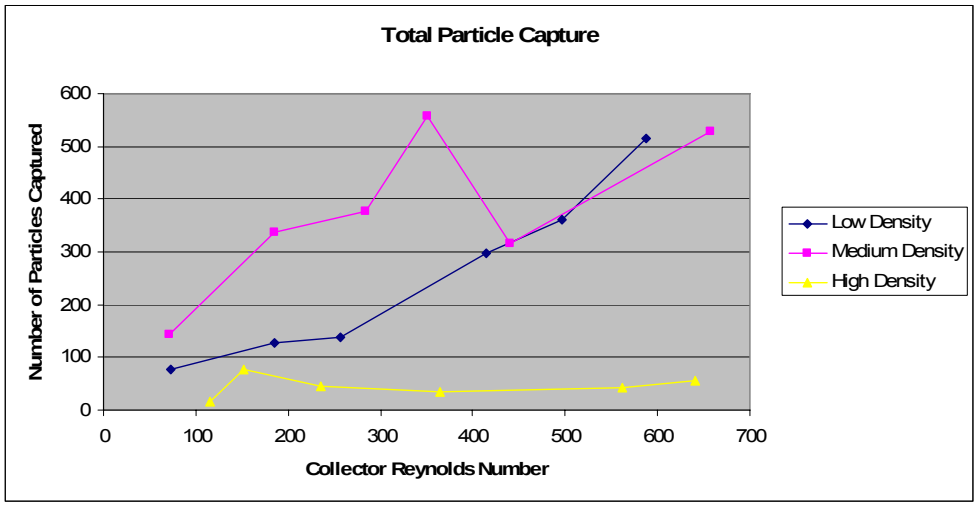

Figure 39: Number of particles captured (on all cylinder faces) versus collector Reynolds number for all experiments.

The percentage of particles captured on the back faces (back left and back right) compared to the total number of particles captured is shown in Figure 40. This shows that the proportion of particles captured on the back faces of cylinders increased with increasing Reynolds number for the low and medium density array experiments. An increase was not observed for the high density experiments.

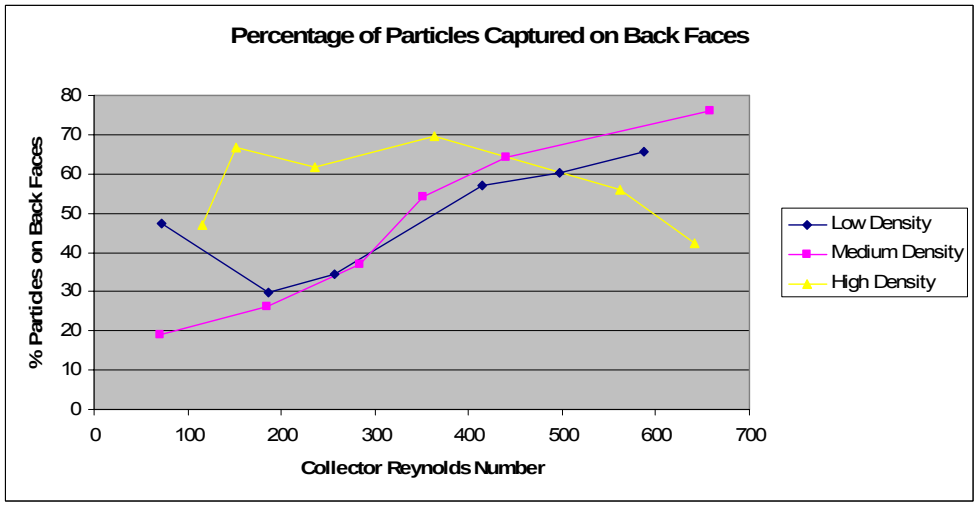

Figure 40: Percentage of particles captured on the back faces (back left and back right) compared to the total number of particles captured.

4.4.2 Cylinder position

The number of particles captured in each test cylinder location is shown below in Figure 41. Cylinder position numbers were the positions of each test cylinder across the flume, with positions 1 and 5 near the flume walls, and position 3 in the middle of the flume. The values plotted in this graph show the total number of particles captured on test cylinders in each cylinder position, for each density array. This is the sum of the number of particles captured over six different experiments with different collector Reynolds numbers. Figure 41 demonstrates that the number of particles collected per cylinder position was the greatest for the medium density array experiments and least for the high density array experiments.

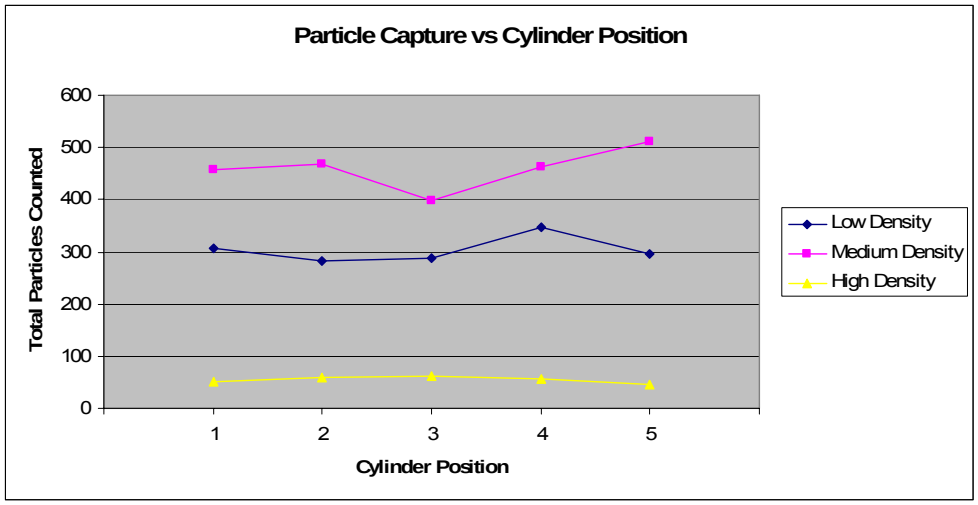

Figure 41: Variation between cylinder position and number of particles collected over the six runs for each array density.

There was some variation in particle capture between test cylinders positions in experiments, but this variation does not appear to be dependent on the cylinder location in the flume. A variation of 63 particles was observed between cylinders in the low array density experiments, with cylinder number 4 capturing noticeably more particles than other cylinders. This variation corresponds to an 18% variation in particle capture between the cylinders capturing the highest and lowest numbers of particles. A variation of 112 particles was observed for the medium density array experiments. Cylinder number 3 captured less, and cylinder number 5 captured more particles than the other cylinders, giving a capture variation of 22% for this array density. For the high array density experiments, a 15 particle range between numbers captured on each cylinder was observed. This equates to a 29% variation in particle capture between the cylinders capturing the highest and lowest numbers of particles.

4.5 Capture efficiencies

The capture efficiencies for each experiment were calculated and the results are shown in Figure 42. The low and high density array capture efficiencies do not show a trend with Reynolds numbers. These capture efficiencies remain approximately constant for all of the Reynolds numbers tested in experiments. The medium density array capture efficiencies decrease as collector Reynolds number increases. The capture efficiencies calculated for the high density array experiments are lower than the capture efficiencies for the low and medium density array experiments for all Reynolds numbers. The medium density capture efficiencies are higher than the low density capture efficiencies at low Reynolds numbers, and approximately equal at high Reynolds numbers. Overall, capture efficiencies ranged from 0.02 – 0.67%.

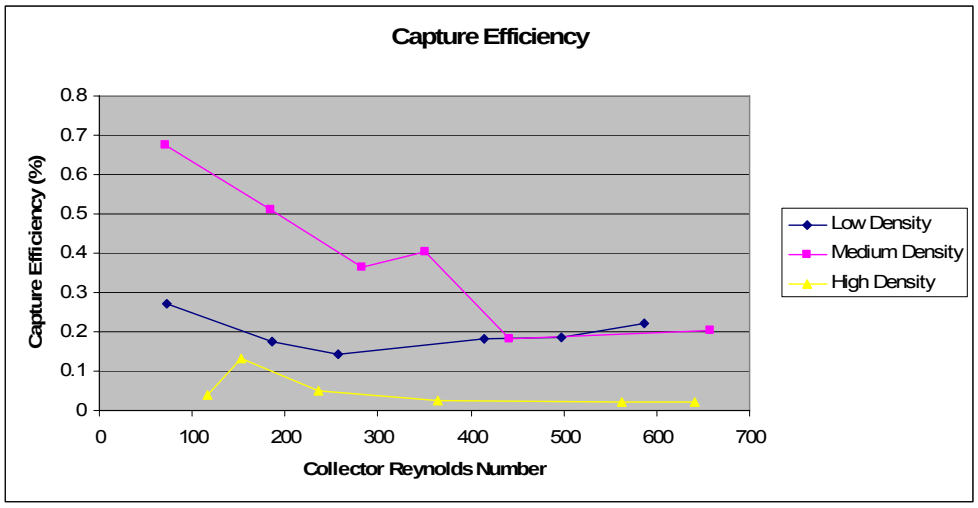

Figure 42: Particle capture efficiency versus collector Reynolds number.

4.6 Particle distribution patterns

Visually analysing photographs found that for some experiments particles are deposited in groups, rather than evenly across the face of a cylinder. Figure 44 below shows the cropped photographs for the front faces of test cylinders for one experiment. Groups of particles are circled to highlight the group deposition patterns.

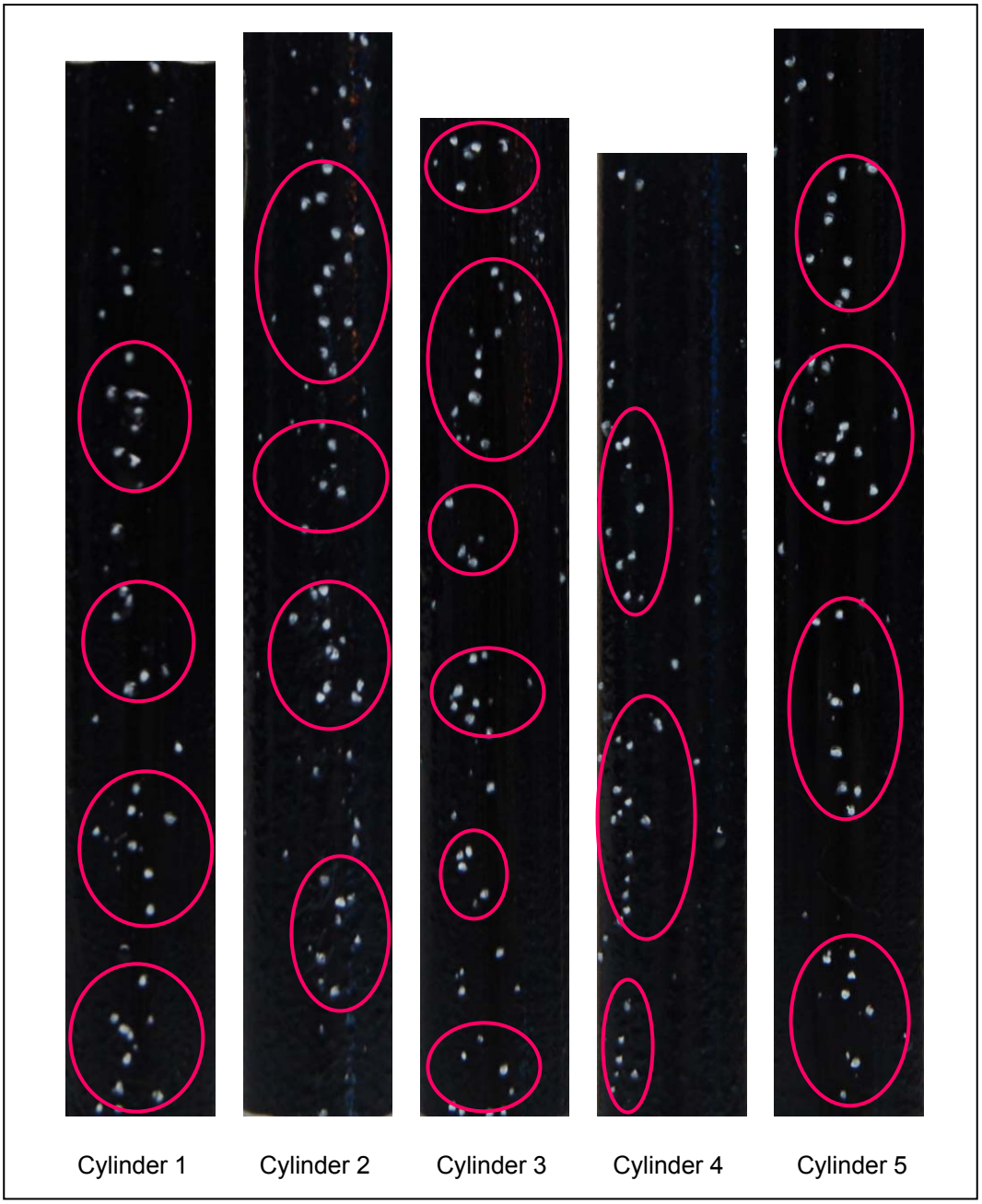

Figure 43: Photographs of the front faces of the cylinders from the medium density array, run 3 experiment.

The graphs produced by analysing the vertical distribution of particles on the cylinders from the low and medium density array experiments are shown below (Figure 44 to Figure 47). Figure 44 shows a small peak at a spatial frequency of 1.9 cm^{-1}, corresponding to a spatial distribution of 0.53 cm between particles on the front faces of test cylinders in the low density array experiments.

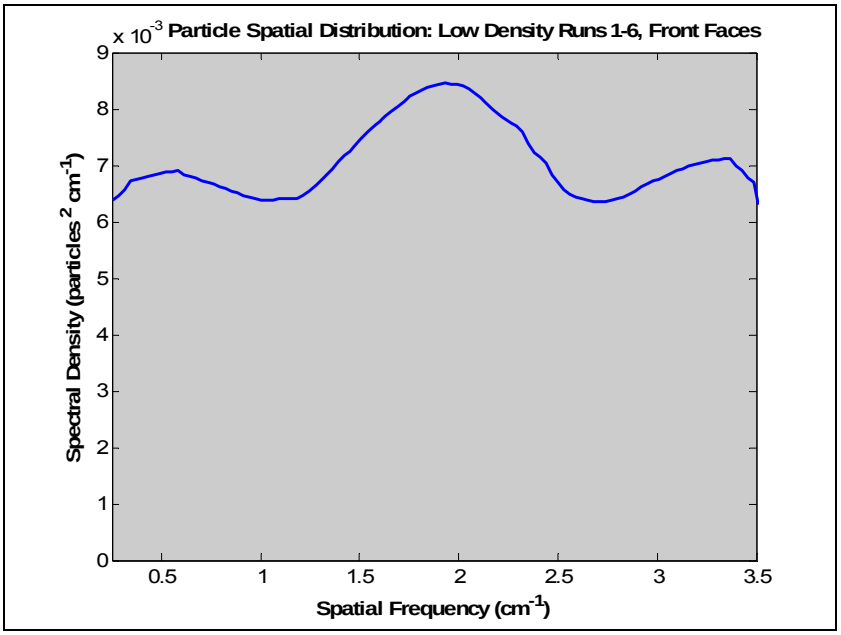

Figure 44: Vertical spatial distribution spectrum for particles deposited on the front face of test cylinders for the low density array experiments.

Figure 45 shows a small peak at a spatial frequency of 2.3 cm^{-1}, corresponding to a spatial distribution of 0.43 cm between particles on the front faces of test cylinders in the medium density array experiments.

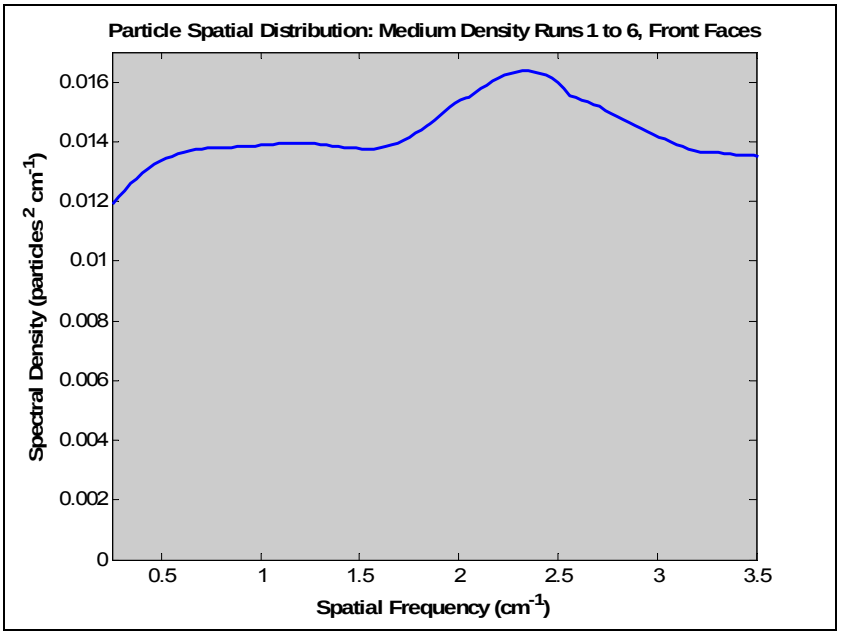

Figure 45: Vertical spatial distribution spectrum for particles deposited on the front face of test cylinders for the medium density array experiments.

No peak is present in Figure 46, the spectral graph produced by analysing the particle distribution on the back faces for runs 4 to 6 of the low density array experiments.

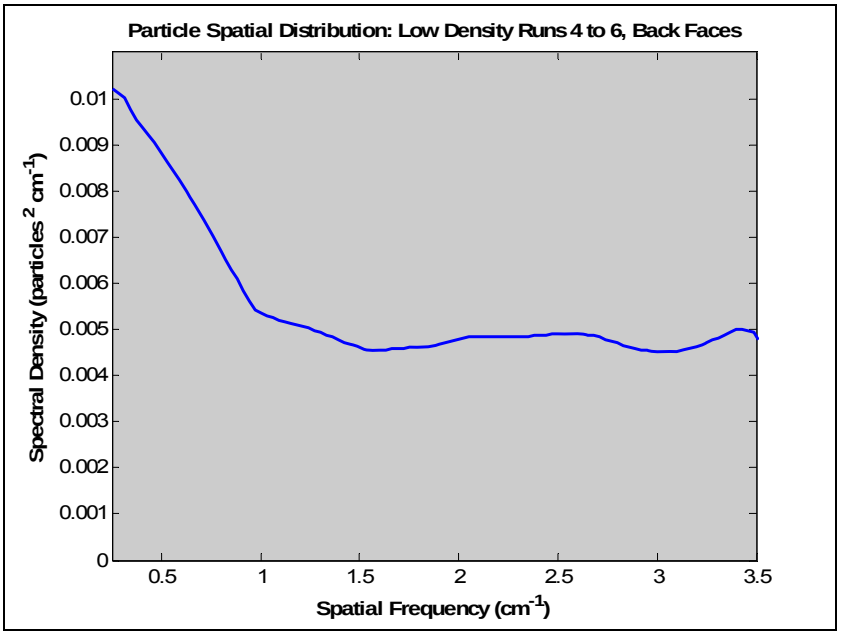

Figure 46: Vertical spatial distribution spectrum for particles deposited on the back faces (left and right) of test cylinders for the runs 4 to 6 of the low density array experiments.

Two small peaks are present in Figure 47, the spectral graph produced by analysing the particle distribution on the back left and right faces for runs 4 to 6 of the medium density experiments. These peaks are at a spatial frequency of 1.6 cm^{-1}, corresponding to a spatial distribution of 0.63 cm between particles, and at a spatial frequency of 3.0 cm^{-1}, corresponding to a spatial distribution of 0.33 cm between particles

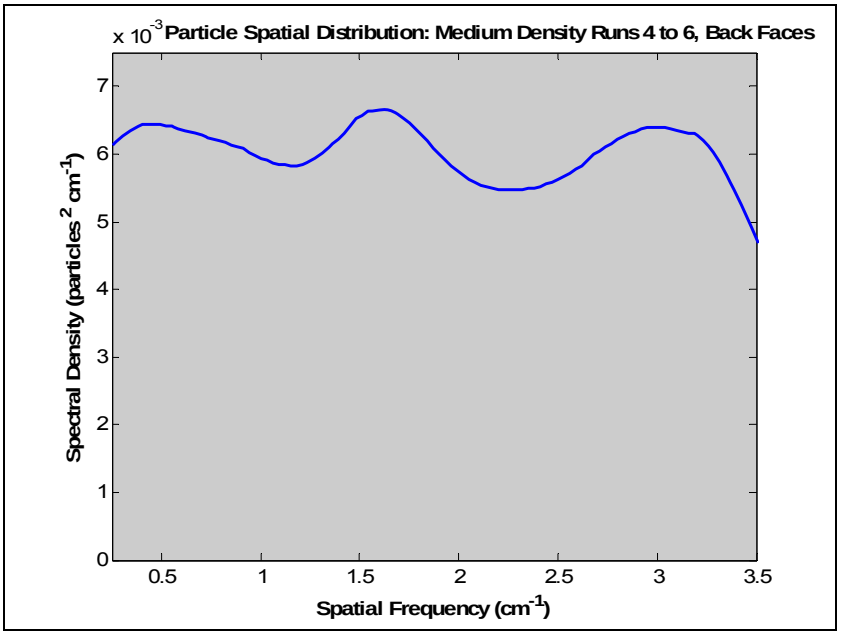

Figure 47: Vertical spatial distribution spectrum for particles deposited on the back faces (left and right) of test cylinders for runs 4 to 6 of the medium density array experiments.

4.7 Resuspension tests

Before the resuspension test, the test cylinder had 28 particles on the front face and 7 particles on the back faces (left and right combined). After ten minutes in the flume, 1 particle had been removed from the back of the cylinder. No particles had been removed from the front face. After the further five minutes in the flume no more particles had been removed. From this it was concluded that removal of particles during experiments was negligible.

5.0 Discussion

This section offers some explanations for the results presented in Section 4.0. The importance of direct particle capture compared to sedimentation as a suspended particle reduction mechanism in different systems is investigated. Findings of this study are also compared to field observations. Finally the limitations of this study are discussed in this section, before the conclusions are presented in Section 6.0.

5.1 Velocity trends

In the experiments conducted the magnitudes of velocities in the direction of flow, lateral to this flow and vertically were measured with the ADV probe and results of these presented in Section 4.2.1. The recorded x-velocities were observed to increase linearly with run number, as these were controlled by adjusting the flow rate through the flume. As the velocity in the direction of flow increased, the magnitude of the lateral and vertical velocities also increased. This shows that as higher Reynolds numbers the flow is more turbulent than at lower Reynolds numbers, as was expected.

5.1.1 Periodicity and shedding frequency

As shown in Section 4.2.2 the velocity measurements made with the ADV probe during experiments contained a periodic component. This periodicity was shown graphically in Figure 21 to Figure 27 and can be accounted for by the periodic formation and shedding of vortices from the dowel rods upstream of the ADV probe.

The periodicity observed in velocity measurements was most defined for the y-direction measurements in the experiments where the velocities in all directions (x, y and z) were analysed, as shown in Figure 30. Typically eddy rotation is more significant in the horizontal (x-y) plane, than vertically. As a result the periodicity in the x and y-velocities is more significant than the periodicity in the z-velocity. In these experiments the directionality associated with flow in the x-direction probably dampened the periodic component of the x-velocity. This explains why the y-velocity data exhibited periodicity most clearly.

The dominant frequency evident in the y-velocity data for all experiments is the shedding frequency (f_s), which was used to calculate the Strouhal number for each experiment, shown in Figure 33. These values can be compared to the Strouhal number for a single cylinder as shown in Figure 2. For a single cylinder, the Strouhal number increases from approximately 0.12 at a Reynolds number of 50, to approximately 0.21 at a Reynolds number of 700. Such a sharp increase in Strouhal number with increasing Reynolds number was not observed in any

of the experiments, which suggests that in cylinder arrays, between Reynolds numbers of approximately 50 to 700 the Strouhal number is less dependent on Reynolds number than for a single cylinder.

Shedding frequency is also affected by proximity of other cylinders (Nepf 1999), and this was evident in results as shown in Figure 31, where different shedding frequencies for different density arrays were observed. As Reynolds number increased, the difference between shedding frequencies in different density arrays also increased. The shedding frequencies for the medium density array experiments were the highest, and the shedding frequencies for the high density array experiments were the lowest for all Reynolds numbers. Shedding frequency increases as the spacing between cylinders decreases (Nepf 1999), which explains why the shedding frequencies for the medium density array experiments are greater than those for the low density array experiments, because cylinders in the medium density array set-up were closer together than in the low density array set-up. Based on this, however, the shedding frequencies for the high density array experiments would be expected to be the highest, but they were observed to be the lowest. This observation could be accounted for if a density threshold for this phenomenon existed, after which a further increase in cylinder density leads to interference in the vortices produced by different cylinders, resulting in a lower shedding frequency.

5.1.2 Standard deviation and eddy rotation

The standard deviations in velocity measurements made during experiments increased approximately linearly with increasing Reynolds number as shown in Figure 18 to Figure 20. Standard deviations of velocity measurements give an indication of the speed of eddy rotation in systems. The increase in standard deviations with Reynolds number suggests that the eddies present in experiments rotate faster at higher Reynolds numbers, as would be expected because higher Reynolds systems have a higher energy.

The standard deviations associated with the y-direction velocities were greater than the standard deviations associated with the x and z-direction velocities, as shown in Table 5. This is consistent with observations of periodicity, where periodicity in the y-direction was most defined, and can be accounted for in the same way.

Previous research into the turbulence in vegetation arrays with different vegetation densities (Nepf 1999) found that turbulence intensity is affected by two competing processes: reduction in velocity and increased turbulence production. In modelling conducted by Nepf (1999)

turbulent intensity was found to increase with the introduction of sparse vegetation, but then decrease as stem population increases further. This was thought to be a result of the competing processes that affect turbulence intensity in a vegetation array.

In all cases except one, the standard deviations of x, y and z-velocity measurements for the medium density array experiments were greater than the standard deviations of velocity measurements for the low and high density array experiments. This observation is consistent with the observations of shedding frequency. The interaction between the competing processes that control turbulence intensity may explain why the standard deviations associated with the medium density array experiments are higher than for the high and low densities. It is thought that at the medium array density the dowel spacings allowed vortices produced from different dowel rods to constructively interfere with each other, leading to a well developed eddy arrangement existing in experiments. At the low array density, cylinders were spaced further apart and less interaction between vortices may have occurred. At the high array density, cylinders were closer together, so vortices may have destructively interfered with each other.

5.2 Drag coefficients

The bulk drag coefficient of vegetation arrays is a function of the stem density because upstream plants can suppress the drag coefficient of trailing cylinders by sheltering them. Therefore, it would be expected that the bulk drag coefficient would decrease as the stem density increases (Nepf 1999). A decrease in the bulk drag coefficient with an increase in array density was observed in the experiments as shown in Figure 35. Also, for collector Reynolds numbers greater than approximately 200 the bulk drag coefficient is only a weak function of Reynolds number (Nepf 1999), as after this Reynolds number the wakes are no longer laminar (Kundu 1990). This too, was observed in experiments for all density arrays, as shown in Figure 35.

5.3 Particle capture trends

5.3.1 Variation in capture between cylinders

There was some variation in the particle capture of cylinders in different positions for any of the experiments as discussed in Section 5.3.1. The position of upstream dowel rods (shown in Appendix C) relative to the test cylinders for each array density was analysed visually in an attempt to explain the variation in cylinder position and capture, however no obvious upstream dowel configuration accounted for the difference in particle capture with cylinder position. There may have been subtle differences in the position of dowel rods which

increased or decreased the probability of particle capture, or otherwise the variation observed may just be experimental variation.

5.3.2 Variation in capture on cylinder faces

The observed increase in proportion of particles captured on the back faces of the test cylinders in the low and medium density array experiments associated with an increase in Reynolds number (Figure 40) suggests that turbulence and wake structures play an important role in particle deposition as a turbulent flow is required to deposit particles on the back of cylinders.

It was noteworthy that the proportion of particles captured on the back of the cylinders in the high density array experiments did not increase with Reynolds number. The close proximity of dowel rods in these experiments would have increased the turbulence present (compared to the lower array density experiments) at low Reynolds numbers. Thus, an increase in Reynolds number would not have altered the deposition patterns as significantly as for the lower array density experiments. Also, because the high array density experiments captured much fewer particles than the low and medium array density experiments (Figure 39), a small variation in the numbers of particles captured on the back of cylinders resulted in a larger change in the proportion of particles captured on the back of cylinders. This explains the variation in the high density array data shown in Figure 40.

5.3.3 Deposition patterns in capture on cylinder faces

For vegetation densities greater than 1%, as were tested in this study, turbulence scales (ℓ) are controlled by the vegetation geometry, with $\ell \sim d_c$ (Nepf 1999). The deposition pattern of particles on the face of cylinders was analysed to determine whether the location that particles were deposited was influenced by the size of eddies in the system.

Weak peaks were observed in the spatial frequency spectral plots produced for the particle distribution on the front face of cylinders as shown in Figure 44 and Figure 45. Peaks corresponding to an average spacing between particle groups of 0.53 cm and 0.43 cm were observed for the low and medium density array experiments respectively. These spacings are of the same order of magnitude as the diameter of the cylinders used in experiments (0.63 cm). These results indicate that the eddies in the arrays may have influenced the location of deposited particles on the front faces of cylinders, but that this is not a dominant effect as spectral peaks were only weak.

No peak was observed in the spatial frequency spectral plot for the back faces of cylinders for the low density array experiments (Figure 46), but two weak peaks were observed for the medium density array experiments (Figure 47). It would not be expected that upstream eddies would influence the particle deposition patterns on the back faces of cylinders, because these back faces would be influenced more by the shedding of vortices from that particular cylinder than by upstream cylinders. The peaks observed for the medium array density experiments may indicate a genuine deposition pattern influenced by vortex shedding, however as similar peaks were not observed for the low density array experiments, there is nothing to compare these peaks to, and thus no conclusions can be drawn.

5.4 Capture efficiencies

Palmer *et al.* (2004) found the particle capture efficiency of a single cylinder to increase with an increasing collector Reynolds number and particle to collector ratio, and that data could be described by the following equation:

$$\eta = 0.224\left(Re_c\right)^{0.718}\left(R\right)^{2.08} \tag{19}$$

The capture efficiency for a single cylinder with the same particle to collector ratio as existed in these experiments was then predicted for the range of Reynolds numbers tested, as is shown below in Figure 48. At low Reynolds numbers the magnitudes of capture efficiency for a cylinder within different array densities are similar to those determined by Palmer *et al.* (2004). As Reynolds number increases, the capture efficiency of an isolated cylinder increases, but the capture efficiency of a cylinder within an array does not increase. This means that at higher Reynolds numbers the capture efficiency of a cylinder within an array is lower than the capture efficiency of an isolated cylinder.

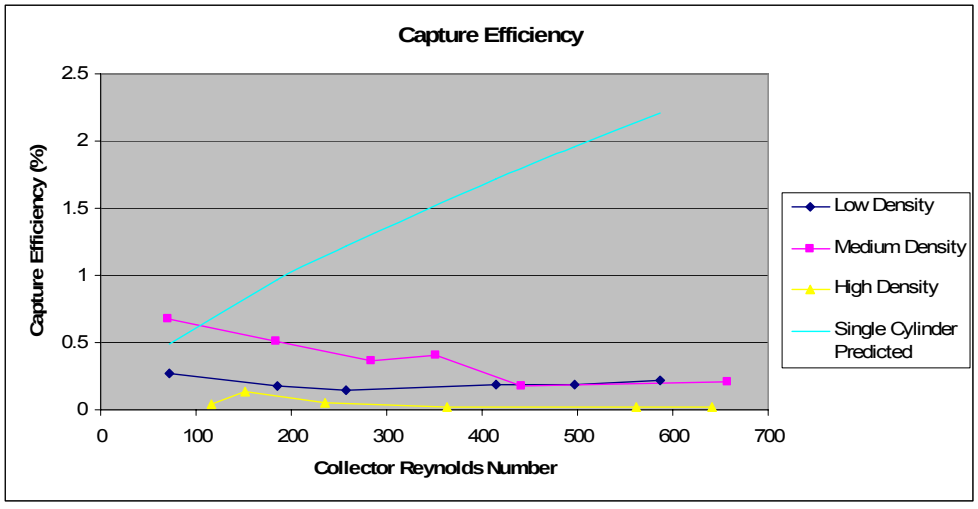

Figure 48: Comparison between observed capture efficiencies and those predicted by Palmer *et al.* (2004) for a single cylinder.

The difference in particle capture efficiency trends with Reynolds number observed for an isolated cylinder and for cylinders in an array may be due to the different flow conditions present, as this may influence what particle capture mechanisms are most dominant. Equation 19 is only valid for particle capture via direct interception. In the isolated cylinder experiments, upstream flow was not turbulent so the dominant particle capture mechanism was direct interception. In arrays of cylinders the existence of turbulence, as was evident from analysis of the velocity measurements, may have affected the dominant particle capture mechanism. For example, diffusional deposition is more important when flow is turbulent, so may have been important in these experiments. Also, local increases in velocity due to turbulence inertial impaction may have been important. The difference in particle capture mechanisms for an isolated cylinder compared to cylinders in an array may account for the different trends with Reynolds number observed for the two situations.

5.4.1 Capture efficiency trends with array density

The capture efficiencies calculated for the medium density array experiments were higher than for the other density experiments. This was an interesting observation; it was expected that the highest capture efficiency would be observed for an extreme (high or low) density array, not for the intermediate density. As well as having the highest capture efficiencies the speed of eddy rotation was determined to be highest in the medium density array experiments, as demonstrated by the larger standard deviations and higher shedding frequencies observed at this medium density array. This may be responsible for the higher capture efficiencies observed at the medium array density.

This is a significant finding. Not only does it suggest that the wakes due to the presence of vegetation in aquatic systems are influenced by the density of the vegetation, and that there is a threshold density which supports the strongest eddy systems in the vegetation array, but also that the existence of these eddies influences the particle capture efficiency of the vegetation. As such, there may be some optimum vegetation density that maximises particle capture efficiency for a particular aquatic system.

5.5 Applying gained knowledge in engineering design

5.5.1 Direct particle capture versus sedimentation

The importance of reductions in suspended particles due to direct particle capture compared to particle reduction by sedimentation can be estimated based on the magnitudes of particle capture efficiencies observed in laboratory experiments and other typical parameters observed in aquatic systems.

To compare the importance of direct particle capture and sedimentation the parameters that each of these processes are dependent on were assessed. Consider the particle flux through a box of length *L*, and width *B*, as shown in Figure 49 below. The flow velocity in this system is defined as *U*, the suspended particle concentration in number of particles per unit area is defined as *P*, and the number of plants in the box is *n*.

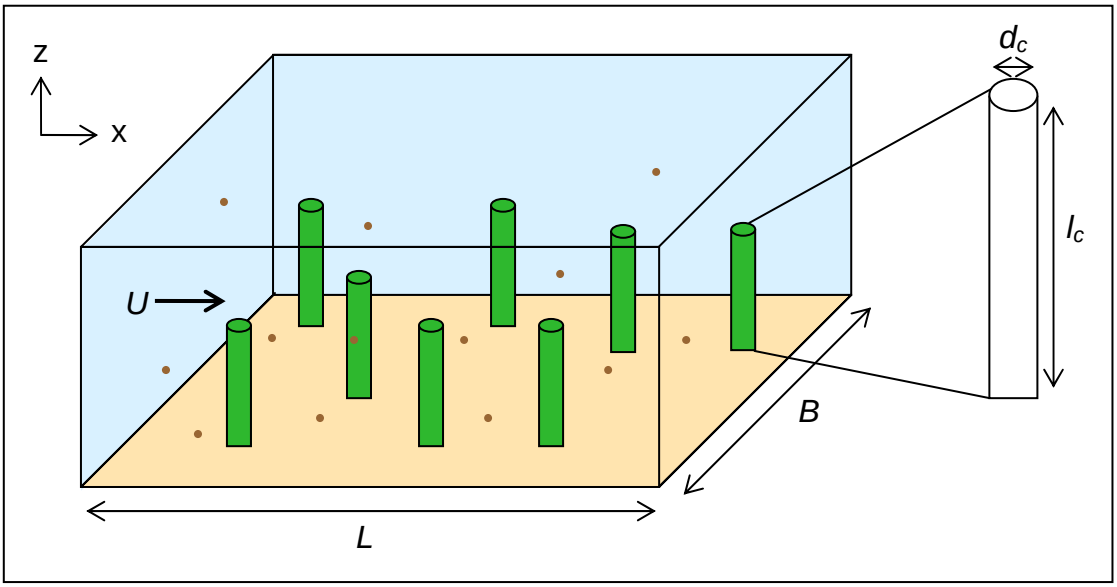

Figure 49: Particle flux through a box of length L, and width B.

The settling flux is governed by the Stokes settling velocity (Equation 6):

$$Settling\ \ flux = w_s(BLP) \tag{20}$$

The capture flux is governed by the particle capture efficiency (Equation 18):

$$Capture\ \ flux = \eta(UAP) \tag{21}$$

The frontal area, where particles can be directly captured, is a function of the size of each collector ($l_c d_c$) and the number of collectors (n):

$$A \sim (l_c d_c)n \tag{22}$$

From Equation 21 and Equation 22 the array capture flux can be expressed as:

$$Capture\ \ flux \sim \eta(U l_c d_c P n) \tag{23}$$

Substituting $D_p = n/(BL)$ where D_p is the plant density in plants per unit area, the ratio of capture flux to settling flux can be expressed as:

$$\frac{Capture\ flux}{Settling\ flux} \sim \eta\left(\frac{U}{w_s}\right)\left(l_c d_c D_p\right) \tag{24}$$

Equation 24 can be used to compare the relative importance of direct particle capture to sedimentation in a number of different systems, based on an order of magnitude analysis. Four different example systems are assessed based on the information summarised in Table 6, to estimate the importance of direct particle capture in each system.

Table 6: Summary of parameters that affect particle reduction in aquatic systems and their typical orders of magnitude. Refer to Section 2.0 for further information.

Parameter	Example	Order of magnitude
Particle capture efficiency (η)	Experimental results	0.01 – 1%
Flow velocity (U)	Freshwater wetlands	0.001 – 0.01 m s^{-1}
	Tidal marshes and seagrasses	0.01 – 0.1 m s^{-1}
Settling velocity (w_s)	Sand particle with diameter 200 µm, density 2650 kg m^{-3}	0.01 m s^{-1}
	Larvae particle with diameter 150 µm, density 1400 kg m^{-3}	0.001 m s^{-1}
	Silt particle with diameter 20 µm, density 2650 kg m^{-3}	0.0001 m s^{-1}
Plant frontal area ($l_c d_c$)	Wetland rushes with stems 0.6 cm diameter, 15 cm submerged	0.001 m^2
	Seagrass blades 1 cm wide, 100 cm long	0.01 m^2
Plant density (D_p)	Wetlands	100 shoots m^{-2}
	Seagrasses	1000 shoots m^{-2}

In general direct particle capture will be more important in systems with high velocities, high plant frontal areas and high plant densities. Direct particle capture will also be more important when the suspended particles are small (for example silts and clays), as these have a lower Stokes settling velocity (Equation 6).

5.5.1.1 Example 1: Wetland system with suspended silt particles

Based on the values in Table 6, order of magnitude assessment of a wetland system with suspended silt particles was conducted:

$$O(\eta) \sim 0.001;\ \ O\left(\frac{U}{w_s}\right) \sim 10-100;\ \ O\left(l_c d_c\right) \sim 0.001;\ \ O\left(D_p\right) \sim 100$$

$$\therefore\ \frac{Capture\ flux}{Settling\ flux} \sim O(0.001-0.01)$$

This shows that for a wetland system with suspended silt particles, the reduction of suspended particles by direct capture compared to by sedimentation is negligible. In this example the low flow velocities, low frontal plant area and low plant density are the causes for this. Flows through wetlands are commonly low, as estimated, however the frontal area of plants and the plant density may be higher than used in this assessment. In these cases the importance of direct particle capture would increase. Also, in the case of smaller suspended particles, such as clay particles, sedimentation would decrease and so the importance of direct particle capture would also increase.

5.5.1.2 Example 2: Seagrass/tidal marsh system with suspended sand particles

Based on the values in Table 6, order of magnitude assessment of a seagrass or tidal marsh system with suspended sand particles was conducted:

$$O(\eta) \sim 0.001; \quad O\left(\frac{U}{w_s}\right) \sim 1-10; \quad O(l_c d_c) \sim 0.01; \quad O(D_p) \sim 1000$$

$$\therefore \quad \frac{Capture\ flux}{Settling\ flux} \sim O(0.01-0.1)$$

This shows that for sand particles, which are some of the larger particles likely to be entrained in aquatic systems, sedimentation is a more important removal process than direct particle capture. This is because the settling velocity of sand particles is relatively high.

5.5.1.3 Example 3: Seagrass/tidal marsh system with suspended silt particles

Based on the values in Table 6, order of magnitude assessment of a seagrass or tidal marsh system with suspended silt particles was conducted:

$$O(\eta) \sim 0.001; \quad O\left(\frac{U}{w_s}\right) \sim 10-100; \quad O(l_c d_c) \sim 0.01; \quad O(D_p) \sim 1000$$

$$\therefore \quad \frac{Capture\ flux}{Settling\ flux} \sim O(1-10)$$

Compared to Example 2, this example shows that for suspended silt particles removal from the water column by direct particle capture is a significant process. In the case of silt particles in seagrass or tidal marsh systems, because silt particles are smaller than sand particles and thus have a much smaller settling velocity, the settling flux for the system is less. Direct particle capture can be equally or an order of magnitude more important than sedimentation in such systems. In the case of suspended clay particles direct particle capture as a removal mechanism would be even more significant.

5.5.1.4 Example 4: Seagrass system with suspended larvae particles

Based on the values in Table 6, order of magnitude assessment of a seagrass system with suspended larvae particles was conducted:

$$O(\eta) \sim 0.001;\ \ O\left(\frac{U}{w_s}\right) \sim 100-1000;\ \ O(l_c d_c) \sim 0.01;\ \ O(D_p) \sim 1000$$

$$\therefore\ \frac{Capture\ flux}{Settling\ flux} \sim O(0.1-1)$$

For suspended larvae particles, such as marine bivalve larvae in seagrass systems, the direct capture by aquatic vegetation is likely to be of a similar order of magnitude to sedimentation. Based on the order of magnitude analysis, direct particle capture could account for up to half of the larvae particles removed from the water column. In this case, approximately half of the larvae would be deposited on seagrass blades, and the other half on or near the seabed. This would have important implications for the population dynamics of the larvae species.

These order of magnitude assessments of the importance of direct particle capture in different aquatic systems do not account for the effect of array density on particle capture efficiency, as was observed in experiments, and discussed in Section 5.4.1. At this stage, the data collected in experiments suggests that particle capture efficiency may be optimised at certain vegetation densities, but results are not conclusive enough to be used in assessments like those performed above.

5.5.2 Filtration capacity of vegetated aquatic systems

The order of magnitude analysis above suggests that, based only on the magnitudes of capture efficiencies measured in experiments, reductions in suspended particles by direct particle capture is particularly important for small suspended particles such as silt, in aquatic systems such as tidal marshes or seagrass meadows, where vegetation densities and flow velocities are typically larger than in freshwater wetlands. The filtration capacity of a hypothetical seagrass meadow is presented to further demonstrate that direct particle capture is an important process in a system such as this.

To estimate the filtration capacity of a hypothetical seagrass meadow based on direct particle capture, an expression for the change in particle concentration of suspended particles with respect to the length of vegetation (x) that water has flowed through is required. Consider a flow with an initial particle concentration of P_0 through a box as shown in Figure 50.

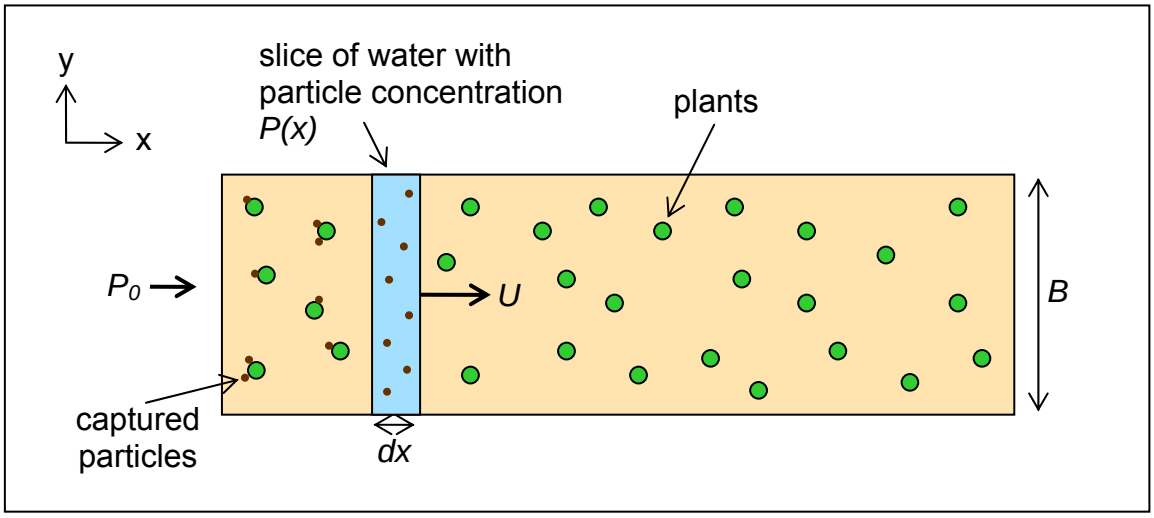

Figure 50: Particle flux through a two dimensional box.

From Equation 16, the number of particles lost to the plants over some time interval can be expressed as:

$$dN_c = \left(-\eta P U d_c l_c n\right) dt \tag{25}$$

Also, N_c is the number of particles lost in a 'slice' of water of some width, so the number of particle lost to plants with respect to distance can be expressed as:

$$dN_c = \left(P l_c B\right) dx \tag{26}$$

Combining Equation 25 and Equation 26, and substituting in the plant density since $D_p = n/(Bdx)$ gives:

$$\frac{dP}{dt} = -\eta U d_c D_p \tag{27}$$

Substituting dt with dx/U then gives:

$$\frac{dP}{dx} = -\eta P d_c D_p \tag{28}$$

Integrating Equation 28 finally gives an expression for the particle concentration in terms of distance (x) through the array:

$$P = P_O \exp\left(-\eta d_c D_p x\right) \tag{29}$$

Equation 29 was used to assess the filtration capacity by direct particle capture of a seagrass meadow for three hypothetical situations: high, medium and low particle removal. The parameters used for each hypothetical situation are shown in Table 7. Seagrass 2 is an example of an average seagrass meadow, with a shoot density within reported ranges (Section

2.2.2), and with a capture efficiency appropriate for this shoot density, based on the relationship between capture efficiency and array density observed in experiments (Section 5.4.1). Seagrass 1 is an example of a seagrass meadow that would capture more suspended particles than the average seagrass meadow over a given distance, and seagrass 3 is an example of a seagrass meadow that would capture less suspended particles than the average seagrass meadow over a given distance. The proportional reduction in suspended particles through a seagrass meadow for these three examples is plotted against length of the meadow in Figure 51.

Table 7: Parameters relevant to determining filtration capacity for three hypothetical seagrasses.

Variable	Seagrass 1	Seagrass 2	Seagrass 3
η (%)	0.7	0.4	0.2
D_p (shoots m^{-2})	3000	2000	1000
d_c (cm)	1.5	1.0	0.7

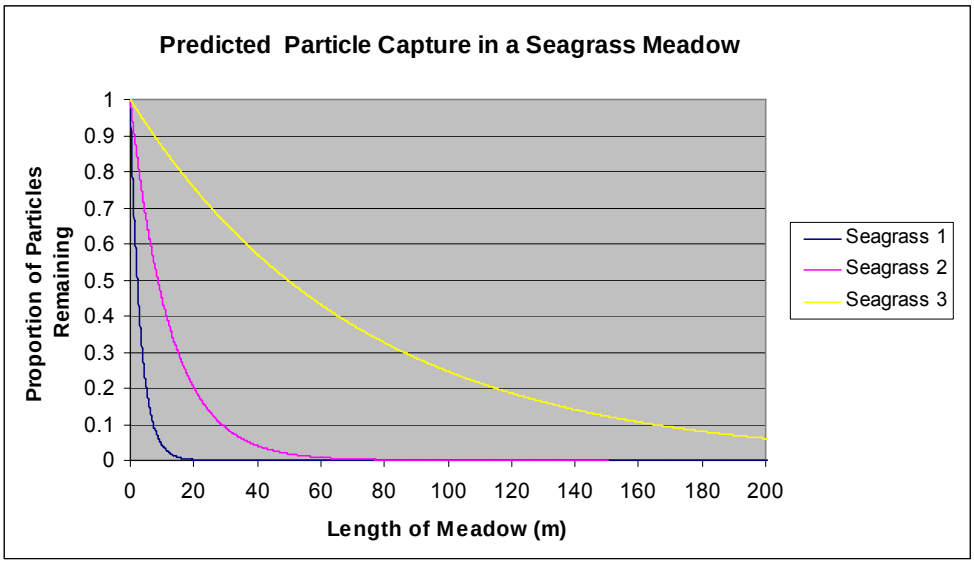

Figure 51: Particle removal for the three hypothetical seagrass meadows listed in Table 7 (predicted by Equation 29).

From Figure 51 it can be seen that, depending on the characteristics of a seagrass meadow, the length of the meadow required for a specific percentage reduction in suspended silt particles can vary dramatically. For an average seagrass meadow (seagrass 2) a reduction in suspended particles of 90% could be obtained through 30 m of the meadow.

Equation 29 was also used to assess the filtration capacity of the different arrays densities used in experiments, if all dowel rods had been coated in grease to allow particles to adhere to them. Calculating the filtration capacity for the experimental densities was undertaken because it allowed the appropriate capture efficiency for each density to be incorporated into

the filter efficiency. The parameters used in filtration calculations are shown in Table 8, and the proportional reduction in suspended particles through the array shown in Figure 52.

Table 8: Parameters relevant to determining filtration capacity for the three density array experiments.

Variable	Low Density Array	Medium Density Array	High Density Array
η (%)	0.20	0.39	0.048
D_p (shoots m^{-2})	1013	2026	4053
d_c (cm)	0.63	0.63	0.63

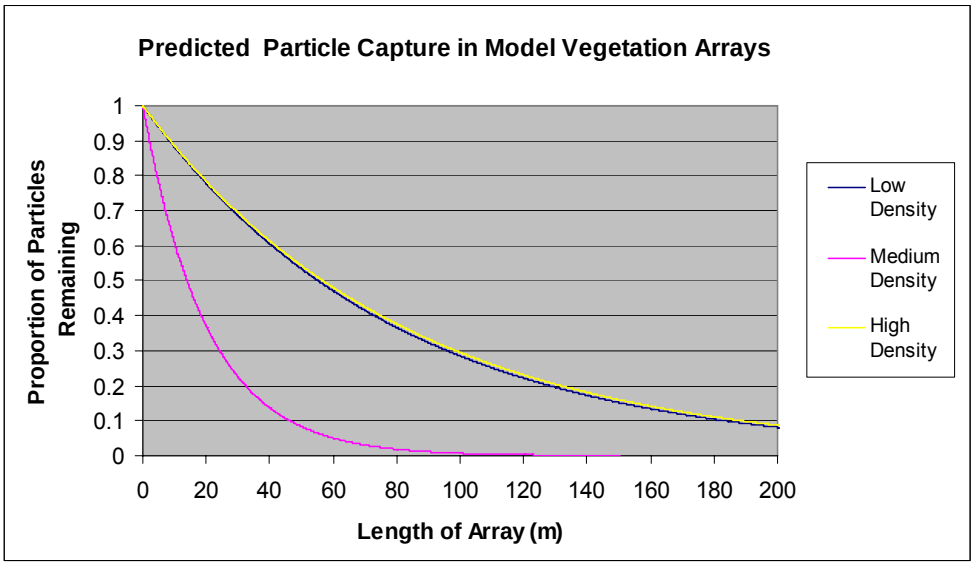

Figure 52: Particle removal for the experimental arrays if all dowel rods had been coated in grease (predicted by Equation 29).

From Figure 52 it can be seen that filtration capacity of the medium density array was the largest of all three array densities. Coincidently, the filtration capacities for the low and high array densities were almost identical, showing the balance between vegetation density and particle capture efficiency which influences the overall filtration capacity of vegetated aquatic systems. From this figure, it can be seen that for the medium density array, a vegetation array length of approximately 46 m would result in only 10% of particles remaining in suspension, whereas for the low and high array densities, this same reduction in particles would require a vegetation array length of approximately 189 m. This demonstrates that the filtration capacity of the medium density array is much higher than those of the low and high density arrays.

5.5.3 Comparison to previous studies

As well as using the experimentally determined particle capture efficiencies to predict the particle reduction potential of hypothetical systems, the experimentally determined capture efficiencies can be used to estimate particle retention in real systems, and these estimates compared to the actual field observations. Two tidal marsh systems in which direct particle

capture was identified as a significant particle removal mechanism are examined here. To estimate what percentage reduction the experimentally determined particle capture efficiencies would account for, the average marsh stem diameter and plant density must be known. For comparison purposes, the length of vegetation over which the observed particle reduction occurred in the field must also be known.

5.5.3.1 Study 1: Smooth cordgrass marsh, Delaware

Stumpf (1983) conducted a study of a salt marsh-creek system in Delaware, USA. Sediment on the stems and leaves of *Spartina alterniflora* (smooth cordgrass) above 3 cm from the seabed was collected, and was found to account for 50% of the suspended sediment lost during a spring tide (Stumpf 1983).

In this system, the observed 50% reduction in suspended sediment occurred within 12 m from the creek mouth. Stem diameters and densities for the cordgrass were not reported by Stumpf (1983); however these can be based on stem diameters and densities observed in nearby *Spartina alterniflora* marshes. A *Spartina alterniflora* marsh in Maryland, USA was found to have an average stem diameter of 0.5 cm and an average plant density of approximately 1000 shoots m^{-2} (Meyer *et al.* 2001). As this plant density is most similar to the low array density investigated in this study, estimating a capture efficiency of 0.2% would be appropriate for this system. With a capture efficiency of 0.2%, from Equation 29, the calculated reduction in suspended particles over 12 m is only 10%, compared to the observed 50% reduction. Based on a capture efficiency of 0.2%, a marsh length of approximately 80 m is required to achieve a 50% reduction in suspended particles. This suggests that in this marsh system the particle capture efficiency was greater than 0.2%. A particle capture efficiency of 1.2% is required to account for a 50% reduction in suspended particles over 12 m as was observed.

5.5.3.2 Study 2: Needlerush marsh, Florida

Leonard *et al.* (1995) studied a *Juncus roemerianus* (needlerush) marsh in west-central Florida. Field observations from this study found that up to 10% of the sediment accreted in tidal marshes is due to adhesion on vegetation, creating a thin layer of sediment over these structures.

In this system the average observed reduction in suspended particle concentration was 9% per metre and average stem densities were reported to be 280 shoots m^{-2} (Leonard *et al.* 1995). An array density similar to this plant density observed was not investigated in this study. The low density array experiments were the closest density to this marsh density, so a particle

capture efficiency of 0.2% was estimated. Stem diameters were not reported in this study and so were estimated to be 1 cm, based on typical wetland plant stem diameters (Chambers *et al.* 1995). Based on a capture efficiency of 0.2% a particle reduction of only 1% per meter was calculated, which is lower than the observed 9%. To achieve a 9% reduction in particle concentration per metre, a capture efficiency of approximately 3.4% is required.

In both of these studies the observed particle capture efficiency required to account for the observed particle reduction was of the order of 1%, which is larger than the experimentally determined capture efficiencies. Given that a significant range of capture efficiency range was observed in experiments (0.02 to 0.67%), the difference between experimental values and field observations of particle capture efficiency does not necessarily imply that the experimentally determined values are lower than actual values, but rather it emphasises that particle capture efficiency needs to be investigated in a wider range of systems before generalisations can be made.

5.6 Limitations to results

5.6.1 Errors

The errors associated with the results obtained in this study must be considered. Errors in the particle counts and ADV measurements, and the impact of these errors on the results are outlined below.

Errors in counting the number of particles collected on cylinder faces may have occurred due to human error and in ambiguous cases. Care was taken during particle counting to minimise the human error associated with results. The error associated with ambiguous cases is likely to be more significant. In some of the photographs analysed, imperfections in the grease and light marks on the cylinder surface (underneath the grease) could not always be distinguished from particles. In these cases comparison between the photograph and the actual cylinder were made where possible. It is estimated that the error associated with particle counts is ± 2 particle per cylinder face. Because capture efficiencies were calculated based on the numbers of particles collected on 15 cylinder faces (three faces per cylinder, five cylinders) errors in particle counts are likely to have averaged to zero and thus would have had a minimal impact on results.

There is also some uncertainty associated with the ADV velocity measurements, which comes from two sources: the input values of temperature and salinity, and Doppler noise. If temperature and salinity are not measured accurately, or if they change during a run, the

velocity measurements made may be biased. In these experiments this uncertainty is likely to be insignificant as the salinity remained constant for all experiments, and the temperature of the water in the flume was measured at the beginning of each experiment and would not have varied much (< 0.5°) over the eight minutes when ADV measurements were collected. Doppler noise is stated by the ADV manufacturer (SonTek) to be an artefact of acoustic scattering and can be assumed to be random noise. At a sampling rate of 25 Hz (as was used in experiments) for a signal to noise ratio above 15 (as was observed in experiments) uncertainty due to Doppler noise is estimated to be 1% of the maximum velocity range (Palmer 2003). This is unlikely to have affected results.

The largest source of error in the results was assuming that the suspended particle concentration remained constant during and between experiment, and that there was no reduction in particles from the original amount added to the flume. This assumption was required because the ADV amplitude measurements made during experiments could not be converted to sensible suspended particle concentrations. Although not ideal, based on the similar density between the water and the particles, and the small number of particles removed on the face of test cylinders, the assumption was reasonable. Some reductions were observed to occur however, as shown in Figure 7. It is estimated that the maximum reduction in suspended particles that would have occurred would be 10% of the initial concentration. Under these circumstances the actual particle capture efficiencies would have been higher than the calculated capture efficiencies. If 90% of the original particle concentration was suspended during an experiment, then the actual capture efficiency for that experiment would be 1.11 times greater than the calculated capture efficiency. Overall, this means that the actual capture efficiencies could be up to 11% higher than those calculated.

5.6.2 Experimental limitations

The conclusions drawn from this study are limited in their applicability to real systems because a limited number of conditions were tested in experiments. Thus, to estimate capture efficiency in systems with flow velocities above and below those tested, for different plant densities, and stem diameters, and for different particle types, results from these experiments must be extrapolated. Also, because each experiment was only performed once the conclusions drawn from results are limited. If experiments had been repeated, conclusions would have been strengthened.

Experiments in this study were constructed for rigid, vertical vegetation, and the wake structure in these arrays investigated. Rigid vegetation such as reeds and rushes exist in

natural aquatic systems, and so results of this study are applicable to these systems. In systems where the vegetation is not rigid, for example in seagrass meadows, where vegetation blades can bend and wave with the currents, the wake structures would be different, and this may alter how particles are captured on the surface of these types of vegetation.

6.0 Conclusion

Before conducting this study, the understanding of the efficiency at which vegetation removes suspended particles from the water column by direct particle capture, and the importance of stem wakes on this process, was limited. This study involved conducting laboratory experiments to test the particle capture efficiency of aquatic vegetation in conditions simulating real systems. The purpose of these experiments was to investigate how the particle capture efficiency of vegetation in arrays varied with two critical parameters, array density and collector Reynolds number, and also to investigate how eddy structures in the modelled vegetation arrays influence the particle capture efficiency.

The results obtained in this study have allowed the magnitude of particle capture efficiency by aquatic vegetation in an array to be estimated, and thus direct particle capture by aquatic vegetation is better quantified. Results from experiments showed that for the conditions tested, the particle capture efficiency of the modelled aquatic vegetation ranged between 0.02 and 0.67%. Particle capture efficiency was highest for modelled vegetation in the medium density array, and lowest for modelled vegetation in the high density array.

Experiments also confirmed that vegetation stem wakes influence particle capture. Analysis of the velocity measurements made during experiments found that the vortex shedding frequency and speed of eddy rotation were highest for the medium density array experiments, in which the highest particle capture efficiencies were observed. Based on the findings of this study, it is hypothesised that there is an optimum vegetation array density required to maximise the particle capture efficiency of that vegetation. Experimental results suggest this is an intermediate density, however further research into how stem wakes influence capture is required, as discussed in Section 7.0.

Capture efficiency was not found to increase with increasing Reynolds numbers for cylinders in the array experiments conducted, unlike observations made previously in particle capture experiments for an isolated cylinder. No obvious trend with Reynolds number was observed in the low and high density array experiments, and a decreasing trend was observed in the medium density array experiments. These observations cannot currently be accounted for. It is suspected that the presence of vortices in arrays influences what particle capture mechanisms dominate, so further investigation into the effect of vortices on particle capture mechanisms may yield an explanation to the Reynolds number trends observed here.

Direct particle capture onto the surface of a single collector within an array system was determined experimentally to remove in the order of 0.01 to 1% of the particles suspended in the water column. Based on this, systems in which direct particle capture is an important mechanism for the removal of suspended particles were identified. It was concluded that in aquatic systems with low flow velocities and relatively sparse vegetation, such as in freshwater wetlands, direct particle capture is not important compared to sedimentation. In aquatic systems with higher flow velocities and denser vegetation, such as in tidal marshes and seagrass meadows, direct particle capture is an important removal mechanism, influencing the fate of suspended particles such as silt and marine bivalve larvae particles.

In conclusion, this study demonstrated that capture of suspended particles by aquatic vegetation is an important process in many aquatic systems. The understanding of the particle capture efficiency by aquatic vegetation and the influence of stem wakes on this efficiency has been improved, achieving the objectives of the study, however considerable further investigation is required before these processes can be described in detail and applied to field scale situations.

7.0 Recommendations

A number of recommendations for future work in the research area of particle capture by aquatic vegetation are made here. Firstly, to build on the results obtained in this study it is recommended that further laboratory work investigating particle capture be undertaken. Experiments repeating the procedures used in this study would be required to verify the results obtained and thus strengthen the conclusions drawn.

Experiments testing particle capture under different conditions would improve the breadth of aquatic systems that experimental findings could be related to. It is recommended that particle capture is investigated for systems with different array densities and different cylinder diameters. Investigation of particle capture by non-cylindrical and flexible vegetation is also suggested, as this is more realistic of certain vegetation types such as seagrasses. Assessing how particle capture efficiency varies with particles of different shapes, sizes and densities in laboratory experiments would also be important. It is recommended that further laboratory work also involve a component of flow visualisation, as this would enable examination of the actual wake structures in arrays.

After conducting further experimental work to test particle capture in the laboratory it is recommended that numerical modelling of the flow through cylinder arrays, typical of aquatic vegetation arrays, be undertaken. Numerical modelling would allow the structure of vortices in the wakes of cylinders to be investigated in greater detail than is possible with laboratory experiments. It is suggested then, that the results from numerical modelling be combined with the results from further laboratory experiments, in particular with flow visualisation results, to describe in detail how the stem wakes from vegetation affect the particle capture efficiency of aquatic vegetation.

It is recommended that when conducting the laboratory experiments and numerical modelling suggested above, particular emphasis be placed on investigating the optimum array density that maximises particle capture efficiency, and why there is an optimum array density. This is recommended because gained knowledge could be used in a number of engineering design applications. Understanding of the optimal vegetation density to maximise particle capture efficiency and thus minimise the concentration of suspended particles could be incorporated into the design of wastewater treatment wetlands, and the revegetation of degraded freshwater and coastal wetlands, to improve the quality of water flowing through these systems.

Ideally, if this recommended research was undertaken, predictions of particle capture in unstudied systems could be made, and field observations of particle capture in studied systems be better understood. A better understanding of particle capture by aquatic vegetation in aquatic systems would in turn lead to a better understanding of the geochemical and biological processes that occur in these systems. Ultimately, a better understanding of the processes occurring in aquatic systems would allow improved conservation and management of these important systems.

8.0 References

Ackerman, J. D. 2002, 'Diffusivity in a marine macrophyte canopy: implications for submarine pollination and dispersal', *American Journal of Botany*, vol. 89, no. 7, pp. 1119-1127.

Ackerman, J. D. & Okubo, A. 1993, 'Reduced Mixing in a Marine Macrophyte Canopy', *Functional Ecology*, vol. 7, pp. 305-309.

Agawin, N. S. R. & Duarte, C. M. 2002, 'Evidence of direct particle trapping by a tropical seagrass meadow', *Estuaries*, vol. 25, pp. 1205-1209.

Ayaz, F. & Pedley, T. J. 1999, 'Flow through and particle interception by an infinite array of closely-spaced circular cylinders', *European Journal of Mechanics - B/Fluids*, vol. 18, no. 2, pp. 173-196.

Beckett, K. P., Freer-Smith, P. H. & Taylor, G. 1998, 'Urban Woodlands: Their role in reducing the effects of particulate pollution', *Environmental Pollution*, vol. 99, pp. 347-360.

Cambridge, M. L. & Hocking, P. J. 1997, 'Annual primary production and nutrient dynamics of the seagrasses *Posidonia sinuosa* and *Posidonia australis* in south-western Australia', *Aquatic Botany*, vol. 59, no. 3-4, pp. 277-295.

Chambers, J. M., Fletcher, N. L. & McComb, A. J. 1995, *A Guide to Emergent Wetland Plants of South-Western Australia*, The Marine & Freshwater Research Laboratory, Murdoch University, Perth.

Eckman, J. E. 1983, 'Hydrodynamic processes affecting benthic recruitment', *Limnology and Oceanography*, vol. 28, no. 2, pp. 241-257.

Elliott, A. H. 2000, 'Settling of fine sediment in a channel with emergent vegetation', *Journal of Hydraulic Engineering*, vol. 126, no. 8, pp. 570-577.

Gacia, E. & Duarte, C. M. 2001, 'Sediment Retention by a Mediterranean *Posidonia oceanica* Meadow: The Balance between Deposition and Resuspension', *Estuarine, Coastal and Shelf Science*, vol. 52, no. 4, pp. 909-919.

Gacia, E., Granata, T. C. & Duarte, C. M. 1999, 'An approach to measurement of particle flux and sediment retention within seagrass (*Posidonia oceanica*) meadows', *Aquatic Botany*, vol. 65, no. 1-4, pp. 255-268.

Gambi, M. C., Nowell, A. R. M. & Jumars, P. A. 1990, 'Flume Observations on Flow Dynamics in Zostera marina (Eelgrass) Beds', *Marine Ecological Progress Series*, vol. 61, pp. 159-169.

Green, E. P. & Short, F. T. 2003, *World Atlas of Seagrasses*, University of California Press, Berkeley.

Grizzle, R. E., Short, F. T., Newell, C. R., Hoven, H. & Kindblom, L. 1996, 'Hydrodynamically induced synchronous waving of seagrasses: 'monami' and its possible effects on larval mussel settlement', *Journal of Experimental Marine Biology and Ecology*, vol. 206, pp. 165-177.

Harvey, M., Bourget, E. & Ingram, R. G. 1995, 'Experimental evidence of passive accumulation of marine bivalve larvae on filamentous epibenthic structures', *Limnology and Oceanography*, vol. 40, no. 1, pp. 94-104.

Hosokawa, Y. & Horie, T. 1992, 'Flow and particulate nutrient removal by wetland with emergent macrophyte', *Science of the Total Environment*, pp. 1271-1281.

Kadlec, R. H. 1990, 'Overland Flow in Wetlands: Vegetation Resistance', *Journal of Hydraulic Engineering*, vol. 116, no. 5, pp. 691-705.

Knight, R. L., Kadlec, R. H. & Ohlendorf, H. M. 1999, 'The Use of Treatment Wetlands for Petroleum Industry Effluents', *Environmental Science & Technology*, vol. 33, no. 7, pp. 973-980.

Kundu, P. K. 1990, *Fluid Mechanics*, Academic Press, Inc., San Diego.

Kundu, P. K. & Cohen, I. M. 2002, *Fluid Mechanics: Second Edition*, Academic Press, Inc., San Diego.

Leonard, L. A., Hine, A. C. & Luther, M. E. 1995, 'Surficial Sediment Transport and Deposition Processes in a *Juncus roemerianus* Marsh, West-Central Florida', *Journal of Coastal Research*, vol. 11, no. 2, pp. 322-336.

Leonard, L. A. & Reed, D. J. 2002, 'Hydrodynamics and Sediment Transport Through Tidal Marsh Canopies', *Journal of Coastal Research*, vol. Special Issue 36, pp. 459-469.

Li, Y. & Park, C. W. 1996, 'Deposition of Brownian Particles on Cylindrical Collectors in a Periodic Array', *Journal of Colloid and Interface Science*, vol. 185, no. 1, pp. 49-56.

Lindegarth, M., Jonsson, P. R. & Andre, C. 1991, 'Fluorescent Microparticles: A New Way of Visualizing Sedimentation and Larval Settlement', *Limnology and Oceanography*, vol. 36, no. 7, pp. 1471-1476.

Lopez, F. & Garcia, M. 1998, 'Open-channel flow through simulated vegetation: Suspended sediment transport modeling', *Water Resources Research*, vol. 34, no. 9, pp. 2341-2352.

Martin, D. & Nokes, R. 1988, 'Crystal settling in a vigorously convecting magma chamber', *Nature*, vol. 332, no. 7, pp. 534-536.

Meyer, D. L., Johnson, J. M. & Gill, J. W. 2001, 'Comparison of nekton use of *Phragmites australis* and *Spartina alterniflora* marshes in the Chesapeake Bay, USA', *Marine Ecological Progress Series*, vol. 209, no. 1, pp. 71-84.

Nepf, H. N. 1999, 'Drag, turbulence, and diffusion in flow through emergent vegetation', *Water Resources Research*, vol. 35, no. 2, pp. 479-489.

Norberg, C. 2001, 'Flow around a circular cylinder: Aspects of fluctuating lift', *Journal of Fluids and Structures*, vol. 15, pp. 459-469.

Palmer, M. P. 2003, Observations of Particle Capture on a Cylindrical Collector: Implications for Particle Accumulation and Removal in Aquatic Systems, Masters, Massachusetts Institute of Technology.

Palmer, M. P., Nepf, H. N. & Petterson, T. J. R. 2004, 'Observations of particle capture on a cylindrical collector: Implications for particle accumulation and removal in aquatic systems', *Limnology and Oceanography*, vol. 49, no. 1, pp. 76-85.

Paterson, D. M. & Black, K. S. 1999, 'Water Flow, Sediment Dynamics and Benthic Biology', *Advances in Ecological Research*, vol. 29, no. 155-193.

Rea, N. & Ganf, G. G. 1994, 'How emergent plants experience water regime in a Mediterranean-type wetland', *Aquatic Botany*, vol. 49, no. 2-3, pp. 117-136.

Stumpf, R. P. 1983, 'Process of Sedimentation on the Surface of a Salt Marsh', *Estuarine, Coastal and Shelf Science*, vol. 17, pp. 495-508.

Terranos, J. & Duarte, C. M. 2000, 'Experimental evidence of reduced particle resuspension within a seagrass (*Posidonia oceanica* L.) meadow', *Journal of Experimental Marine Biology and Ecology*, vol. 243, no. 1, pp. 45-53.

Turner, S. J. & Schwarz, A.-M. 2006, 'Biomass development and photosynthetic potential of intertidal Zostera capricorni in New Zealand estuaries', *Aquatic Botany*, vol. 85, no. 1, pp. 53-64.

White, B. & Nepf, H. N. 2003, 'Scalar transport in random cylinder arrays at moderate Reynolds numbers', *Journal of Fluid Mechanics*, vol. 487, pp. 43-79.

Whitlow, R. 2001, *Basic Soil Mechanics, 4th ed.*, Sydney, Prentice Hall.

Appendix A

MATLAB code for counting particles

```
%Counting particles
clear, close all, imtool close all
ypos=[];
zpos=[];

%%%%%User input
fig_name ='cyl1 front.jpg';

disk_size = 200;
%Used to evaluate background (number must be bigger, in pixels, than size
of particles)

size_threshold_min = 5;
size_threshold_max = 130;

size_to_count_as_double = 60;
%Used to count very big particles as two different particles

%Load figure
Iraw = imread(fig_name);
Iraw2 = rgb2gray(Iraw);
imshow(Iraw2)

%Crop figure
I=imcrop(Iraw2);
imshow(I)

I = Iraw2;

se=ones(4);
erodedI=imerode(I,se);
I=erodedI;
figure, imshow(I)

%Evaluate background intensity
background = imopen(I,strel('disk',disk_size));
figure, imshow(background)

%Subtract uneven background
I2 = imsubtract(I,background);
figure, imshow(I2)

%Adjust contrast
%Code not used because did not give good results for specific use
%I3 = imadjust(I2);
%figure, imshow(I3);
%Manually assign I3 instead
I3=I2;

%Create a binary version of the image
%Code not used because did not give good results for specific use
%level = graythresh(I3);
%Manually assign threshold level instead
level = 0.2;
bw = im2bw(I3,level);
figure, imshow(bw)

%Determine number of particles in image (the '4' refers to how connectivity
%is defined)
[labeled,numObjects] = bwlabel(bw,8);

numObjects
```

```
%Data quality check
graindata = regionprops(labeled,'basic');

figure, imshow(I)

for i=1:numObjects
    hold on

    if  graindata(i).Area  >=  size_threshold_min  &  graindata(i).Area  <=
    size_threshold_max & graindata(i).Area < size_to_count_as_double
        ypos=[ypos graindata(i).Centroid(1)];
        zpos=[zpos graindata(i).Centroid(2)];
        plot(graindata(i).Centroid(1),graindata(i).Centroid(2),'*')

    elseif graindata(i).Area >= size_threshold_min & graindata(i).Area <=
    size_threshold_max & graindata(i).Area >= size_to_count_as_double
        ypos=[ypos graindata(i).Centroid(1) graindata(i).Centroid(1)];
        zpos=[zpos graindata(i).Centroid(2) graindata(i).Centroid(2)];
        plot(graindata(i).Centroid(1), graindata(i).Centroid(2),'ro')

    end
end

numObjects_just_the_right_size=length(ypos)

%%%%%%%%%%%%%%%%%%%%%%%%%%%%%%%%%%%%%%%%%%%%%%%%%%%%%%%%%%%%%%%%%%%%%%%%%%%%%%%

% Analysing particle deposition patterns
number_of_bins=32;
[n,x] = hist(zpos,number_of_bins);
figure, plot(x,n)

% Plots spectrum with # diameters as x-axis
[P,f] = pwelch(nmean(n), number_of_bins/2, [], [],
                                number_of_bins*size(I3,2)/(size(I3,1)*0.6));
cumuldata=[cumuldata
    rot90(P,-1)
    rot90(f,-1)];
ypos=[];
zpos=[];
        end
    end

meanP=mean(cumuldata(1:2:size(cumuldata,1)-1,:));
meanf=mean(cumuldata(2:2:size(cumuldata,1),:));
figure, plot(meanf,meanP)
title('Particle Spatial Distribution: Low Density Run 1, Front Face',
                                                    'FontWeight', 'bold')
xlabel('Spatial Frequency (cm^-^1)','FontWeight','bold')
ylabel('Spectral Density (particles^2.cm^-^1)','FontWeight','bold')
   save meanf-left meanf
   save meanP-left meanP
```

Appendix B

Tables of experimental results

Table 9: ADV amplitude results from the in-flume calibration.

			Counts				
Calibration	**Mass (g)**	**Concentration (g m^{-3})**	**Run 1**	**Run 2**	**Run 3**	**Run 4**	**Average Amplitude**
1	8.0064	66.72	85.44	85.13	86.29	-	85.62
2	8.5081	70.90	88.41	90.57	-	-	89.49
3	9.0086	75.07	91.05	90.05	87.85	86.44	88.85
4	9.5089	79.24	88.92	87.66	86.88	-	87.82
5	10.0065	83.39	86.64	93.56	89.25	-	89.82
6	11.0000	91.67	94.30	92.28	91.06	-	92.55
7	12.0032	100.03	91.34	92.92	90.06	-	91.44
8	13.0000	108.33	95.30	92.82	90.04	-	92.72
9	14.0011	116.68	92.91	93.93	94.33	-	93.72

Table 10: ADV amplitude results from the bucket calibration.

Volume (L)	**Concentration (g m^{-3})**	**Amplitude (counts)**
6	129.7	113.6
7	111.2	113.6
8	97.3	112.9
9	86.5	112.3
10	77.8	112.2

Table 11: Average ADV results for each experiment.

LOW DENSITY ARRAY	Run 1	Run 2	Run 3	Run 4	Run 5	Run 6	Average
Number of samples	11228	13219	12279	11634	10945	11174	11747
Average x velocity (cm s^{-1})	-1.12	-2.88	-3.97	-6.42	-7.70	-9.09	-5.20
Positive x velocity	1.12	2.88	3.97	6.42	7.70	9.09	5.20
Std dev of x velocity (cm s^{-1})	0.19	0.51	0.68	0.97	1.12	1.31	0.80
Average y velocity (cm s^{-1})	-0.01	0.02	-0.01	0.02	-0.22	-0.18	-0.06
Std dev of y velocity (cm s^{-1})	0.25	0.54	0.75	1.15	1.20	1.48	0.90
Average absolute value of y velocity (cm s^{-1})	0.20	0.43	0.59	0.90	0.95	1.17	0.71
Average absolute value of z velocity (cm s^{-1})	-0.02	-0.08	-0.08	-0.13	-0.15	-0.17	-0.11
Std dev of z velocity (cm s^{-1})	0.13	0.34	0.48	0.66	0.78	0.94	0.56
Average abs z velocity (cm s^{-1})	0.10	0.27	0.38	0.53	0.63	0.76	0.45
Average amplitude (cm s^{-1})	92.22	91.71	91.29	92.78	91.82	93.97	92.30
MEDIUM DENSITY ARRAY	**Run 1**	**Run 2**	**Run 3**	**Run 4**	**Run 5**	**Run 6**	**Average**
Number of samples	10677	13075	12909	13071	10461	10590	11797
Average x velocity (cm s^{-1})	-1.10	-2.86	-4.39	-5.43	-6.83	-10.18	-5.13
Positive x velocity	1.10	2.86	4.39	5.43	6.83	10.18	5.13
Std dev of x velocity (cm s^{-1})	0.42	0.77	1.06	1.53	1.58	1.98	1.22
Average absolute value of y velocity (cm s^{-1})	-0.05	-0.09	0.05	0.04	0.10	0.02	0.01
Std dev of y velocity (cm s^{-1})	0.41	0.82	1.16	1.82	1.70	2.53	1.41
Average abs y velocity (cm s^{-1})	0.33	0.64	0.92	1.45	1.37	2.01	1.12
Average z velocity (cm s^{-1})	-0.01	-0.04	-0.10	-0.02	-0.15	-0.26	-0.10
Std dev of z velocity (cm s^{-1})	0.17	0.44	0.64	0.95	0.98	1.33	0.75
Average absolute value of z velocity (cm s^{-1})	0.13	0.34	0.51	0.76	0.77	1.07	0.60
Average amplitude (cm s^{-1})	81.36	80.96	79.00	76.98	85.29	89.15	82.12
HIGH DENSITY ARRAY	**Run 1**	**Run 2**	**Run 3**	**Run 4**	**Run 5**	**Run 6**	**Average**
Number of samples	12839	11858	12523	11871	11283	10400	11798
Average x velocity (cm s^{-1})	-1.79	-2.35	-3.65	-5.63	-8.71	-9.92	-5.35
Positive x velocity	1.79	2.35	3.65	5.63	8.71	9.92	5.35
Std dev of x velocity (cm s^{-1})	0.20	0.47	0.61	1.14	1.79	1.81	1.00
Average absolute value of y velocity (cm s^{-1})	-0.05	0.01	-0.14	0.19	0.27	0.05	0.05
Std dev of y velocity (cm s^{-1})	0.13	0.50	0.72	1.06	1.42	1.48	0.88
Average abs y velocity (cm s^{-1})	0.11	0.40	0.58	0.86	1.15	1.19	0.71
Average z velocity (cm s^{-1})	0.02	-0.06	-0.11	-0.16	-0.18	-0.17	-0.11
Std dev of z velocity (cm s^{-1})	0.05	0.29	0.42	0.71	0.97	1.01	0.57
Average absolute value of z velocity (cm s^{-1})	0.04	0.23	0.34	0.57	0.78	0.81	0.46
Average amplitude (cm s^{-1})	85.27	79.71	87.35	90.87	89.09	94.33	87.77

Table 12: Manual particle counts for experiments.

LOW DENSITY ARRAY		Number of Particles Counted						
Cylinder	**Face**	**Run 1**	**Run 2**	**Run 3**	**Run 4**	**Run 5**	**Run 6**	**Total**
Cylinder 1	Front	6	19	18	19	37	41	140
	Back Left	3	3	2	5	20	48	81
	Back Right	13	5	6	20	23	18	85
	Cylinder Total	22	27	26	44	80	107	306
Cylinder 2	Front	14	23	17	15	22	34	125
	Back Left	2	7	5	17	22	22	75
	Back Right	2	3	6	29	24	19	83
	Cylinder Total	18	33	28	61	68	75	283
Cylinder 3	Front	8	13	15	36	28	32	132
	Back Left	3	7	7	15	27	44	103
	Back Right	1	0	2	11	12	26	52
	Cylinder Total	12	20	24	62	67	102	287
Cylinder 4	Front	6	19	32	37	28	44	166
	Back Left	2	5	3	31	15	54	110
	Back Right	2	0	9	7	29	23	70
	Cylinder Total	10	24	44	75	72	121	346
Cylinder 5	Front	7	16	9	21	28	26	107
	Back Left	1	4	1	25	23	60	114
	Back Right	8	4	7	10	22	23	74
	Cylinder Total	16	24	17	56	73	109	295
Run	Run Total	78	128	139	298	360	514	1517
MEDIUM DENSITY ARRAY		**Number of Particles Counted**						
Cylinder	**Face**	**Run 1**	**Run 2**	**Run 3**	**Run 4**	**Run 5**	**Run 6**	**Total**
Cylinder 1	Front	26	52	54	41	31	29	233
	Back Left	2	1	13	14	21	29	80
	Back Right	4	10	12	35	29	54	144
	Cylinder Total	32	63	79	90	81	112	457
Cylinder 2	Front	20	57	54	52	18	26	227
	Back Left	2	10	7	30	11	55	115
	Back Right	3	10	23	29	28	32	125
	Cylinder Total	25	77	84	111	57	113	467
Cylinder 3	Front	28	44	42	61	16	17	208
	Back Left	9	2	5	14	7	11	48
	Back Right	2	9	17	47	20	47	142
	Cylinder Total	39	55	64	122	43	75	398
Cylinder 4	Front	43	43	47	55	19	32	239
	Back Left	1	10	3	12	15	14	55
	Back Right	4	14	28	42	24	56	168
	Cylinder Total	48	67	78	109	58	102	462
Cylinder 5	Front	28	52	41	47	29	22	219
	Back Left	5	3	4	17	23	66	118
	Back Right	2	19	28	62	25	37	173
	Cylinder Total	35	74	73	126	77	125	510
Run	Run Total	179	336	378	558	316	527	2294

HIGH DENSITY ARRAY		Number of Particles Counted						
Cylinder	**Face**	**Run 1**	**Run 2**	**Run 3**	**Run 4**	**Run 5**	**Run 6**	**Total**
Cylinder 1	Front	2	9	2	2	6	6	27
	Back Left	1	3	2	0	6	3	15
	Back Right	3	2	0	1	1	1	8
	Cylinder Total	6	14	4	3	13	10	50
Cylinder 2	Front	0	4	3	2	4	3	16
	Back Left	0	5	3	3	1	3	15
	Back Right	0	9	6	4	3	7	29
	Cylinder Total	0	18	12	9	8	13	60
Cylinder 3	Front	4	10	3	5	6	2	30
	Back Left	1	3	2	6	4	1	17
	Back Right	2	4	1	3	3	3	16
	Cylinder Total	7	17	6	14	13	6	63
Cylinder 4	Front	2	14	3	3	4	1	27
	Back Left	0	1	3	4	1	0	9
	Back Right	0	5	1	5	8	1	20
	Cylinder Total	2	20	7	12	13	2	56
Cylinder 5	Front	1	8	2	1	5	3	20
	Back Left	1	1	3	3	4	8	20
	Back Right	0	0	0	1	1	3	5
	Cylinder Total	2	9	5	5	10	14	45
Run	Run Total	17	78	34	43	57	45	274

Appendix C

Location of dowel rods near test cylinders

The location of dowel rods near the test cylinders for the different array densities are shown below (Figure 53, Figure 54 and Figure 55). Pegboard is shown in grey, with the holes in the pegboard shown as circles. Test cylinders are shown in black, and dowel rods in yellow.

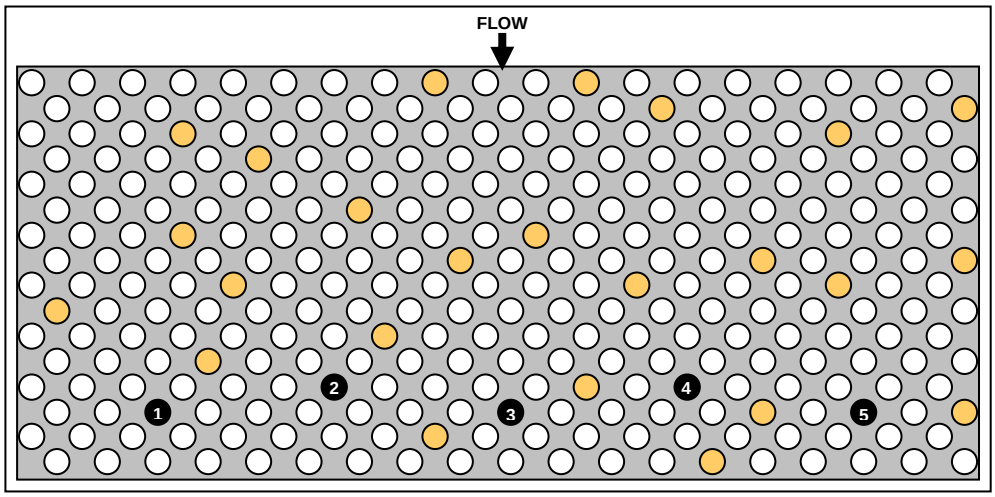

Figure 53: Position of dowel rods in vicinity of test cylinders for the low density array experiments.

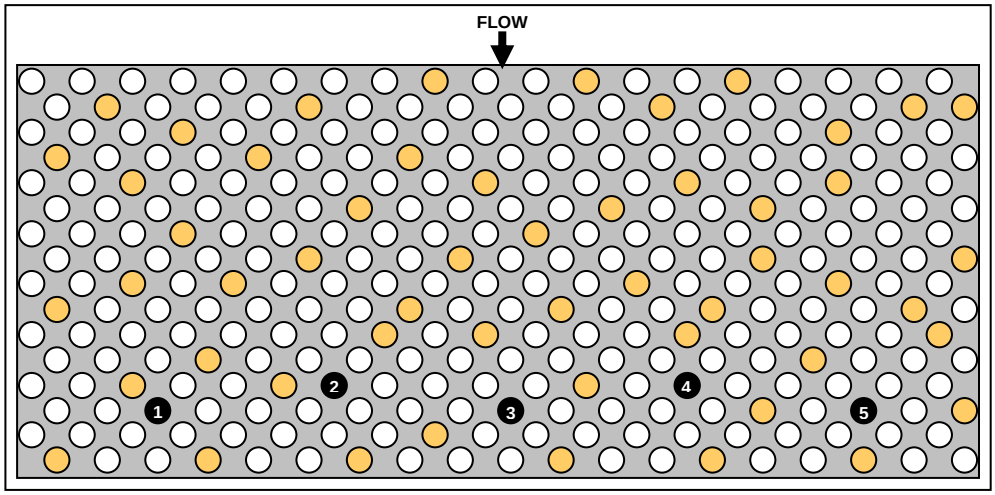

Figure 54: Position of dowel rods in vicinity of test cylinders for the medium density array experiments.

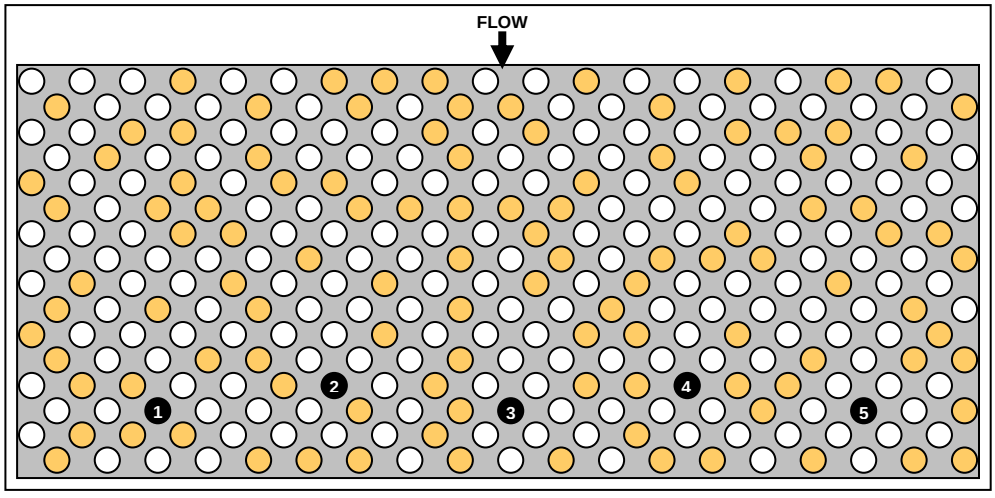

Figure 55: Position of dowel rods in vicinity of test cylinders for the high density array experiments.